



HAL
open science

α -Synuclein fibrils subvert lysosome structure and function for the propagation of protein misfolding between cells through tunneling nanotubes

Aysegul Dilsizoglu Senol, Maura Samarani, Sylvie Syan, Carlos M. Guardia, Takashi Nonaka, Nalan Liv, Patricia Latour-Lambert, Masato Hasegawa, Judith Klumperman, Juan S Bonifacino, et al.

► To cite this version:

Aysegul Dilsizoglu Senol, Maura Samarani, Sylvie Syan, Carlos M. Guardia, Takashi Nonaka, et al.. α -Synuclein fibrils subvert lysosome structure and function for the propagation of protein misfolding between cells through tunneling nanotubes. PLoS Biology, 2021, 19 (7), pp.e3001287. 10.1371/journal.pbio.3001287 . pasteur-03274582

HAL Id: pasteur-03274582

<https://pasteur.hal.science/pasteur-03274582>

Submitted on 30 Jun 2021

HAL is a multi-disciplinary open access archive for the deposit and dissemination of scientific research documents, whether they are published or not. The documents may come from teaching and research institutions in France or abroad, or from public or private research centers.

L'archive ouverte pluridisciplinaire **HAL**, est destinée au dépôt et à la diffusion de documents scientifiques de niveau recherche, publiés ou non, émanant des établissements d'enseignement et de recherche français ou étrangers, des laboratoires publics ou privés.



Distributed under a Creative Commons Attribution 4.0 International License

1 **α -Synuclein fibrils subvert lysosome structure and function for the**
2 **propagation of protein misfolding between cells through tunneling**
3 **nanotubes**

4 Aysegul Dilsizoglu Senol^{1§}, Maura Samarani^{1§}, Sylvie Syan¹, Carlos M. Guardia², Takashi
5 Nonaka³, Nalan Liv⁴, Patricia Latour Lambert⁵, Masato Hasegawa³, Judith Klumperman⁴, Juan
6 S. Bonifacino², Chiara Zurzolo^{1*}

7 ¹Unité de Trafic Membranaire et Pathogénèse, Département de Biologie Cellulaire et de
8 l'Infection, Institut Pasteur, Paris, France.

9 ²Neurosciences and Cellular and Structural Division, *Eunice Kennedy Shriver* National
10 Institute of Child Health and Human Development, National Institutes of Health, Bethesda,
11 MD, USA.

12 ³Dementia Research Project, Tokyo Metropolitan Institute of Medical Science, Tokyo, Japan.

13 ⁴Section Cell Biology, Center for Molecular Medicine, University Medical Center Utrecht,
14 Utrecht University, Utrecht, Netherlands.

15 ⁵Dynamique des Interaction Hôte-Pathogène, Département de Biologie Cellulaire et de
16 l'Infection, Institut Pasteur, Paris, France.

17
18 §These authors contributed equally

19 *Corresponding Author

20 E-mail: chiara.zurzolo@pasteur.fr (CZ)

21 **Abstract**

22 The accumulation of α -synuclein aggregates in specific brain regions is a hallmark of
23 synucleinopathies including Parkinson's disease. α -Synuclein aggregates propagate in a "prion-
24 like" manner and can be transferred inside lysosomes to recipient cells through tunneling
25 nanotubes (TNTs). However, how lysosomes participate in the spreading of α -synuclein
26 aggregates is unclear. Here, by using super-resolution and electron microscopy, we find that α -
27 synuclein fibrils affect the morphology of lysosomes and impair their function in neuronal cells.
28 In addition, we demonstrate that α -synuclein fibrils induce peripheral redistribution of
29 lysosomes, likely mediated by TFEB, increasing the efficiency of α -synuclein fibrils' transfer
30 to neighboring cells. We also show that lysosomal membrane permeabilization allows the
31 seeding of soluble α -synuclein in cells that have taken up α -synuclein fibrils from the culture
32 medium and, more importantly, in healthy cells in co-culture, following lysosome-mediated
33 transfer of the fibrils. Moreover, we demonstrate that seeding occurs mainly at lysosomes in
34 both donor and acceptor cells, after uptake of α -syn fibrils from the medium and following their
35 transfer, respectively. Finally, by using a heterotypic co-culture system, we determine the origin
36 and nature of the lysosomes transferred between cells and we show that donor cells bearing α -
37 synuclein fibrils transfer damaged lysosomes to acceptor cells, while also receiving healthy
38 lysosomes from them. These findings thus contribute to the elucidation of the mechanism by
39 which α -synuclein fibrils spread through TNTs, while also revealing the crucial role of
40 lysosomes, working as a Trojan horse for both seeding and propagation of disease pathology.

41 **Introduction**

42 The accumulation of amyloidogenic proteins in different regions of the brain is a hallmark of
43 neurodegenerative diseases (NDs) leading to cellular dysfunction, loss of synaptic
44 communication, and deficits in specific brain functions [1,2]. The misfolded α -synuclein (α -
45 syn) protein accumulates in intraneuronal inclusions known as Lewy bodies and Lewy neurites
46 in NDs known as synucleinopathies, including the second most common ND, Parkinson's
47 Disease (PD) [3–5]. These inclusions are associated with loss of neuronal and glial cells in
48 specific brain regions, leading to both motor (e.g., bradykinesia, tremor, rigidity) and non-motor
49 (e.g., cognitive impairment, depression, anxiety) symptoms [6,7].

50 α -Syn is a small (140 amino acids) cytoplasmic protein enriched in the brain and localized to
51 presynaptic terminals [8]. Although the precise function of α -syn remains poorly understood, it
52 has been shown to promote membrane curvature, thus contributing to synaptic trafficking and
53 vesicle budding [9–12], to modulate dopamine release through its association with presynaptic
54 terminal SNARE complexes [13], and to be involved in synaptic attenuation [14]. A recent
55 study has characterized *in vitro* a mechanism by which α -syn stabilizes, in a concentration-
56 dependent manner, the docking of synaptic vesicles on the plasma membrane by establishing a
57 dynamic link between the two membranes [15]. In PD brains, the spread of the pathology
58 correlates with the presence of α -syn inclusions and follows a specific and predictable route
59 through interconnected brain regions, mirroring the different stages of the disease [5,16]. These
60 findings supported the hypothesis, later confirmed experimentally, that α -syn aggregates can
61 be transferred from one cell to another both *in vitro* [17–22], and *in vivo* [23–27]. Furthermore,
62 mounting evidence suggests that α -syn aggregates spread in a “prion-like” manner, as they are
63 able to self-propagate by acting as “seeds” and inducing the misfolding of soluble native α -syn
64 [19,27–35]. Thus, understanding how α -syn aggregates spread and how/where in the cell they
65 induce misfolding of the soluble protein is crucial: i) to elucidate the pathogenesis of the
66 disease, and ii) to devise a therapy to inhibit the progression of the pathology. Different
67 mechanisms depending on either cell-to-cell contact or secretion have been proposed for the
68 spread of α -syn fibrils [35]. We and others have found that, in *in vitro* and *ex vivo* cultures,
69 tunneling nanotubes (TNTs) play a major role in this process [19–21,36].

70 TNTs are actin-based, thin cellular protrusions that connect remote cells [37]. They have been
71 identified in various cell types *in vitro* [38–41] and *in vivo* [42–47]. TNTs are open-ended
72 structures [48,49] that allow the exchange of various cargos, including entire organelles, such
73 as mitochondria and lysosomes, between cells [19,37–40]. In addition to α -syn fibrils, other

74 amyloidogenic proteins such as prion protein [50–52], huntingtin [53], and tau [52,54,55] use
75 TNTs as highways for transfer to naïve cells, suggesting that TNTs are common routes for the
76 spread of pathogenic proteins between cells. Of particular interest, we showed that α -syn fibrils
77 can be efficiently transferred between neuronal CAD cells, primary neurons, primary
78 astrocytes, and human neural progenitor cells, and between organotypic hippocampal slices and
79 astrocytes. We found that α -syn fibrils are mostly localized inside lysosomes in all of these cell
80 types [19,21,56] and could be transferred inside lysosomes through TNTs from “infected”
81 donor cells to naïve acceptor cells in co-cultures. Importantly, once arrived in the acceptor cells,
82 α -syn fibrils were able to induce the aggregation of soluble α -syn [19]. How this occurs,
83 however, is not clear.

84 Lysosomes are cytoplasmic, membrane-enclosed, acidic organelles that have long been
85 considered as the “dustbin” and “recycling center” of the cells, as they are responsible for the
86 degradation of both exogenous and intracellular cargos destined to lysosomes via endocytic,
87 phagocytic [57,58], and autophagic pathways [59,60]. However, in recent years, mounting
88 evidence revealed that lysosomes play a more complex role in the regulation of cellular
89 homeostasis, as they are involved in crucial processes such as plasma membrane repair,
90 transcriptional control, nutrient sensing, signaling, and energy metabolism [61–65]. It is
91 therefore not surprising that lysosomal dysfunction is involved in a plethora of pathological
92 conditions, including NDs [66]. Notably, the levels of lysosome-associated membrane proteins
93 1 and 2 (LAMP1 and LAMP2) and lysosomal enzymes Cathepsin B and D were found to be
94 significantly reduced in PD patient brains, mouse and cell models [67–72]. Moreover,
95 lysosomal membrane permeabilization (LMP) has been reported in cells treated with protein
96 aggregates including α -syn [73,74].

97 In the present study, we focused on the role of lysosomes in the intercellular spread of α -syn
98 fibrils in neuronal cells. Particularly, we studied how α -syn fibrils affect lysosomes and how
99 these organelles contribute to the spread and propagation of α -syn aggregates through TNTs.
100 We found that α -syn fibrils alter the morphology of lysosomes and compromise lysosomal
101 function. We demonstrated that α -syn fibrils induce the peripheral distribution of the lysosomes
102 exhibiting functional impairment, likely mediated by TFEB, and showed that this peripheral
103 positioning enhances the efficiency of α -syn fibrils’ transfer in a cell-to-cell contact-dependent
104 manner. In addition, we demonstrated that TFEB translocated to the nucleus in the presence of
105 α -syn fibrils, probably contributing to the peripheral distribution of lysosomes. We also found
106 that LMP, which is well described in cells following the uptake of α -syn fibrils from the
107 medium, also occurs in acceptor cells following the transfer of lysosomes bearing α -syn fibrils

108 from neighboring donor cells. Thus, by facilitating the escape of α -syn fibrils from lysosomes
109 after their transfer, LMP appears to be a relevant mechanism for the seeding of soluble α -syn
110 and propagation of the pathology in neighboring cells. Importantly, our super-resolution
111 microscopy data suggest that lysosomes create an optimal environment for seeding and are a
112 hub for the conversion of soluble α -syn into aggregates. Finally, by using a heterotypic cell co-
113 culture, we were able to track the origin and nature of the lysosomes transferred between cells.
114 We found that cells overwhelmed by the presence of α -syn fibrils impairing lysosomal function
115 transfer more damaged lysosomes to recipient cells and, in return, they receive healthy
116 lysosomes from neighboring cells devoid of α -syn, suggesting a potential rescue mechanism in
117 α -syn pathology.

118 **Results**

119 **α -Syn fibrils affect the morphology and function of lysosomes.**

120 We have previously reported that the majority of exogenous α -syn fibrils internalized by
121 neuronal catecholaminergic cell line CAD localize to lysosomes [19]. We confirmed these
122 findings by performing object-based 3D colocalization analysis (<https://imaris.oxinst.com>) in
123 CAD cells challenged with α -syn fibrils for 18 h prior to labelling for the lysosomal marker
124 LAMP1. We detected $74 \pm 1\%$ of α -syn fibrils colocalizing with lysosomes (LAMP1+
125 organelles), confirming that the majority of α -syn fibrils localize to lysosomes following their
126 uptake (Fig 1A). In addition, we found $60 \pm 1\%$ of lysosomes colocalizing with α -syn fibrils
127 (Fig 1A). To further investigate the lysosomal localization of α -syn fibrils and the possible
128 morphological consequences of this localization, we performed structured illumination
129 microscopy (SIM). We found that α -syn fibrils localized either inside lysosomes (Fig 1B,
130 magenta arrow and enlarged images on the right) or at the lysosomal membrane (Fig 1B, green
131 arrow and enlarged images on the right). We then measured the diameter of lysosomes in
132 control cells and in α -syn fibril-treated cells (where we distinguished between lysosomes
133 containing or not containing α -syn fibrils). The average diameter of lysosomes in control cells
134 and of lysosomes not containing α -syn fibrils in treated cells was almost identical (0.43 ± 0.01
135 μm) whereas lysosomes containing α -syn fibrils increased their diameter by 50% (0.63 ± 0.01
136 μm ; Fig 1B, graph), demonstrating that the enlargement induced by α -syn fibrils is restricted to
137 the lysosomes containing fibrils.

138 To further investigate the morphology of compartments containing α -syn fibrils, we used a
139 correlative light-electron microscopy (CLEM) approach to identify α -syn-positive and -
140 negative lysosomes by fluorescence microscopy (FM) and study their corresponding
141 morphology by electron microscopy (EM). First, we cultured CAD cells transiently transfected
142 with a plasmid encoding LAMP1-GFP and loaded with Alexa 568-tagged α -syn fibrils on
143 gridded coverslips, and imaged α -syn fibril-treated cells in FM while marking coordinates of
144 α -syn positive (Alexa568+/GFP+) and negative (Alexa568-/GFP+) LAMP1-GFP lysosomes.
145 Following FM imaging, the CAD cells were prepared for EM by keeping their orientation, and
146 serial sections were collected from the region containing the previously marked coordinates
147 (see also Material and Methods) [75,76]. Then, the FM signal was correlated to EM images.
148 Using this approach, we overcame the lack of suitable tools to identify α -syn fibrils directly by
149 EM and were able to compare the structural properties of lysosomes containing or not
150 containing α -syn fibrils. LAMP1-GFP-positive organelles colocalizing with α -syn fibrils in FM

151 were structurally identified as lysosomes by the presence of electron-dense heterogenous
152 luminal content, degraded membranes, and occasional intraluminal vesicles as morphological
153 criteria [77]. Lysosomes not containing α -syn fibrils presented a healthy lysosome morphology
154 with spherical shape and smooth membranes [77,78] (Fig 1C, green square, number 1).
155 Interestingly, most lysosomes containing α -syn fibrils were found to be quite heterogeneous in
156 structure (Fig 1C, red squares numbers 2, 3, and 4). Some had an unusual luminal content and
157 displayed curvy limiting membrane, suggesting that the presence of the fibrils could deform the
158 organelles (Fig 1C, red squares numbers 3, and 4). The aberrant, curvy organelles were
159 completely absent in control cells not treated with α -syn fibrils (S1A Fig). A subset of
160 lysosomes containing α -syn fibrils, as defined by FM, had a healthy morphology (Fig 1C, red
161 square, number 2), which could represent an early stage of fibrillar accumulation.

162 Next, we used another CLEM approach to analyse the morphology and size of α -syn-positive
163 lysosomes with high-resolution. CAD cells loaded with Alexa 568-tagged α -syn fibrils were
164 prepared for EM following the flat embedding Tokuyasu technique. This technique preserves
165 the fluorescence signal of α -syn fibrils in ultrathin sections prepared for EM, and in addition
166 allows to perform immunolabelling (both gold and fluorescent) of endogenous LAMP1 [79]
167 (Fig 1D). Following a recently developed high-throughput on-section CLEM approach [80],
168 we analysed 50 LAMP1-immunolabelled lysosomes in control cells (S1B Fig), 50 α -syn-
169 positive, and 50 α -syn-negative lysosomes in treated cells. For each lysosome, we correlated
170 EM ultrastructural details (surface area and perimeter) and the presence of LAMP1 to the FM
171 images showing the presence or absence of α -syn fibrils. Using this approach, we confirmed
172 that the lysosomes bearing α -syn fibrils were significantly larger (perimeter: $2.24 \pm 0.14 \mu\text{m}$
173 and area: $0.16 \pm 0.01 \mu\text{m}^2$) compared to lysosomes devoid of α -syn fibrils (perimeter: $1.16 \pm$
174 $0.06 \mu\text{m}$ and area: $0.08 \pm 0.01 \mu\text{m}^2$) and control lysosomes (perimeter: $1.16 \pm 0.04 \mu\text{m}$ and area:
175 $0.08 \pm 0.01 \mu\text{m}^2$; Fig 1D, graphs).

176

177 **Fig 1. α -Syn fibrils affect the morphology of lysosomes. (A)** Representative confocal images
178 of control and Alexa 568-tagged α -syn fibril-treated (18 h) CAD cells, immunolabelled for
179 LAMP1 (green). Colocalization between LAMP1+ puncta and α -syn fibrils is indicated by
180 arrows in the inset of a selected region delimited by a square. % of α -syn fibrils colocalizing
181 with LAMP1+ puncta ($74 \pm 1\%$) and % of LAMP1+ puncta colocalizing with α -syn fibrils (60
182 $\pm 1\%$) performed by object-based 3D colocalization method (Imaris software) is presented.
183 Mean \pm S.E.M, $n=3$ (30 cells per condition). Scale bar: $10 \mu\text{m}$ (for inset: $2 \mu\text{m}$). (B) Super-

184 resolution (SR) images of control (left panel) and Alexa 568-tagged α -syn fibril-treated CAD
185 cells for 18 h (right panel), immunolabelled for LAMP1 (far-red) antibody (pseudo colored in
186 grey). Merge images of each condition are presented with additional HCS CellMaskTM Blue
187 staining. Magenta and green arrows indicate the selected lysosomes having α -syn fibrils inside
188 the lysosomal lumen and on the lysosomal membrane, respectively, where higher
189 magnifications of these lysosomes and 3D reconstructions are represented in magenta and green
190 squares, respectively. Scale bar: 10 μ m (for insets: 2 μ m, for magenta and green insets: 0.5 μ m).
191 Average diameter (μ m) of lysosomes in control (0.43 ± 0.01) and in α -syn fibril-treated cells,
192 the latter sub-grouped as: lysosomes without α -syn fibrils (0.43 ± 0.01) and lysosomes with α -
193 syn fibrils (0.63 ± 0.01), is presented. Mean \pm S.E.M, lysosomes' diameters were measured in
194 SR images of eight α -syn fibril-treated cells and seven control cells (155 lysosomes per
195 condition). Images were acquired by spinning-disk microscopy with SR module. ns=not
196 significant, ****P<0.0001 by Kruskal-Wallis nonparametric ANOVA test followed by Dunn's
197 multiple comparison tests. **(C)** FM image of LAMP1-GFP transfected and α -syn fibril-treated
198 CAD cells for 18 h (left panel). Enlarged merged images of correlative resin EM and FM images
199 of four selected lysosomes not containing (number 1, indicated by green square) and containing
200 α -syn fibrils (numbers 2, 3, 4, indicated by red squares) are presented. Lysosomes number 1
201 and 2 are further magnified (blue squares) and presented within the same image. Lyso:
202 lysosome, PM: plasma membrane, LD: lipid droplets. Scale bar: 10 μ m (for red and green
203 insets: 0.5 μ m, for blue insets: 0.2 μ m). **(D)** Overlay of on-section correlative EM images
204 immuno-gold labelled for LAMP1¹⁰ and FM images of LAMP1-GFP transfected and α -syn
205 fibril-treated CAD cells (18 h). Insets of three selected regions (indicated by red, purple, and
206 black squares) are presented. Average perimeter (μ m) of lysosomes in control (1.16 ± 0.04) and
207 in α -syn fibril-treated cells: lysosomes without α -syn fibrils (1.16 ± 0.06) and lysosomes with
208 α -syn fibrils (2.24 ± 0.14 ; upper graph) is presented. ns=not significant, ****P<0.0001 by one-
209 way ANOVA followed by Tukey's multiple comparison tests. Average area (μ m²) of
210 lysosomes in control (0.08 ± 0.01) and in α -syn fibril-treated cells: lysosomes without α -syn
211 fibrils (0.08 ± 0.01) and lysosomes with α -syn fibrils (0.16 ± 0.01 ; lower graph) is presented.
212 Mean \pm S.E.M. (50 cells per condition). ns=not significant, ****P<0.0001 by Kruskal-Wallis
213 nonparametric ANOVA test followed by Dunn's multiple comparison tests. Scale bar: 10 μ m
214 (for insets: 0.5 μ m). The data underlying this Figure may be found in S1 Data.

215

216 In spite of these changes in lysosome morphology, the presence of α -syn fibrils had no effect
217 on the abundance of lysosomes. Indeed, the average number of LAMP1-positive lysosomes per
218 cell (control cells: 222 ± 6 ; α -syn fibril-treated cells: 218 ± 7 ; Fig 2A, left panel) and the level
219 of LAMP1 (control: 0.9 ± 0.2 AU; α -syn: 0.7 ± 0.1 AU; Fig 2A, right panel) did not show any
220 significant difference in the presence or absence of α -syn fibrils. Overall, these results indicate
221 that, while the overall amount of lysosomes is not affected by α -syn fibrils, lysosomes
222 containing α -syn exhibit changes in size and morphology.

223 α -Syn fibrils have been shown to impair lysosomal function [67–72]. Thus, next we addressed
224 their effect on lysosomes in our model system. We first assessed the acidity of the lysosomes
225 in cells treated or not with α -syn fibrils by using a fluorogenic acidotropic dye, LysoTracker
226 Deep Red (LysoTracker DR). The fluorescence intensity of LysoTracker DR was significantly
227 decreased (~ 41 %) in α -syn fibril-treated cells compared to untreated control cells (Fig 2B),
228 suggesting alkalization of lysosomes in the presence of α -syn fibrils. Second, we used a DQ-
229 BSA assay in which the fluorescent signal is detected only when the fluorogenic substrate is
230 hydrolyzed by lysosomal proteases. We observed that the DQ-BSA fluorescence intensity was
231 significantly decreased (~ 45 %) in the presence of α -syn fibrils compared to the control (Fig
232 2C), suggesting that the activity of the lysosomal proteases was compromised. Finally, we used
233 a more specific approach to evaluate lysosomal function by quantifying the activity of the
234 lysosomal enzyme Cathepsin B (CathB). The intracellular activity of CathB was detected as
235 fluorescent puncta produced by the hydrolysis of the fluorogenic substrate Magic Red in live
236 cells. We observed a significant decrease (~ 42 %) in CathB enzyme activity in cells challenged
237 with α -syn fibrils compared to control cells (Fig 2D). Since the lysosomal pool was similar in
238 control and α -syn fibril-treated cells, these data indicate that the decrease in the fluorescent
239 signal of LysoTracker DR, DQ-BSA, and Magic Red is likely due to the presence of α -syn
240 fibrils.

241 Altogether, our data indicate that the majority of the α -syn fibrils localize to the lysosomes,
242 where they induce lysosomal enlargement and structural changes, and impair lysosome
243 function.

244

245 **Fig 2. α -Syn fibrils affect the function of lysosomes.** (A) Average number of lysosomes
246 (LAMP1+ puncta) per cell in control (222 ± 6) and in α -syn fibril-treated CAD cells for 18 h
247 (218 ± 7) is presented. Mean \pm S.E.M, $n=5$ (50 cells per condition). ns=not significant by
248 Whitney-Mann *U*- test (left panel). Western blot showing LAMP1 and α -tubulin expression in

249 control and α -syn fibril-treated cells. Integrated Density of LAMP1 protein expression levels
250 normalized to α -tubulin in control (0.9 ± 0.2) and α -syn fibril-treated cells (0.7 ± 0.1) are
251 presented in Arbitrary Units (AU). Mean \pm S.E.M, $n=3$. ns=not significant by paired t -test. **(B)**
252 Representative confocal images of control and Alexa 568-tagged α -syn fibrils challenged CAD
253 cells (18 h), labelled with LysoTracker DR (20 nM for 20 min; LysoTracker DR is pseudo
254 colored in grey). Dashed lines represent the cell contour. Average Integrated Density of control
255 cells ($1.4 \times 10^7 \pm 9 \times 10^5$) and α -syn fibril-treated cells ($8.3 \times 10^6 \pm 5 \times 10^5$) is presented. Mean
256 \pm S.E.M, $n=3$ (40 cells per condition). **** $P < 0.0001$ by Mann-Whitney U -test. Scale bar: 10
257 μ m. **(C)** Representative confocal images of control and Alexa 568-tagged α -syn fibrils (red)
258 challenged CAD cells for 18 h, treated with DQ-BSA (green) for 90 min. Dashed lines represent
259 the cell contour. Average Integrated Density measured for control cells ($3.8 \times 10^6 \pm 1 \times 10^5$)
260 and α -syn fibril-treated cells ($1.7 \times 10^6 \pm 6 \times 10^4$) is presented. Mean \pm S.E.M, $n=3$ (25 cells per
261 condition). **** $P < 0.0001$ by Mann-Whitney U -test. Scale bar: 10 μ m. **(D)** Representative
262 confocal images of control and Alexa 488-tagged α -syn fibrils (green) challenged CAD cells
263 for 18 h treated with 1X Magic Red Cathepsin B (red). Dashed lines represent the cell contour.
264 Average Integrated Density measured for control cells ($1.3 \times 10^6 \pm 6 \times 10^4$) and α -syn fibril-
265 treated cells ($7.5 \times 10^5 \pm 5 \times 10^4$) is presented. Mean \pm S.E.M, $n=5$ (100 cells per condition).
266 **** $P < 0.0001$ by Mann-Whitney U -test. Scale bar: 10 μ m. The data underlying this Figure
267 may be found in S1 Data.

268

269 **Lysosomes containing α -syn fibrils undergo Lysosomal Membrane Permeabilization** 270 **(LMP).**

271 α -Syn [73,74], as well as other amyloidogenic aggregates such as tau [81,82] and amyloid beta
272 [83], induce LMP following their uptake from the culture medium in different cell types. This
273 allows escape of α -syn aggregates from the lysosome to act on the soluble α -syn in the cytosol.
274 However, the fate of these lysosomes has not been assessed. Furthermore, we previously
275 demonstrated that α -syn spread between cells occurs mainly by direct cell-to-cell transfer of
276 lysosomes bearing aggregates through tunneling nanotubes (TNTs), cytoplasmic protrusions
277 extending from the cell periphery and connecting distant cells [21,35,52] (S2 Fig). Therefore,
278 the question arises as to whether LMP also occurs after lysosomes bearing α -syn have been
279 transferred to healthy neighboring cells. To address this question, we assessed first whether α -
280 syn fibrils also induced LMP in our neuronal CAD cells. We used the Galectin-3 (Gal3) puncta

281 assay, based on the localization of Gal3 to damaged lysosomes. CAD cells were transiently
282 transfected with Gal3-GFP and challenged or not with α -syn fibrils for 18 h, prior to labelling
283 for LAMP1 (Figs 3A and S3A number 1). After image acquisition by confocal microscopy, we
284 quantified Gal3-GFP puncta formation in α -syn fibril-treated and non-treated cells. We detected
285 a significantly higher percentage of cells exhibiting Gal3-GFP puncta in the presence of α -syn
286 fibrils ($46 \pm 2\%$) compared to the control condition ($7 \pm 1\%$) (Fig 3B, left graph), in which most
287 cells displayed cytosolic Gal3-GFP [73,74]. However, in cells exhibiting Gal3-GFP puncta,
288 there was no significant difference in the average number of puncta between control and α -syn
289 fibril-treated cells (8 ± 1 and 12 ± 1 respectively; Fig 3B, right graph). In addition, we performed
290 object-based 3D colocalization analysis to evaluate the association of Gal3-GFP with both α -
291 syn fibrils and LAMP1+ lysosomes. We detected $38 \pm 4\%$ of Gal3-GFP puncta colocalizing
292 with α -syn fibrils, $47 \pm 3\%$ of Gal3-GFP puncta colocalizing with LAMP1+ lysosomes, and 35
293 $\pm 3\%$ of Gal3-GFP puncta colocalizing with both α -syn fibrils and lysosomes (Fig 3A, magenta
294 arrowheads, and C). These findings demonstrate that more than one third of Gal3-GFP puncta
295 are recruited to the ruptured lysosomes containing α -syn fibrils. Furthermore, by using SIM,
296 we could clearly observe the recruitment of Gal3-GFP to the damaged lysosomes positive for
297 α -syn fibrils, which appeared to be either inside their lumen (Fig 3D) or at their membrane (Fig
298 3E).

299 Since lysosomes under LMP can be targeted to the autophagy pathway in order to be degraded
300 (a process called lysophagy) [84], next we investigated this possible scenario in CAD cells
301 treated with α -syn fibrils in comparison with control cells. As a positive control we treated CAD
302 cells with L-leucyl-L-leucine methyl ester (LLOMe), which is a well-known inducer of LMP.
303 Cells were then labeled for ubiquitin, LC3, and LAMP1, and colocalization of these markers
304 were analysed. As expected, in CAD cells treated with LLOMe, we could detect good
305 colocalization between LC3, ubiquitin and LAMP1, whereas in control cells we could only
306 detect a few LC3 and ubiquitin puncta and no colocalization between these puncta and
307 lysosomes (S4 Fig). In three independent experiments, we could only detect one lysosome that
308 colocalized with LC3 and ubiquitin in α -syn fibril-treated cells (S4 Fig); thus, lysophagy was
309 an extremely rare event under these conditions and was not statistically different from the
310 control condition.

311

312 **Fig 3. α -Syn fibrils induce LMP.** (A) Representative confocal images of Gal3-GFP transfected
313 control (upper panel) and Alexa 568-tagged α -syn fibril-treated CAD cells for 18 h (lower

314 panel), labelled with LAMP1-Alexa 647 antibody (pseudo colored in grey). Higher
315 magnifications of the selected region in α -syn fibril-treated cells (white squares) are presented
316 on the upper-left part of each image. Arrowheads indicate a lysosome having α -syn fibrils
317 colocalizing with Gal3 puncta. Scale bar: 10 μ m (for insets: 5 μ m). **(B)** % of control ($7 \pm 1\%$)
318 and α -syn fibril-treated CAD cells for 18 h ($46 \pm 2\%$) under LMP (left graph), and average
319 number of Gal3-GFP puncta for control (8 ± 1) and α -syn fibril-treated cells (12 ± 1) under
320 LMP (right graph). Mean \pm S.E.M, $n=3$ (50 cells per condition). **** $P<0.0001$ by Mann-
321 Whitney U-test. **(C)** % of Gal3-GFP puncta colocalizing with α -syn fibrils ($38 \pm 4\%$), with
322 LAMP1 ($47 \pm 3\%$), and with both α -syn fibrils and LAMP1 ($35 \pm 3\%$) calculated by object-
323 based 3D colocalization (Imaris software). Mean \pm S.E.M, $n=3$ (30 cells per condition). **(D)** SR
324 image showing the recruitment of Gal3-GFP to a lysosome containing α -syn fibrils puncta in
325 its lumen. **(E)** SR image showing the recruitment of Gal3-GFP to a lysosome having α -syn
326 fibrils at its membrane. In D and E, insets of two selected regions (white squares) from different
327 Z-planes of the same Gal3-GFP transfected and α -syn fibril-treated CAD cell, labelled for HCS
328 CellMask™ Blue, DAPI, and LAMP1 (pseudo colored in grey) are presented. Images were
329 acquired with SR SIM (Zeiss, LSM 780-Elyra PS.1). Scale bars: 10 μ m (for insets: 1 μ m). The
330 data underlying this Figure may be found in S1 Data.

331

332 **α -Syn fibrils seed *de novo* formation of aggregates at the lysosomes.**

333 LMP has been proposed to be a relevant mechanism for α -syn fibrils to escape from lysosomes
334 and interact with soluble α -syn to induce seeding [19,85]. Therefore, we investigated the
335 seeding activity of exogenous α -syn fibrils in CAD cells. To this aim, CAD cells were
336 transiently transfected with a plasmid encoding α -syn-GFP, a soluble fluorescent reporter of α -
337 syn, and the cells were challenged or not with Alexa 568-tagged α -syn fibrils for 18 h. The
338 formation of α -syn-GFP aggregates detected as green puncta was then quantified (Figs 4A and
339 S3A number 2). We found that $76 \pm 5\%$ of cells treated with α -syn fibrils produced newly
340 formed α -syn-GFP aggregates, whereas this percentage was significantly lower ($13 \pm 2\%$) in
341 control cells transfected with α -syn-GFP only (Fig 4B, left graph). In addition, the average
342 number of newly formed α -syn-GFP puncta detected in the cells treated with the fibrils ($27 \pm$
343 3) was significantly higher than the α -syn-GFP puncta detected in the control condition ($12 \pm$
344 1 ; Fig 4B, right graph), suggesting that the exogenous α -syn fibrils induce efficient seeding of
345 the soluble protein. These data were in line with previous findings [86–89]; however, the

346 question remains as to whether lysosomes participate to this seeding event and how/where in
347 the cell it occurs. To investigate whether seeding is associated with the lysosomes, we
348 performed super-resolution microscopy in CAD cells transfected with α -syn-GFP, loaded with
349 α -syn fibrils and labelled for LAMP1. We observed three different scenarios: i) lysosomes with
350 both α -syn fibrils and α -syn-GFP aggregates colocalizing at the lysosomal membrane (Fig 4C),
351 ii) lysosomes with α -syn fibrils and α -syn-GFP aggregates colocalizing inside their lumen (Fig
352 4D), and iii) lysosomes containing both α -syn fibrils and α -syn-GFP aggregates inside their
353 lumen, but not necessarily co-localizing (Fig 4E). In addition, we performed object-based 3D
354 colocalization analysis between newly formed α -syn aggregates (α -syn-GFP puncta), α -syn
355 fibrils and lysosomes. We observed that 69 ± 6 % of the newly formed aggregates colocalized
356 with LAMP1+ lysosomes, 74 ± 7 % colocalized with α -syn fibrils, and 63 ± 6 % of them were
357 positive for both α -syn fibrils and LAMP1+ organelles (Fig 4F), indicating that in CAD cells
358 the majority of the seeding takes place at lysosomal compartments following α -syn fibrils
359 uptake.

360 To understand whether the localization of α -syn-GFP aggregates to lysosomes was consistent
361 with the beginning of the seeding event and not a post seeding delivery of newly formed fibrils,
362 we monitored the occurrence of seeding by live imaging microscopy. We first transfected CAD
363 cells with soluble α -syn-GFP and then immediately after the addition of α -syn fibrils we started
364 to monitor the seeding event by detecting the formation of green puncta (α -syn-GFP newly
365 formed aggregates) in these cells compared to control cells by live spinning-disk microscopy.
366 We found that the seeding first became apparent about 2 h from the addition of the α -syn fibrils
367 and increased with time (S1 Movie and S5A Fig). We did not observe any newly formed α -syn-
368 GFP puncta in untreated control cells (S2 Movie and S5B Fig). Next, we performed super-
369 resolution microscopy in order to investigate whether these newly formed aggregates were
370 associated with the lysosomes by immunolabelling LAMP1 at different time points (1h, 2h, and
371 4h). Interestingly, at all these time points (even in the rare events found at 1 hour), we found
372 that newly formed aggregates colocalized with α -syn fibrils and LAMP1 (Fig 4G-I). Therefore,
373 newly formed α -syn-GFP aggregates following α -syn fibrils addition are associated with
374 lysosomes at the very beginning of the seeding event, supporting our hypothesis that lysosomes
375 function as hubs for the seeding of newly formed α -syn aggregates.

376 Overall, these results indicate that exogenous α -syn fibrils induce *de novo* aggregation of
377 soluble α -syn in association with lysosomes.

378

379 **Fig 4. α -Syn fibrils seed *de novo* formation of aggregates associated with lysosomes. (A)**
380 Representative confocal images of α -syn-GFP transfected control or Alexa 568-tagged α -syn
381 fibril-treated CAD cells (18 h). Scale bar: 10 μ m (for insets: 5 μ m). **(B)** % of control ($13 \pm 2\%$)
382 and α -syn fibril-treated CAD cells for 18 h ($76 \pm 5\%$) that formed α -syn-GFP aggregates (left
383 graph). Mean \pm S.E.M, $n=3$ (45 cells per condition). **** $P < 0.0001$ by two tailed t -test. Average
384 number of α -syn-GFP puncta per cell in control (12 ± 1) and α -syn fibril-treated cells (27 ± 3)
385 (right graph). Mean \pm S.E.M, $n=3$ (45 cells per condition). ** $P = 0.005$ by Mann-Whitney U -
386 test. **(C)** SR image showing α -syn fibrils puncta and α -syn-GFP+ aggregate colocalizing on the
387 lysosomal membrane in CAD cells treated with α -syn fibrils for 18 h. **(D)** SR image showing
388 colocalization between α -syn fibrils puncta and α -syn-GFP+ aggregate inside the lysosomal
389 lumen, and α -syn fibrils on the lysosomal membrane in CAD cells treated with α -syn fibrils for
390 18 h. **(E)** SR image showing α -syn fibrils puncta and α -syn-GFP+ aggregate inside the
391 lysosomal lumen in CAD cells treated with α -syn fibrils for 18 h. **(F)** Object-based 3D
392 colocalization analysis (Imaris software) between α -syn-GFP aggregates and α -syn fibrils (74
393 $\pm 7\%$), α -syn-GFP aggregates and LAMP1+ lysosomes ($69 \pm 6\%$), and α -syn-GFP aggregates
394 with both α -syn fibrils and LAMP1+ lysosomes ($63 \pm 6\%$). Mean \pm S.E.M, $n=2$ (16 super-
395 resolution images, ~ 2000 lysosomes were analysed). **(G)** SR image showing α -syn fibrils
396 puncta and α -syn-GFP+ aggregate colocalizing with LAMP1 on the lysosomal membrane in
397 CAD cells treated with α -syn fibrils for 1 h. **(H)** SR image demonstrating α -syn fibrils puncta
398 and α -syn-GFP+ aggregate colocalizing with LAMP1 both on the lysosomal membrane and
399 inside the lysosomal lumen in CAD cells treated with α -syn fibrils for 2 h. **(I)** SR image showing
400 α -syn fibrils puncta and α -syn-GFP+ aggregate colocalizing with LAMP1 on the lysosomal
401 membrane in CAD cells treated with α -syn fibrils for 4 h. In C, D, E, G, H, I insets of selected
402 regions (white squares) from different α -syn-GFP transfected and α -syn fibril-treated CAD
403 cells, labelled for DAPI and LAMP1 (pseudo colored in grey) are presented. Images were
404 acquired with a spinning-disk microscope with SR module. Scale bars: 10 μ m (for insets: 1 μ m;
405 0.5 μ m for inset in G). The data underlying this Figure may be found in S1 Data.

406

407 **α -Syn-loaded lysosomes localize to the cell periphery and are less functional.**

408 The results presented above highlight the role of lysosomes in the propagation of α -syn
409 misfolding after uptake of the fibrils from the culture medium. However, they do not address i)
410 how propagation of misfolding occurs following the transfer of lysosomes containing α -syn
411 aggregates to healthy neighboring cells [19,21], and ii) whether/how lysosome damage induced

412 by α -syn aggregates favors the spread of pathology [19,32]. Lysosomes are dynamic organelles
413 that move bidirectionally between the perinuclear and peripheral regions of the cell [90–92].
414 As our results indicate that the α -syn fibrils interfere with lysosome morphology and function,
415 we hypothesized that they could also have an impact on lysosome positioning. Therefore, we
416 evaluated the distribution of lysosomes in CAD cells challenged with α -syn fibrils compared to
417 control cells. Cells were labelled for LAMP1, HCS CellMaskTM Blue (cell outline stain), and
418 DAPI (nuclear stain), and the number of lysosomes in the perinuclear and peripheral regions in
419 each condition was quantified (see Materials and Methods; Fig 5A). In agreement with previous
420 findings that lysosomes are mainly located in the perinuclear region in healthy non-polarized
421 cells [93], we detected $57 \pm 1\%$ of the lysosomes at the perinuclear region in control CAD cells
422 (Fig 5A, white arrows, and B). In contrast, in cells treated with α -syn fibrils, the situation was
423 reversed, with the majority of lysosomes ($56 \pm 1\%$) found in the peripheral region (Fig 5A,
424 green, red, yellow arrows, and B).

425 Since our results indicate that α -syn fibrils affect lysosomal pH and function (Fig 2B-D), to
426 understand whether there is a correlation between lysosome distribution and function, we next
427 evaluated the distribution of lysosomes containing α -syn fibrils and quantified the perinuclear
428 and peripheral distribution of only functional lysosomes positive for LysoTracker DR and
429 Magic Red CathB. We found that α -syn fibril-containing LysoTracker DR positive and Magic
430 Red CathB positive lysosomes were more perinuclear ($54 \pm 2\%$ and $56 \pm 1\%$, respectively; Fig
431 5C), suggesting that peripheral lysosomes containing α -syn fibrils are less functional.

432 These results thus show that α -syn fibrils promote redistribution of lysosomes towards the cell
433 periphery. Furthermore, this pool of peripheral lysosomes is less acidic and has less degradative
434 capacity.

435

436 **Peripheral α -syn-loaded lysosomes are preferentially transferred to neighboring cells.**

437 Our next question was to understand whether the effect of α -syn on lysosome positioning could
438 be relevant for the propagation of the pathology and in which way. Peripheral lysosomes could
439 be more prone to exocytosis and therefore could increase the secretion of α -syn fibrils to the
440 extracellular environment. Alternatively, peripheral lysosomes could be more apt for transfer
441 to healthy neighboring cells through TNTs. To distinguish between these alternative scenarios,
442 we first examined lysosomal exocytosis by comparing the amount of CathB released into the
443 culture medium of control and α -syn fibril-treated CAD cells using an ELISA method. These
444 experiments showed no significant difference in the amount of CathB released by control (70

445 ± 1 ng/mL) and α -syn fibril-treated cells (75 ± 7 ng/mL; Fig 5D). As an alternative approach,
446 we measured the integrated fluorescence density of LAMP1 at the plasma membrane (PM) in
447 cells treated or not treated with α -syn fibrils. To this end, we used an antibody recognizing a
448 luminal epitope of LAMP1, which is displayed to the extracellular milieu after fusion of
449 lysosomes with the PM in non-permeabilized cells (Fig 5E). We did not observe a difference
450 in the average integrated density of PM-associated LAMP1 between control ($9 \times 10^4 \pm 2 \times 10^4$
451 AU) and α -syn fibril-treated cells ($9 \times 10^4 \pm 3 \times 10^4$ AU; Fig 5E, graph). These results indicate
452 that, despite their different distributions, lysosomes are exocytosed at a similar rate in α -syn
453 fibril-treated and control cells.

454 Next, to understand whether the peripheral positioning of lysosomes could affect their transfer
455 to neighboring cells, we compared the efficiency of lysosome transfer by using a co-culture
456 assay where donor cells were transiently transfected with LAMP1-GFP and either treated or
457 not with α -syn fibrils for 18 h (α -syn co-culture and control co-culture, respectively), and
458 acceptor cells were transiently transfected with H2B-mCherry (Figs 5F and S3B). We observed
459 that the percentage of acceptor cells that received LAMP1-GFP puncta (lysosomes) from donor
460 cells was significantly higher in the α -syn co-culture compared to the control co-culture ($29 \pm$
461 3% and $18 \pm 2\%$, respectively) (Fig 5G, left graph). Lysosome transfer through secretion was
462 evaluated by a “secretion test” (S3I Fig) whereby acceptor cells treated with the conditioned
463 medium of control or α -syn fibril-loaded donor cells were quantified for the presence of
464 LAMP1-GFP puncta. We did not observe a significant difference between the two secretion
465 tests ($9 \pm 2\%$ and $7 \pm 1\%$ in control and α -syn secretion, respectively; Fig 5G, left graph). In
466 addition, we did not observe any difference in the average number of LAMP1-GFP puncta
467 detected per acceptor cell either in the co-culture conditions (2 ± 0.2 for both co-culture
468 conditions) or in the secretion test conditions (1 ± 0.1 for both secretion conditions; Fig 5G,
469 right graph). These results confirm our previous data that lysosome transfer from donor to
470 acceptor cells is predominantly mediated by cell-to-cell contact, likely through TNTs rather
471 than secretion [19,21,22]. Importantly, we showed that donor cells challenged with α -syn fibrils
472 transfer lysosomes more efficiently to the acceptor cells compared to control donor cells.
473 Moreover, we performed object-based 2D colocalization analysis in the acceptor cells that
474 received both LAMP1-GFP+ lysosomes and α -syn fibrils in order to evaluate the number of
475 lysosomes containing α -syn fibrils transferred to the acceptor cells. We found $51 \pm 6\%$ of α -
476 syn fibrils colocalizing with LAMP1-GFP+ lysosomes and $51 \pm 6\%$ of lysosomes colocalizing

477 with α -syn fibrils, suggesting that half of the lysosomes transferred from donor to acceptor cells
478 carried α -syn fibrils (Fig 5H).

479 Taken together, our data indicate that lysosomes that are more peripherally located in the
480 presence of α -syn fibrils are not secreted more compared to control cells, but instead are more
481 efficiently transferred to acceptor cells by cell-to-cell contact.

482

483 **Fig 5. α -Syn-loaded lysosomes localize to the cell periphery, are less functional, and are**

484 **preferentially transferred to neighboring cells. (A)** Representative confocal images of

485 control and Alexa 568-tagged α -syn fibril-treated CAD cells (18 h) labelled for LAMP1-Alexa

486 488 antibody, HCS CellMaskTM Blue, and DAPI. White arrows indicate the perinuclear

487 lysosome clusters in control cells; green, red, and yellow arrows indicate peripheral lysosomes,

488 α -syn fibrils, and lysosomes colocalizing with α -syn fibrils, respectively. Scale bar: 10 μ m. **(B)**

489 % of LAMP1+ lysosomes in perinuclear (purple dots) and peripheral regions (black dots) of

490 the control cells and cells challenged with α -syn fibrils is presented. In control cells: % of

491 perinuclear lysosomes: $57 \pm 1\%$, and peripheral lysosomes: $43 \pm 1\%$; in α -syn fibril-treated

492 cells: % of perinuclear lysosomes: $44 \pm 1\%$, and peripheral lysosomes: $56 \pm 1\%$. Mean \pm S.E.M,

493 $n=5$ (40 cells per condition). ns=not significant, **** $P<0.0001$ by one-way ANOVA followed

494 by Tukey's multiple comparison tests. **(C)** Graph representing the distribution of LysoTracker

495 DR+ and Magic Red CathB+ lysosomes colocalizing with the α -syn fibrils in perinuclear

496 (purple dots) and peripheral region (black dots). % of LysoTracker DR+ lysosomes colocalizing

497 with α -syn fibrils in perinuclear region: $54 \pm 2\%$, and in peripheral region: $46 \pm 2\%$. % of Magic

498 Red CathB+ lysosomes colocalizing with α -syn fibrils in perinuclear region: $56 \pm 1\%$, and in

499 peripheral region: $44 \pm 1\%$. Mean \pm S.E.M, $n=4$ (40 cells per condition). ns=not significant by

500 one-way ANOVA followed by Tukey's multiple comparison tests. **(D)** Quantity of secreted

501 CathB (ELISA) in the media of control (70 ± 1 ng/mL) and α -syn fibril-treated CAD cells (75

502 ± 7 ng/mL). Mean \pm S.E.M, $n=3$. ns=not significant by Mann-Whitney U -test. **(E)**

503 Representative confocal images of control and Alexa 568-tagged α -syn fibril-treated CAD cells

504 for 18 h, immuno-labelled for LAMP1-Alexa 488 antibody in non-permeabilized conditions.

505 Scale bar: 10 μ m. Average Integrated Density of LAMP1 immunofluorescence at the cell

506 surface in control ($9 \times 10^4 \pm 2 \times 10^4$) and in α -syn fibril-treated cells ($9 \times 10^4 \pm 3 \times 10^4$) is presented.

507 Mean \pm S.E.M, $n=3$ (20 cells per condition). ns=not significant by paired t -test. Scale bar: 10

508 μ m. **(F)** Representative confocal images of donor and acceptor cells after 24 h of co-culture.

509 Donor cells were transfected with LAMP1-GFP and treated with Alexa 568-tagged α -syn fibrils

510 or not (referred to as “ α -syn co-culture” and “control co-culture”, respectively). Acceptor cells
511 were transfected with H2B-mCherry. Scale bar: 20 μ m. **(G)** % of acceptor cells that received
512 LAMP1+ puncta (lysosomes) from donor cells in control co-culture ($18 \pm 2\%$), in α -syn co-
513 culture ($29 \pm 3\%$), in control secretion test ($9 \pm 2\%$), and in α -syn secretion test ($7 \pm 1\%$) (left
514 graph). Mean \pm S.E.M, $n=4$ (150 acceptor cells per condition). ns=not significant, *** $P=0.0004$
515 by one-way ANOVA followed by Tukey’s multiple comparison tests. The average number of
516 LAMP1-GFP+ puncta detected per acceptor cell in control co-culture (2 ± 0.2), in α -syn co-
517 culture (2 ± 0.2), in control secretion (1 ± 0.1), and in α -syn secretion (1 ± 0.1) is presented
518 (right graph). Mean \pm S.E.M, $n=4$ (150 acceptor cells per condition). ns=not significant,
519 *** $P=0.0004$ by Kruskal-Wallis nonparametric ANOVA test followed by Dunn’s multiple
520 comparison tests. **(H)** % of α -syn fibril puncta colocalizing with LAMP1-GFP+ puncta ($51 \pm$
521 6%) and % of LAMP1-GFP+ puncta colocalizing with α -syn fibrils puncta ($51 \pm 6\%$) is
522 presented. Mean \pm S.E.M, $n=4$ (20 acceptor cells that received both α -syn fibrils and LAMP1-
523 GFP puncta were analysed). The data underlying this Figure may be found in S1 Data.

524

525 **TFEB as a player in lysosome redistribution upon α -syn loading.**

526 The Transcription Factor EB (TFEB) regulates lysosome biogenesis and function by
527 coordinating the expression of lysosomal components [94]. Furthermore, TFEB has also been
528 shown to influence lysosome positioning [95–97]. To investigate a possible role of TFEB in
529 the peripheral redistribution of lysosomes upon α -syn loading, we first asked whether the
530 lysosomal loading of α -syn fibrils triggers TFEB nuclear translocation. To address this
531 question, we expressed TFEB-WT-GFP in CAD cells challenged or not with α -syn fibrils for
532 18 h (S3A Fig number 3). We found a significant increase in the percentage of CAD cells
533 having nuclear TFEB upon α -syn loading compared to control cells (control: $18 \pm 4\%$; α -syn:
534 $57 \pm 6\%$, Fig 6A).

535 Next, we assessed the effect of TFEB overexpression on lysosome distribution in CAD cells.
536 We transiently transfected CAD cells with plasmids encoding wild-type TFEB (TFEB-WT-
537 GFP) or constitutively active mutant TFEB (TFEB-mut-GFP) (i.e., nuclear TFEB), or with
538 empty plasmid CMV-GFP (control), and quantified the number of lysosomes in the perinuclear
539 and peripheral regions. We found that cells overexpressing the constitutively active form of
540 TFEB showed more peripheral lysosomes compared to both control cells and cells
541 overexpressing TFEB-WT-GFP (TFEB-mut-GFP: $59 \pm 1\%$; TFEB-WT-GFP: $54 \pm 2\%$; CMV-

542 GFP: $52 \pm 1\%$; Fig 6B). These results indicate that TFEB promotes the peripheral distribution
543 of lysosomes in CAD cells.

544 To determine whether TFEB participates in peripheral redistribution of lysosomes upon α -syn
545 loading, we silenced the expression of TFEB in CAD cells by RNA interference (Fig 6C). CAD
546 cells transfected with scrambled siRNA (control) or siTFEB were challenged with α -syn fibrils
547 for 18 h. Then, we quantified the positioning of lysosomes containing α -syn fibrils (Fig 6D).
548 As expected, control cells showed more peripheral α -syn-loaded lysosomes ($52.1 \pm 1\%$). In
549 contrast, in siTFEB-treated CAD cells α -syn-loaded lysosomes were slightly but significantly
550 more perinuclear ($50.7 \pm 1\%$). These findings indicate that silencing of endogenous TFEB
551 reduced the peripheral redistribution of lysosomes upon α -syn loading, suggesting the
552 involvement of TFEB in this event.

553

554 **Fig 6. The role of TFEB in lysosome redistribution upon α -syn loading.** (A) % of cells
555 overexpressing TFEB-WT-GFP having nuclear TFEB in control CAD cells ($18 \pm 4\%$) and α -
556 syn fibril-treated CAD cells for 18 h ($57 \pm 6\%$). Mean \pm S.E.M, $n=3$ (50 cells per condition).
557 **** $P<0.0001$ by Unpaired t test. (B) % of LAMP1+ lysosome distribution in perinuclear
558 (purple dots) and peripheral regions (black dots) of cells overexpressing CMV-GFP (control),
559 TFEB-WT-GFP, or TFEB-mut-GFP. In control CMV-GFP cells: % of perinuclear lysosomes:
560 $48 \pm 1\%$, and peripheral lysosomes: $52 \pm 1\%$; in TFEB-WT-GFP cells: % of perinuclear
561 lysosomes: $46 \pm 2\%$, and peripheral lysosomes: $54 \pm 2\%$; in TFEB-mut-GFP cells: % of
562 perinuclear lysosomes: $41 \pm 1\%$, and peripheral lysosomes: $59 \pm 1\%$. Mean \pm S.E.M, $n=3$ (30
563 cells per condition). *** $P<0.001$ by one-way ANOVA followed by Tukey's multiple
564 comparison tests. (C) Western blot prepared from cell extracts collected from control,
565 scrambled siRNA (sicontrol)-, and siTFEB-pretreated CAD cells for 60 h, showing TFEB and
566 GAPDH (loading control) expression. (D) Graph representing the distribution of lysosomes
567 containing α -syn fibrils in perinuclear (purple dots) and peripheral region (black dots) of α -syn
568 fibril-treated sicontrol and siTFEB cells. % of lysosomes containing α -syn fibrils of sicontrol
569 cells in perinuclear region: $49 \pm 1\%$, and in peripheral region: $52 \pm 1\%$. % of lysosomes
570 containing α -syn fibrils of siTFEB cells in perinuclear region: $51 \pm 1\%$, and in peripheral
571 region: $49 \pm 1\%$. Mean \pm S.E.M, $n=4$ (30 cells per condition). ns=not significant, * $P=0.0288$
572 by one-way ANOVA followed by Tukey's multiple comparison tests. The data underlying this
573 Figure may be found in S1 Data.

574

575 **Lysosome positioning affects the efficiency of α -syn fibrils' transfer.**

576 To further investigate the effect of lysosome positioning on α -syn fibrils transfer, we set-up
577 different co-culture assays where we monitored the amount of α -syn transfer using donor cells
578 with more peripheral or more perinuclear lysosomes. To this end, we respectively
579 overexpressed or silenced the Arf-like small GTPase Arl8b, which controls the movement of
580 lysosomes towards the cell periphery [98,99]. To examine the effect of peripheral lysosome
581 redistribution, Arl8b-GFP transfected or control donor CAD cells were loaded with α -syn fibrils
582 and co-cultured with acceptor CAD cells transiently transfected with H2B-GFP to distinguish
583 them from the donors (referred to as Arl8b-GFP co-culture and control co-culture, respectively;
584 Figs 7A and S3C). We then quantified the presence of α -syn fibrils in the acceptor cells in each
585 co-culture condition. We detected a significant increase in the percentage of acceptor cells that
586 received α -syn fibrils in the Arl8b-GFP co-culture ($65 \pm 4\%$) compared to control co-culture
587 ($49 \pm 4\%$; Fig 7B, left graph). As a control, we monitored the transfer of α -syn fibrils through
588 the culture supernatant, thus checking a possible effect on transfer through a secretion
589 mechanism. As previously found [19], the amount of α -syn transfer by secretion was very low
590 compared with the transfer in co-culture, and did not significantly change in the two co-culture
591 conditions ($8 \pm 2\%$ and $10 \pm 2\%$, in control and Arl8b-GFP secretion conditions, respectively;
592 Fig 7B, left graph). Despite changes in the percentage of cells that took up α -syn fibrils in co-
593 cultures, we did not find a significant difference in the average number of α -syn puncta per
594 acceptor cell in any of these conditions (in average: 3 ± 0.4 , 3.4 ± 0.4 , 1.3 ± 0.4 , 2 ± 0.3 α -syn
595 fibrils puncta per acceptor cell in control co-culture, Arl8b-GFP co-culture, control secretion,
596 and Arl8b-GFP secretion, respectively; Fig 7B, right graph).

597 To corroborate these observations in a different cell type, we performed the same experiment
598 in HeLa cells (Figs S3D and S6) in which the effect of Arl8b on lysosome positioning was
599 extensively characterized [90,91]. We observed that the percentage of acceptor cells that
600 received α -syn fibrils was $28 \pm 3\%$ and $60 \pm 5\%$ in control and Arl8b-GFP co-cultures,
601 respectively (S6A and B Fig, left graph). Again, we did not observe any significant increase in
602 the transfer of α -syn fibrils through secretion from the donors overexpressing Arl8b-GFP in
603 comparison to control donors ($8 \pm 3\%$ and $1 \pm 1\%$ respectively; S6B Fig, left graph). As in
604 CAD cells, the average number of α -syn puncta per acceptor cell was not significantly different
605 in HeLa co-cultures and secretion conditions (3 ± 1 and 5 ± 1 in control and Arl8b-GFP co-
606 cultures, respectively; 1 ± 0.0 and 2 ± 0.2 in control and Arl8b-GFP secretion tests, respectively;
607 S6B Fig, right graph).

608 Furthermore, we silenced the expression of Arl8b in CAD cells by RNA interference (Fig 7C).
609 Briefly, we pretreated donor cells with siRNA targeting Arl8b (siArl8b) and scrambled siRNA
610 (sicontrol) for 60 h prior to loading with α -syn fibrils for 18 h; in parallel, untreated control
611 cells were challenged with α -syn fibrils. These donors were then co-cultured with acceptor cells
612 transiently transfected with H2B-GFP (Figs 7D and S3E). In control co-culture and in siicontrol
613 co-culture, the percentage of acceptor cells that received α -syn fibrils was $55 \pm 4\%$ and $60 \pm$
614 3% , respectively, whereas in siArl8b co-culture we observed a significant lower percentage of
615 $28 \pm 3\%$ (Fig 7E, left graph). We did not detect any significant difference in α -syn transfer
616 through secretion ($6 \pm 1\%$, $9 \pm 1\%$, and $6 \pm 1\%$ in control, siicontrol, and siArl8b secretion
617 conditions, respectively; Fig 7E, left graph). The average number of α -syn puncta detected in
618 acceptor cells in co-cultures and secretion conditions was not significantly changed (1-2 puncta
619 per cell in all the conditions; Fig 7E, right graph).

620 To further test the importance of lysosome positioning in α -syn fibrils transfer, we performed
621 similar experiments in HeLa cells with knock out (KO) of components of the lysosome-
622 positioning machinery. These components included the myrlysin (also known as BORCS5)
623 subunit of BORC, which promotes recruitment of Arl8b to membranes [100], and the kinesins
624 KIF1B and KIF5B [101–105], which drive lysosome movement towards the cell periphery [90].
625 KO of these proteins impairs lysosome movement towards the cell periphery [90,100]. These
626 KO donor cells, in parallel to control donors (WT HeLa) were loaded with α -syn fibrils and co-
627 cultured with WT HeLa cells expressing H2B-GFP (Figs S3F and S6C). Acceptor cells were
628 then analysed for the presence of α -syn fibrils. The percentage of acceptor cells that received
629 α -syn fibrils in control co-culture was $29 \pm 2\%$, whereas in myrlysin-KO and KIF1B-KIF5B-
630 double-KO (KIF1B-5B dKO) co-cultures this percentage was significantly decreased to $16 \pm$
631 2% and $12 \pm 2\%$, respectively (S6D Fig, left graph). α -Syn fibrils' transfer through secretion
632 was similar in all the conditions ($5 \pm 2\%$, $6 \pm 1\%$, $6 \pm 1\%$ in control, myrlysin-KO, and KIF1B-
633 5B dKO secretion conditions, respectively; S6D Fig, left graph). We did not observe a
634 significant difference in the average number of transferred α -syn puncta in any of the co-
635 cultures/secretion conditions (1-2 puncta per cell in all the conditions; S6D Fig, right graph).
636 Overall, these data indicate that the contact-dependent transfer of α -syn is affected by the
637 position of lysosomes, with more transfer when lysosomes are peripheral and less transfer when
638 lysosomes are perinuclear.

639 As we have shown that lysosomes containing α -syn are transferred from acceptor cells inside
640 TNTs [52] (S2 Fig), we wondered whether TNT formation was affected by the manipulations

641 that alter lysosome positioning. Thus, we performed two sets of TNT counting experiments in
642 control, Arl8b-GFP-overexpressing or siArl8b/sicontrol-treated CAD cells in the presence or
643 absence of α -syn fibrils. These cells were labelled with WGA and the percentage of TNT-
644 connected cells was quantified for each condition (see Materials and Methods). We did not
645 observe a significant difference in the percentage of TNT-connected cells between control (45
646 $\pm 3\%$) and Arl8b-GFP-overexpressing cells ($46 \pm 2\%$; Fig 7F, left graph). However, in the
647 presence of α -syn fibrils the percentage of TNT-connected cells was significantly increased to
648 $60 \pm 5\%$ in control and $64 \pm 5\%$ in Arl8b-GFP-overexpressing cells (Fig 7F, left graph).
649 Similarly, the percentage of TNT-connected cells remained unchanged between control ($44 \pm$
650 4%), sicontrol ($45 \pm 4\%$), and siArl8b ($43 \pm 4\%$) pretreated cells, whereas in the presence of α -
651 syn fibrils the percentage of TNT-connected cells significantly increased to $62 \pm 4\%$ in control,
652 $62 \pm 5\%$ in sicontrol, and $66 \pm 3\%$ in siArl8b-treated cells (Fig 7F, right graph). These data
653 indicate that lysosome positioning has no effect on TNT formation per se, but it is the presence
654 of α -syn fibrils that increases the number of TNT-connected cells, in line with previous findings
655 [19].

656 Taken together, these results indicate that lysosome positioning affects the efficiency of α -syn
657 fibrils' transfer. Moreover, α -syn fibrils increase the number of TNT-connected cells
658 independent of lysosome positioning.

659

660 **Fig 7. Lysosome positioning affects the efficiency of α -syn fibrils' transfer. (A)**

661 Representative confocal images of donor and acceptor cells after 24 h of co-culture. Donor cells
662 were either loaded with Alexa 568-tagged α -syn fibrils only (control co-culture) or transfected
663 with Arl8b-GFP prior to be treated with α -syn fibrils (Arl8b-GFP co-culture). Acceptor cells
664 were transfected with H2B-GFP. Co-cultures were labelled with HCS CellMask™ Blue and
665 DAPI. Arrows indicate the α -syn fibrils received by acceptor cells and asterisks indicate the
666 cells having α -syn fibrils in each co-culture condition. Scale bar: 10 μ m. **(B)** % of acceptor cells
667 received α -syn fibrils in control co-culture ($49 \pm 4\%$), in Arl8b-GFP co-culture ($65 \pm 4\%$), in
668 control secretion ($8 \pm 2\%$), and in Arl8b-GFP secretion ($10 \pm 2\%$) (left graph). Mean \pm S.E.M,
669 $n=3$ (90 acceptor cells per condition). ns=not significant, ** $P=0.0038$ by Kruskal-Wallis
670 nonparametric ANOVA test followed by Dunn's multiple comparison tests. Average number
671 of α -syn fibrils puncta in control co-culture (3 ± 0.4), in Arl8b-GFP co-culture (3.4 ± 0.4), in
672 control secretion (1.3 ± 0.4), and in Arl8b-GFP secretion (2 ± 0.3) (right graph). Mean \pm S.E.M,
673 $n=3$ (90 acceptor cells per condition). ns=not significant, by one-way ANOVA followed by

674 Tukey's multiple comparison tests. **(C)** Western blot prepared from cell extracts collected from
675 control, scrambled siRNA (sicontrol)-, and siArl8b-pretreated CAD cells for 60 h, showing
676 Arl8b and α -tubulin (loading control) expression. Integrated Density of Arl8b protein
677 expression levels normalized to α -tubulin in control (0.80 ± 0.03), sicontrol- (0.82 ± 0.02), and
678 siArl8b-pretreated cells (0.19 ± 0.09) are presented in Arbitrary Units (AU). Mean \pm S.E.M,
679 $n=3$. ns= not significant, *** $P=0.0004$ by one-way ANOVA followed by Tukey's multiple
680 comparison tests. **(D)** Representative confocal images of donor and acceptor cells after 24 h of
681 co-culture. Donor CAD cells were pretreated with sicontrol or siArl8b for 60 h or left untreated
682 prior to be challenged with Alexa 568-tagged α -syn fibrils (referred to as control, sicontrol, and
683 siArl8b co-cultures, respectively). Acceptor cells were transfected with H2B-GFP. Co-cultures
684 were labelled with HCS CellMaskTM Blue and DAPI. Arrows indicate the α -syn fibrils received
685 by acceptor cells and asterisks indicate the cells having α -syn fibrils in each co-culture
686 condition. Scale bar: 10 μ m. **(E)** % of acceptor cells that received α -syn fibrils in control co-
687 culture ($55 \pm 4\%$), sicontrol co-culture ($60 \pm 3\%$), siArl8b co-culture ($28 \pm 3\%$), control
688 secretion ($6 \pm 1\%$), sicontrol secretion ($9 \pm 1\%$), and siArl8b secretion ($6 \pm 1\%$) (left graph).
689 Mean \pm S.E.M, $n=4$ (80 acceptor cells per condition). ns= not significant, **** $P<0.0001$ by
690 one-way ANOVA followed by Tukey's multiple comparison tests. Average number of α -syn
691 puncta per acceptor cell in control co-culture (2 ± 0.2), sicontrol co-culture (2 ± 0.1), siArl8b
692 co-culture (2 ± 0.3), control secretion (1 ± 0.2), sicontrol secretion (2 ± 0.2), and siArl8b
693 secretion (2 ± 0.3) (right graph). Mean \pm S.E.M, $n=4$ (80 acceptor cells per condition). ns= not
694 significant by Kruskal-Wallis nonparametric ANOVA test followed by Dunn's multiple
695 comparison tests. **(F)** Control, Arl8b-GFP transfected, and sicontrol- or siArl8b-pretreated
696 CAD cells for 60 h were challenged or not with α -syn fibrils (18 h) and labelled with WGA for
697 TNT counting experiments. % of TNT-connected cells in control ($45 \pm 3\%$), Arl8b-GFP ($46 \pm$
698 2%), control- α -syn ($60 \pm 5\%$), and Arl8b-GFP- α -syn ($64 \pm 5\%$) conditions. Mean \pm S.E.M, $n=4$
699 (115 cells per condition). ns= not significant (left graph). % of TNT-connected cells in control
700 ($44 \pm 4\%$), sicontrol ($45 \pm 4\%$), siArl8b ($43 \pm 4\%$), control- α -syn ($62 \pm 4\%$), sicontrol- α -syn
701 ($62 \pm 5\%$), and siArl8b- α -syn ($66 \pm 3\%$) is presented (right graph). Mean \pm S.E.M, $n=3$ (90
702 cells per condition). ns= not significant, * $P<0.05$, ** $P<0.01$ by one-way ANOVA followed by
703 Tukey's multiple comparison tests. The data underlying this Figure may be found in S1 Data.

704

705 **α -Syn fibrils induce LMP upon arrival in the acceptor cells.**

706 Our data show that more than 50% of α -syn fibrils in acceptor cells colocalize with LAMP1,
707 indicating that they are still associated with lysosomes after the transfer (Fig 5H). Moreover,
708 we have previously reported that α -syn fibrils can induce seeding of soluble α -syn once they
709 are transferred to acceptor cells [19]. Based on the results presented here one possible
710 explanation for this observation would be that α -syn fibrils also trigger LMP in acceptor cells
711 following their transfer, similar to what we have observed in donor cells (Fig 3A and B). To
712 assess this hypothesis, we performed co-culture experiments where donor cells were either
713 transiently transfected with H2B-mCherry (control co-culture) or treated with α -syn fibrils for
714 18 h (α -syn co-culture), and co-cultured with acceptor cells transiently transfected with Gal3-
715 GFP (Figs 8A and S3G number 1). Acceptor cells were then evaluated for the presence of Gal3-
716 GFP puncta. The percentage of acceptor cells exhibiting LMP (Fig 8A, white arrows) was
717 significantly higher in the α -syn co-culture ($33 \pm 5\%$) compared to control co-culture ($6 \pm 2\%$)
718 (Fig 8B, upper graph). We also quantified the average number of Gal3-GFP puncta per acceptor
719 cell and we found a significant increase in α -syn co-culture (14 ± 1) compared to control co-
720 culture where some LMP occurs spontaneously (8 ± 1 ; Fig 8B, lower graph). We also performed
721 super-resolution microscopy in α -syn co-culture labelled for lysosomes with antibody to
722 LAMP1 and observed Gal3-GFP and α -syn fibrils puncta both in close proximity inside the
723 lysosomal lumen (Fig 8C) and colocalizing on the lysosomal membrane (Fig 8D). These results
724 thus show that, following their transfer, α -syn-containing lysosomes undergo LMP in acceptor
725 cells.

726

727 **Fig 8. α -Syn fibrils induce LMP upon arrival in the acceptor cells.** (A) Representative
728 confocal images of donor and acceptor cells after 24 h of co-culture. Donor cells were
729 transfected with H2B-mCherry (control co-culture) or treated with Alexa 568-tagged α -syn
730 fibrils (α -syn co-culture). Acceptor cells were transfected with Gal3-GFP. Co-cultures were
731 labelled with HCS CellMaskTM Blue. Red arrows indicate the α -syn fibrils received by acceptor
732 cells, white arrows indicate the Gal3-GFP puncta formation (LMP) in the acceptor cells that
733 received α -syn fibrils. Scale bar: 10 μ m. (B) % of acceptor cells under LMP in control ($6 \pm 2\%$)
734 and α -syn ($33 \pm 5\%$) co-cultures (upper graph). Average number of Gal3-GFP puncta formation
735 in acceptor cells under LMP in control (8 ± 1) and α -syn (14 ± 1) co-cultures (lower graph).
736 Mean \pm S.E.M, $n=5$ (50 acceptor cells per condition). * $P=0.04$, **** $P<0.0001$ by Mann-
737 Whitney U - test. (C) SR image of a co-culture where donor cells were treated with α -syn fibrils
738 for 18 h and acceptor cells were transfected with Gal3-GFP, labelled for LAMP1-Alexa 647

739 antibody (pseudo colored in grey). A selected region where Gal3-GFP puncta were observed
740 (indicated by a white square in the acceptor cell of the co-culture image), was further magnified
741 to observe one lysosome (indicated by the small white square) having α -syn fibrils puncta and
742 recruited Gal3-GFP. Image was acquired with a Spinning Disk microscope with SR module.
743 Scale bar: 10 μ m (for the inset: 0.2 μ m). **(D)** SR image of an acceptor cell demonstrating Gal3-
744 GFP puncta recruited at the lysosomal membrane where α -syn fibrils were detected in close
745 proximity. Selected lysosome is indicated by a white square. Image was acquired by SR SIM
746 (Zeiss, LSM 780-Elyra PS.1). Scale bar: 5 μ m (for the inset: 0.5 μ m). In C, the signal was
747 boosted to make the selected lysosome visible; in D, the acceptor cell was presented with HCS
748 CellMask™ Blue labelling as this cell was poorly transfected but accumulation of Gal3-GFP
749 puncta was clearly detectable. The data underlying this Figure may be found in S1 Data.

750

751 **α -Syn fibrils induce seeding after their transfer into acceptor cells and this event is**
752 **preferentially associated with lysosomes.**

753 To further investigate the seeding mechanism in acceptor cells that received lysosomes
754 containing α -syn fibrils, we used again our α -syn-GFP soluble fluorescent reporter expressed
755 in acceptor cells co-cultured with donor cells, either challenged with α -syn fibrils or transfected
756 with H2B-mCherry (α -syn co-culture and control co-culture respectively; Figs 9A and S3G
757 number 2). We then quantified the presence of α -syn-GFP puncta (indicating aggregation of the
758 soluble protein; Fig 9A, white arrows) in the acceptor cells that received α -syn fibrils (Fig 9A,
759 red arrows). We found that 27 ± 4 % of acceptor cells contained 7 ± 1 α -syn-GFP puncta in α -
760 syn co-culture, whereas in control co-culture only 10 ± 4 % of the acceptor cells had 2 ± 0.2 α -
761 syn-GFP puncta (Fig 9B).

762 Next, to address whether the seeding in acceptor cells was associated with lysosomes, we
763 performed super-resolution microscopy. After labelling the cells in co-culture with antibody to
764 LAMP1, we examined the subcellular localization of α -syn-GFP aggregates in acceptor cells.
765 We observed four different scenarios: i) lysosomes containing α -syn fibrils and colocalizing
766 with α -syn-GFP puncta surrounding the lysosomal membrane (Fig 9C), ii) lysosomes filled
767 with α -syn fibrils with discrete α -syn-GFP deposits on their membrane (Fig 9D), iii) lysosomes
768 containing α -syn-GFP puncta with α -syn fibrils in close proximity (Fig 9E), and iv) lysosomes
769 containing both α -syn fibrils and α -syn-GFP puncta partially colocalizing in their lumen (Fig
770 9F). In addition, we performed 3D object-based colocalization analysis between α -syn-GFP

771 puncta, α -syn fibrils, and LAMP1+ lysosomes. We observed that $60 \pm 7\%$ of the newly formed
772 α -syn-GFP aggregates colocalized with LAMP1+ lysosomes (Fig 9G). Overall, these data
773 indicate that the majority of the seeding of endogenously expressed soluble α -syn takes place
774 at lysosomal compartments in acceptor cells after the transfer of α -syn fibrils.
775

776 **Fig 9. α -syn fibrils induce seeding after their transfer into acceptor cells and this event is**
777 **frequently associated with lysosomes. (A)** Representative confocal images of donor and
778 acceptor cells after 24 h of co-culture. Donor cells were transfected with H2B-mCherry (control
779 co-culture) or treated with Alexa 568-tagged α -syn fibrils for 18 h (α -syn co-culture). Acceptor
780 cells were transfected with α -syn-GFP. Inset of acceptor cells (indicated by white squares) is
781 presented at the right top corner of acceptor cells' panel. White arrows indicate α -syn-GFP
782 aggregate formation, red arrows indicate α -syn fibrils received by acceptor cells in α -syn co-
783 culture. Scale bar: 10 μm (for the inset: 5 μm). **(B)** % of acceptor cells that formed α -syn-GFP
784 aggregates in control ($10 \pm 4\%$) and in α -syn ($27 \pm 4\%$) co-cultures (left graph). Average
785 number of α -syn-GFP puncta detected in acceptor cells in control (2 ± 0.2) and in α -syn (7 ± 1)
786 co-cultures is presented (right graph). Mean \pm S.E.M, $n=3$ (150 acceptor cells per condition).
787 * $P=0.01$ and ** $P=0.003$ for % of aggregates and average number of aggregates in control
788 versus α -syn co-cultures, respectively, by Mann Whitney U -test. **(C)** SR image showing a
789 lysosome containing α -syn fibrils puncta colocalizing with α -syn-GFP+ aggregate at the
790 lysosomal membrane. **(D)** SR image showing a lysosome containing α -syn fibrils where α -syn-
791 GFP+ aggregate is located mostly in a restricted portion of the lysosomal membrane. **(E)** SR
792 image showing a lysosome having α -syn-GFP+ aggregate where α -syn fibrils puncta were
793 found to be in close proximity of the lysosomes. **(F)** SR image showing a lysosome where both
794 α -syn fibrils and α -syn-GFP aggregates are located to the lumen of the lysosome and partially
795 colocalizing. **(G)** Object-based 3D analysis (Imaris software) of colocalization between α -syn-
796 GFP and LAMP1+ lysosomes ($60 \pm 7\%$). Mean \pm S.E.M, $n=2$ (15 super-resolution images,
797 ~ 3000 lysosomes were analysed). Insets of images in C, D (acquired with Spinning-Disk
798 microscope with SR module) and E, F (acquired with SR SIM, Zeiss, LSM 780-Elyra PS.1)
799 from four selected regions (white squares) and from different acceptor cells transfected with α -
800 syn-GFP and that received α -syn fibrils, labelled for LAMP1 Alexa 647 antibody (pseudo
801 colored in grey). Scale bars: 10 μm (for the insets: 1 μm). The data underlying this Figure may
802 be found in S1 Data.
803

804 **α -Syn-loaded cells transfer damaged lysosomes to healthy cells and receive healthy**
805 **lysosomes in return.**

806 In our homotypic co-culture system between CAD cells, we could not address the nature of the
807 transferred lysosomes (i.e., whether the lysosomes that are transferred have LMP or not) nor
808 the directionality of lysosome transfer (from donor to acceptor and/or from acceptor to donor).
809 To answer these fundamental questions, we designed a heterotypic co-culture assay using
810 mouse CAD cells as donors and human HeLa cells as acceptors. Briefly, CAD cells were
811 transiently transfected with Gal3-GFP, loaded or not with α -syn fibrils, and used as the donor
812 cell population; on the other hand, HeLa cells stably expressing Gal3-Turquoise were used as
813 the acceptor cell population. Donor and acceptor cells were co-cultured for 24 h prior to be
814 fixed and immunolabelled with either a specific anti-mouse LAMP1 antibody (to detect the
815 lysosomes originated from donor cells) or a specific anti-human LAMP1 antibody (to detect
816 the lysosomes originated from acceptor cells; S3H Fig).

817 First, we tested this heterotypic system by evaluating: i) the efficiency of α -syn fibrils' transfer
818 from donor CAD cells to acceptor HeLa cells, and ii) the occurrence of seeding in the acceptor
819 cells. The percentage of acceptor HeLa cells that received α -syn fibrils from donors was $65 \pm$
820 3% with an average of 4 ± 0.2 α -syn puncta per acceptor cell (S7A-B Fig). As expected, also
821 in this case, both the percentage of α -syn fibrils ($7 \pm 2\%$) and the average number of α -syn
822 fibrils puncta per acceptor cell (2 ± 0.2) was significantly lower in the secretion condition (S7B
823 Fig). When donor CAD cells loaded with α -syn fibrils were co-cultured with HeLa cells
824 transiently transfected with soluble α -syn-GFP, we again observed the aggregation of soluble
825 α -syn-GFP (S7C Fig, green arrows) in acceptor HeLa cells that received α -syn fibrils from
826 donor CAD cells (S7C Fig, red arrows). Taken together, these results indicate that α -syn fibrils
827 can be efficiently transferred in a cell-to-cell contact manner and can induce seeding in the
828 acceptor cells following their transfer also in a heterotypic mouse-human co-culture assay.

829 As we could recognize the origin of lysosomes, we then used this system to better quantify the
830 transfer of all lysosomes and of lysosomes under LMP from donor to acceptor cells. To this
831 end, CAD cells were either loaded or not with α -syn fibrils and co-cultured with HeLa cells
832 expressing Gal3-Turquoise. Cells in co-culture were then immunolabelled with the antibody to
833 mouse LAMP1 to detect the transfer of lysosomes originated from donor cells (Fig 10A). The
834 percentage of acceptor HeLa cells that received donors' lysosomes was significantly higher in
835 α -syn co-culture ($52 \pm 4\%$) compared to control co-culture ($32 \pm 5\%$), whereas the average
836 number of transferred lysosomes (LAMP1+ puncta) did not change (3 ± 0.3 in both co-cultures;

837 Fig 10B). Furthermore, we observed that in α -syn co-culture both lysosomes containing α -syn
838 fibrils (Figs 10A, yellow arrows, and S7G, red arrow) or not (Figs 10A, white arrows, and S7G,
839 white arrow) were transferred to acceptor cells.

840 Next, to evaluate the amount of lysosomes having LMP that were transferred from CAD cells
841 to HeLa cells, we quantified the occurrence of LMP in CAD cells in our heterotypic co-culture
842 condition. Thus, we counted the number of Gal3-GFP puncta in donor CAD cells transfected
843 with Gal3-GFP, challenged or not with α -syn fibrils, and co-cultured with HeLa-Gal3-
844 Turquoise cells (S7D Fig, green arrows). As expected, the percentage of donor CAD cells
845 having LMP was significantly higher in α -syn loaded donor cells ($11 \pm 4\%$) compared to control
846 donors ($2 \pm 2\%$), whereas the average number of Gal3-GFP puncta per cell did not show any
847 statistically significant change (10 ± 2 and 14 ± 4 in control and α -syn donors, respectively;
848 S7E Fig). These findings indicate that, in co-culture conditions, donor CAD cells challenged
849 with α -syn fibrils undergo LMP similar to what we showed earlier (Fig 3A and B). Next, we
850 evaluated the transfer of donors' lysosomes with LMP by quantifying the presence of Gal3-
851 GFP puncta in acceptor HeLa-Gal3-Turquoise cells both in control and α -syn co-cultures (Fig
852 10C). We found a significantly higher percentage of HeLa cells with Gal3-GFP puncta in the
853 α -syn co-culture ($13 \pm 2\%$; Fig 10C, green arrows, and D, left graph) compared to control co-
854 culture ($4 \pm 1\%$; Fig 10D, left graph). We did not observe a significant difference between the
855 average number of Gal3-GFP puncta per acceptor cell in the two co-cultures (2 ± 0.2 and $2 \pm$
856 0.3 in control and α -syn co-cultures, respectively; Fig 10D, right graph). These data indicate
857 that CAD cells challenged with α -syn fibrils transfer more damaged lysosomes (i.e., undergoing
858 LMP) to acceptor cells compared to control CAD cells. In addition, we were able to detect
859 donors' lysosomes colocalizing both with α -syn fibrils and Gal3-GFP puncta in acceptor HeLa
860 cells (Fig 10E), demonstrating that damaged lysosomes carrying α -syn fibrils are transferred
861 into the acceptor cells.

862 By taking advantage of HeLa cells stably expressing Gal3-Turquoise as acceptor cells, we also
863 evaluated the occurrence of LMP in acceptor cells by assessing the Gal3-Turquoise puncta (Fig
864 10F, turquoise arrows). We found that $18 \pm 3\%$ of acceptor cells undergo LMP with an average
865 of 10 ± 1 Gal3-Turquoise puncta per cell in α -syn co-culture (Fig 10G). LMP in the acceptor
866 cells of control co-culture was significantly lower ($3 \pm 1\%$) with an average of 9 ± 1 Gal3-
867 Turquoise puncta per cell (Fig 10G). In addition, by using antibody to human LAMP1, we also
868 detected colocalization with Gal3-Turquoise puncta in acceptor cells (S7F Fig, arrow). These
869 results suggest that α -syn fibrils derived from CAD cells are able to induce LMP in the acceptor

870 HeLa cells following their transfer. Interestingly, in very few cases we could also detect
871 colocalization between Gal3-Turquoise puncta and donors' lysosomes labelled with anti-mouse
872 LAMP1 antibody in acceptor HeLa cells (S7G Fig, white arrow), suggesting that damaged
873 donors' lysosomes can undergo LMP upon arrival to the acceptor cells.

874 Finally, to evaluate lysosome transfer from acceptor to donor cells, the CAD-HeLa co-culture
875 was immunolabelled with anti-human LAMP1 antibody and donor CAD cells were evaluated
876 for the presence of acceptors' lysosomes (Fig 10H). The percentage of donor cells that received
877 acceptors' lysosomes in control co-culture was $14 \pm 4\%$ whereas in α -syn co-culture this
878 percentage was significantly higher ($34 \pm 5\%$; Fig 10I, left graph). The average number of
879 acceptors' lysosomes per donor cell in both co-culture conditions was similar (2 ± 0.3 and $2 \pm$
880 0.1 in control and α -syn co-cultures, respectively; Fig 10I, right graph). To understand whether
881 lysosomes transferred from acceptor to donor cells were damaged, we quantified the presence
882 of Gal3-Turquoise puncta in donor CAD cells in both in the α -syn and control co-cultures (S7H
883 Fig). Only $4 \pm 1\%$ of donor cells resulted positive for Gal3-Turquoise puncta in α -syn co-
884 culture, while we could barely ($0.3 \pm 0.3\%$) observe donor cells positive for Gal3-Turquoise
885 puncta in control co-culture (S7I Fig). Taken together, these results demonstrate that donor cells
886 challenged with α -syn fibrils receive healthy lysosomes from acceptor cells, while the transfer
887 of damaged lysosomes from the acceptor cells is a rare event. This suggests the occurrence of
888 a rescue mechanism towards donor cells overloaded with α -syn, similar to what was previously
889 reported in the case of a lysosomal disease [106].

890

891 **Fig 10. Intercellular lysosome transfer is reciprocal. (A)** Representative confocal image of
892 CAD-HeLa co-culture where donor mouse CAD cells were treated with Alexa 568-tagged α -
893 syn fibrils (18 h) and co-cultured with acceptor human HeLa stable Gal3-Turquoise cells for 24
894 h, labelled for anti-LAMP1 mouse antibody and DAPI. In acceptor HeLa Gal3-Turquoise cells,
895 arrows indicate donors' lysosomes containing (yellow) or not (white) α -syn fibrils. Inset
896 represents a selected region (white square) of one acceptor cell containing donors' lysosomes.
897 Scale bar: $10 \mu\text{m}$ (for the inset: $2 \mu\text{m}$). **(B)** % of acceptor HeLa cells that received lysosomes
898 from donor CAD cells in control ($32 \pm 5\%$) and in α -syn ($52 \pm 4\%$) co-cultures (left graph).
899 $**P=0.006$ by two-tailed *t*-test. Average number of lysosomes transferred from donor to
900 acceptor cells in control (3 ± 0.3) and in α -syn (3 ± 0.3) co-cultures (right graph). Mean \pm
901 S.E.M. ns= not significant by Mann-Whitney *U*-test. **(C)** Representative confocal image of
902 CAD-HeLa co-culture where Gal3-GFP transfected donor CAD cells were treated with Alexa

903 568-tagged α -syn fibrils for 18 h and co-cultured with HeLa Gal3-Turquoise for 24 h, labelled
904 with DAPI. In acceptor HeLa Gal3-Turquoise cells, red arrows indicate α -syn fibrils, green
905 arrows indicate Gal3-GFP puncta (lysosomes under LMP received from donor cells). Scale bar:
906 10 μ m. **(D)** % of acceptor HeLa cells that received Gal3-GFP puncta from donor cells in control
907 ($4 \pm 1\%$) and in α -syn ($13 \pm 2\%$) co-cultures (left graph); average number of Gal3-GFP puncta
908 per acceptor HeLa cell in control (2 ± 0.3) and in α -syn (2 ± 0.2) co-cultures (right graph). Mean
909 \pm S.E.M. ns= not significant, * $P=0.04$ by Mann-Whitney *U*-test. **(E)** Acceptor HeLa Gal3-
910 Turquoise cell that received a donor's lysosome containing α -syn fibrils and under LMP.
911 Colocalization between LAMP1 (labelled with anti-LAMP1 mouse antibody), α -syn fibrils, and
912 Gal3-GFP is presented in the inset of the selected area (white square). Scale bar: 10 μ m (for the
913 inset: 1 μ m). **(F)** Representative confocal image of LMP in HeLa Gal3-Turquoise (pseudo
914 colored in yellow) acceptor cell in CAD-HeLa co-culture. In acceptor HeLa Gal3-Turquoise
915 cells, red arrows indicate the α -syn fibrils, turquoise arrows indicate the Gal3Turquoise puncta.
916 Scale bar: 10 μ m. **(G)** % of acceptor HeLa cells under LMP in control ($3 \pm 1\%$) and in α -syn
917 ($18 \pm 3\%$) co-cultures is presented (left graph); average number of Gal3-Turquoise puncta per
918 acceptor cell under LMP in control (9 ± 1) and in α -syn (10 ± 1) co-cultures is presented (right
919 graph). Mean \pm S.E.M. ns= not significant, * $P=0.03$ by Mann-Whitney *U*-test. **(H)**
920 Representative confocal image of CAD-HeLa co-culture where donor CAD cells were treated
921 with Alexa 568-tagged α -syn fibrils for 18 h and co-cultured with HeLa Gal3-Turquoise for 24
922 h, labelled for anti-LAMP1 human antibody and DAPI. In donor CAD cells, white arrows
923 indicate acceptors' lysosomes. Inset of a selected region of a donor CAD cell (white square)
924 showing acceptors' lysosomes in higher magnification. Scale bar: 10 μ m (for the inset: 5 μ m).
925 **(I)** % of acceptors' lysosomes transferred from acceptor to donor cells in control ($14 \pm 4\%$) and
926 in α -syn ($34 \pm 5\%$) co-cultures (left graph). ** $P=0.002$ by two-tailed *t*-test. Average number of
927 acceptors' lysosomes per donor cell in control (2 ± 0.3) and in α -syn (2 ± 0.1) co-cultures (right
928 graph). Mean \pm S.E.M. ns= not significant by Mann-Whitney *U*-test. In CAD-HeLa co-culture
929 model, data was collected from seven independent experiments in which four and three of them
930 were labelled with anti-LAMP1 mouse and human antibodies, respectively. According to the
931 experiment, in average 100 acceptor or donor cells were analysed for each condition per
932 experiment. The data underlying this Figure may be found in S1 Data.

933 **Discussion**

934 α -Syn plays a crucial role in the generation and progression of synucleinopathies including PD.
935 Indeed, the pathology correlates with the presence of α -syn inclusions spreading through
936 interconnected brain regions in a “prion-like” manner [5,16,107]. By using a co-culture system,
937 we previously demonstrated that α -syn fibrils can be transferred from donor to acceptor cells
938 inside of lysosomes through TNTs and induce the seeding in the recipient cells [19]. However,
939 fundamental questions regarding how lysosomes participate in this process remained open. In
940 the current study, we focused on the role of lysosomes and the crosstalk between α -syn fibrils
941 and lysosomes in the context of intercellular spread of α -syn fibrils and the subsequent seeding
942 mechanism.

943 By using super-resolution microscopy, we looked precisely at the subcellular localization of
944 the α -syn fibrils and we found them mainly in the lysosomal lumen or at the lysosomal
945 membrane (Fig 1B). In both cases, lysosomes associated with α -syn fibrils had a larger diameter
946 compared to control lysosomes. Lysosomal enlargement in the presence of α -syn fibrils has
947 been reported before [70,108]; however, here we showed that this morphological change is
948 specific to the lysosomes containing α -syn fibrils. Indeed, in α -syn fibril-treated cells, the
949 diameter of the lysosomes devoid of fibrils was comparable to that of the control lysosomes
950 (Fig 1B, graph). This finding was supported by correlative EM analysis that indicated an α -syn-
951 dependent enlargement of lysosomes both in the perimeter and area (Fig 1D, graphs). In
952 addition, we found that lysosomes containing α -syn fibrils exhibit structural alterations (e.g.,
953 enlargement in size, aberrant luminal content), directly supporting that α -syn fibrils cause
954 changes in lysosome morphology (Fig 1C). The exact mechanism of lysosomal enlargement
955 needs to be further investigated; in agreement with studies demonstrating lysosome dilation
956 accompanied by lysosomal dysfunction [70,108,109], one possibility is that dysfunction results
957 from accumulation of undegraded α -syn fibrils. Consistently, while the total number of
958 lysosomes did not vary, we detected lysosomal dysfunction in α -syn fibril-treated cells
959 compared to control cells. Specifically, in the presence of α -syn fibrils, we observed disturbance
960 of lysosomal pH and decrease of lysosomal enzyme activities (Fig 2B and D). These changes
961 could be a consequence of the LMP induced by α -syn fibrils that we and others detected in α -
962 syn fibril-treated cells [73,74]. Indeed, LMP causes the release of cathepsins and other
963 hydrolases from the lysosomal lumen to the cytosol [72,110].

964 LMP can be induced by different protein aggregates (e.g., α -syn, tau, huntingtin), and it has
965 been proposed to be a common mechanism used by exogenous fibrils to spread through the

966 cells [74]. Specifically, LMP has been described in several cell types challenged with α -syn
967 fibrils, such as the neuronal cell lines SH-SY5Y and N27, as well as human dopaminergic
968 neurons derived from induced pluripotent stem cells [73,74]. Here, we showed that α -syn fibrils
969 induce LMP also in neuronal CAD cells (Fig 3A and B). By using SIM, we observed the
970 recruitment of Gal3 to the damaged lysosomes displaying α -syn fibrils in their lumen or limiting
971 membrane (Fig 3D and E). Importantly, we demonstrated that α -syn fibrils trigger LMP also in
972 the recipient cells following their intercellular transfer (Fig 8A and B). LMP in acceptor cells
973 has been only reported in a co-culture system where donor N27 cells expressing α -syn were
974 pretreated with the mitochondrial toxin MPP⁺ (1-methyl-4-phenylpyridine) to induce PD-like
975 pathology and co-cultured with acceptor cells stably expressing Gal3 [73]. Our results indicate
976 that, without inducing a PD-like pathology in donor cells, the transfer of α -syn fibrils ‘per se’
977 is sufficient to induce LMP in acceptor cells both in homotypic (Fig 8A and B) and heterotypic
978 co-culture systems (Fig 10F and G). In addition, by performing super-resolution microscopy,
979 we also detected the recruitment of Gal3 to damaged lysosomes bearing α -syn fibrils either in
980 their lumen or at their membrane in the acceptor cells, similar to what we observed in donor
981 cells (Fig 8C and D). Interestingly, our results show that lysosomes containing α -syn fibrils are
982 not targeted for lysophagy [84] (S4 Fig), possibly suggesting a rescue mechanism such as the
983 one orchestrated by the ESCRT machinery [111,112]. Considering the evidence supporting
984 autophagy impairment in neurodegenerative diseases and more specifically following α -syn
985 accumulation [55,113], and the recent findings that impaired autophagic flux contributes to the
986 occurrence of LMP [114], it will be interesting to assess the contribution of autophagy to LMP,
987 lysosomal dysfunction, and propagation of α -syn.

988 The underlying mechanism of LMP induction by α -syn fibrils is unclear. Several studies have
989 reported the ability of α -syn protofibrils to permeabilize membranes [115–117]; thus, as
990 suggested by Freeman et al., the luminal α -syn fibrils could induce membrane curvature causing
991 the rupture of lysosomes [73]. Our correlative EM data show a wavy limiting membrane in
992 lysosomes containing α -syn fibrils compared to lysosomes devoid of α -syn fibrils, supporting
993 this hypothesis. Moreover, oxidative stress could also compromise lysosomal integrity [118].
994 Consistently, we have previously reported that α -syn fibrils increase ROS levels in CAD cells
995 [19], and enhanced ROS levels have been found in PD mouse models and PD patients [68,119].
996 Since α -syn fibrils located to the lysosomes need to directly interact with the soluble cytosolic
997 α -syn in order to induce the seeding, LMP has been proposed as a relevant mechanism to allow
998 the escape of α -syn fibrils from the lysosomes [19,85]. Co-localization between Gal3 and
999 aggregated α -syn has been reported in the basal forebrain of Diffused Lewy Body Disease

1000 patients but not in normal, age-matched controls, supporting the role of lysosome rupture in α -
1001 syn pathology and progression [85]. In the current study, we detected efficient seeding of
1002 soluble α -syn both in donor cells treated with α -syn fibrils and in acceptor cells that received
1003 the fibrils inside lysosomes from donor cells (Figs 4A and B and 9A and B). By using super-
1004 resolution microscopy, we observed that $69 \pm 6\%$ and $60 \pm 7\%$ of the newly formed α -syn
1005 aggregates colocalize with LAMP1+ lysosomes in the donor and acceptor cells, respectively.
1006 These data together with live imaging show that the seeding event begins shortly after the
1007 internalization of α -syn fibrils and occurs preferentially at the lysosomes (Figs 4C-I, 9C-G,
1008 S5A, and S1 Movie). It has been shown that specific environments inside membranous and
1009 vesicular structures favor the aggregation of the α -syn protein [120,121]; thus, our results
1010 indicate that lysosomes can create a confined environment facilitating the conversion of soluble
1011 α -syn.

1012 Do lysosomes contribute to the spread of the disease? Lysosomes are highly dynamic organelles
1013 that move bidirectionally along microtubules between the center and the periphery of the cell
1014 [122]. In non-polarized cells, lysosomes are mostly clustered at the perinuclear region, but a
1015 more dynamic pool is located at the cell periphery [90,92,100]. Here, we demonstrated that α -
1016 syn fibrils act on lysosome positioning by inducing their peripheral redistribution (Fig 5A and
1017 B). We also found that peripheral α -syn-containing lysosomes exhibit lysosomal dysfunction
1018 (i.e., disturbed pH and decreased lysosomal enzyme activities; Fig 5C). In addition, we showed
1019 that donor cells challenged with α -syn fibrils, thus having more peripheral lysosomes, transfer
1020 lysosomes more efficiently to the recipient cells compared to untreated donor cells (Fig 5F and
1021 G). Moreover, the peripheral distribution of lysosomes positively affects α -syn fibrils' transfer
1022 both in CAD and HeLa cells (Figs 7A and B and S6A and B).

1023 The induction of LMP has been recently shown to promote nuclear translocation of TFEB
1024 [123], which influences lysosomal motility and exocytosis [95]. Furthermore, TFEB
1025 overexpression promotes α -syn clearance [124]. Thus, we investigated whether the loading of
1026 lysosomes with α -syn fibrils triggers TFEB nuclear translocation and whether this translocation
1027 participates in α -syn-induced distribution of lysosomes to the cell periphery. We found that α -
1028 syn fibrils induced TFEB translocation to the nucleus (Fig 6A). Moreover, expression of active
1029 TFEB correlates with more peripheral distribution of lysosomes (Fig 6B), while silencing of
1030 the endogenous TFEB prevents the peripheral redistribution of lysosomes upon α -syn loading
1031 (Fig 6D) suggesting the involvement of TFEB in this event. However, how this occurs is not
1032 yet clear. Previous reports suggested that TFEB-regulated transcription induced lysosomal
1033 docking to the plasma membrane, thus promoting the peripheral distribution of lysosomes in

1034 HeLa cells [95]. However, TFEB and the related transcription factor TFE3 have been reported
1035 to contribute to perinuclear positioning of lysosomes through transcriptional activation of the
1036 lysosomal protein TMEM55B under starvation conditions in HeLa cells [96]. It has also been
1037 reported that overexpression of TFEB promotes perinuclear positioning of the lysosomes in
1038 mouse fibroblast cells defective for the lysosomal transporter cystinosin [97]. Given these
1039 controversies in the literature, the exact role of TFEB in the regulation of lysosome positioning
1040 remains to be addressed in the future.

1041 To our knowledge, this is the first report showing that α -syn fibrils influence lysosome
1042 positioning, favoring α -syn fibrils transfer in a cell-to-cell contact-dependent manner via
1043 lysosomes. These findings suggest that lysosomes play an important role in the intercellular
1044 trafficking of α -syn fibrils. It is worth noting that α -syn fibrils do not affect lysosomal
1045 exocytosis (Fig 5D and E). In addition, in the secretion tests used in each co-culture experiment,
1046 we never detected any significant difference in the transfer of α -syn fibrils and/or lysosomes
1047 through the cell supernatant. Although this was not the aim of our study, these results further
1048 confirm that transfer of α -syn fibrils primarily relies on TNT- and/or cell-to-cell-contact-
1049 dependent mechanisms in accordance with our previous findings [19,20,22]. The mechanism
1050 by which α -syn fibrils enhance TNT formation is still largely unknown. However, we and others
1051 demonstrated that cells form more TNTs under stress, such as when they are treated with H₂O₂
1052 [125,126]. In line with these findings, we previously reported that CAD cells bearing α -syn
1053 fibrils exhibit sustained increase in ROS levels [19]. Therefore, α -syn fibrils can indeed trigger
1054 stress in the cells in order to induce TNT formation. In addition, it has been reported that α -syn
1055 could induce membrane remodeling, such as membrane expansion and formation of cylindrical
1056 tubes, and that the extent of membrane expansion correlated linearly with the density of α -syn
1057 [127]. Thus, further studies are essential to address how α -syn fibrils participate in the formation
1058 of TNTs.

1059 Lysosome transfer through TNTs has been shown to be bidirectional [106]. However, there is
1060 no study on the directionality/origin and the nature (whether they are healthy or damaged) of
1061 the lysosomes transferred between cells in the presence of the α -syn fibrils. Thus, in the current
1062 study, we studied the transfer of both healthy and damaged (i.e., under LMP) lysosomes
1063 between CAD (donor) and HeLa (acceptor) cells and found that the transfer of both types of
1064 lysosomes is bidirectional (Fig 10A, B, H, and I). We showed that α -syn fibril-treated donor
1065 cells transfer more lysosomes (both healthy and damaged) to acceptor cells compared to
1066 untreated control donor cells. Interestingly, we observed the recruitment of acceptor's Gal3 to
1067 the donor's lysosomes transferred in an acceptor cell (S7G Fig), suggesting that the rupture of

1068 donors' lysosomes containing α -syn fibrils could occur after their transfer in the recipient cells.
1069 Focusing on the transfer of lysosomes from acceptors to donors, we found that α -syn fibril-
1070 treated donor cells received more healthy acceptors' lysosomes compared to control untreated
1071 donor cells (Fig 10H and I). We also detected damaged acceptors' lysosomes in α -syn fibril-
1072 treated donor cells although this was a very rare event (S7H and I Fig). Based on these data we
1073 suggest that in the context of α -syn spreading, donor cells loaded with α -syn fibrils, try to get
1074 rid of α -syn fibrils through the transfer of lysosomes, thus promoting the spreading of the fibrils.
1075 On the other hand, donor cells receive healthy lysosomes from acceptor cells, suggesting a
1076 potential rescue mechanism. A similar rescue mechanism has been previously reported in
1077 cystinosis-deficient fibroblasts, which receive cystinosis-bearing lysosomes from healthy
1078 macrophages through TNTs [106].

1079 In light of these findings, we propose a working model on how lysosomes contribute to the
1080 transfer and propagation of α -syn fibrils (Fig 11). After internalization, α -syn fibrils localize to
1081 lysosomes (Fig 11, number 1), where they induce LMP and recruit Gal3 (Fig 11, number 2). α -
1082 Syn fibrils escape from damaged lysosomes and seed soluble α -syn in donor cells, an event that
1083 occurs mostly in association with the lysosomes (Fig 11, number 3). Following α -syn fibrils
1084 internalization, TFEB translocates to the nucleus (Fig 11, number 4) and participates in the
1085 redistribution of lysosomes containing α -syn fibrils, likely under LMP or functionally impaired,
1086 towards the cell periphery (Fig 11, number 5). Here, lysosomes are not exocytosed (Fig 11,
1087 number 6), but are more prone to be transferred to other cells through TNTs. Indeed, cells
1088 loaded with α -syn fibrils transfer more lysosomes (both under LMP or not) to acceptor cells
1089 compared to healthy cells through TNTs (Fig 11, number 7). Once lysosomes reach the acceptor
1090 cells, α -syn fibrils escape from lysosomes already under LMP or from lysosomes that undergo
1091 LMP when they arrive in the acceptor cells. This again allows α -syn fibrils to seed soluble α -
1092 syn in the acceptor cells, mostly in association with the lysosomes (Fig 11, number 8) and
1093 further triggering LMP (Fig 11, number 9). In an attempt to rescue α -syn-overloaded donor
1094 cells, acceptor cells transfer healthy lysosomes to donor cells (Fig 11, number 10).

1095 In conclusion, our data explain how lysosomes are involved in the transfer and propagation of
1096 α -syn aggregates, and the crucial role that they play in this process. In agreement with these
1097 findings, we have previously reported that α -syn fibrils can be efficiently transferred between
1098 neurons, primary astrocytes, neurons and astrocytes, astrocytes and organotypic hippocampal
1099 slices and between iPSCs and they were associated to lysosomes in these co-culture systems
1100 [19,21,56]; however we have used here undifferentiated neuronal CAD cells line, for their easy
1101 manipulation. Although our results contribute to a better understanding of the mechanism of

1102 development and progression of α -syn pathology, opening new avenues for possible therapeutic
1103 approaches against synucleinopathies, it will be necessary in the future to investigate the
1104 transfer of α -syn containing lysosomes in differentiated primary neurons and/or in ex-vivo/in-
1105 vivo systems to further validate our data and overcome the limitation of this study.

1106

1107 **Fig 11. Working Model. 1)** α -Syn fibrils localize to lysosomes following their uptake. **2)** α -
1108 Syn fibrils induce LMP (i.e., recruit Gal3 to the ruptured lysosomes) in donor cells following
1109 their uptake, allowing their escape from lysosomes. **3)** α -Syn fibrils interact with soluble α -syn
1110 and induce seeding in donor cells. **4)** Following α -syn fibrils internalization, TFEB translocates
1111 to the nucleus. **5)** Lysosomes (possibly under LMP, as their pH is higher and lysosomal
1112 activities is lower) having the α -syn fibrils move towards the cell periphery. **6)** Peripheral
1113 lysosomes are not preferentially exocytosed. **7)** Lysosomes having α -syn (both under LMP or
1114 not) are transferred to acceptor cells along with healthy lysosomes. **8)** α -Syn fibrils induce LMP
1115 following their transfer to acceptor cells. **9)** α -Syn fibrils induce further seeding following their
1116 transfer to acceptor cells. **10)** Acceptor cells transfer healthy lysosomes to donors.

1117 **Materials and Methods**

1118

1119 **Cell culture, transfection, siRNA treatment**

1120 The mouse catecholaminergic neuronal cells (CAD cells) generated from a brain tumour of
1121 transgenic mice by targeted oncogenesis (kind gift of Hubert Laude; Institut National de la
1122 Recherche Agronomique, Jouy-en-Josas, France), were cultured in Opti-MEM^R GlutaMAXTM
1123 (Gibco) including 10% foetal bovine serum (FBS) and 1% penicillin-streptomycin (Pen-Strep).
1124 CAD cells express neuronal properties, but they lack neuronal morphology, thus stay
1125 undifferentiated in the presence of serum in their medium. This situation can be reversed by
1126 serum starvation and differentiation can be induced [128]. In this study, we used CAD cells in
1127 their undifferentiated state as this condition is optimal to study TNTs [19,125,129–131]. HeLa
1128 cells WT, HeLa cells myrlysin-KO and KIF1B-KIF5B double KO [100,132] and HeLa cells
1129 stably expressing Gal3-Turquoise were cultured in DMEM-GlutaMAXTM including 4.5 g/L D
1130 glutamine and pyruvate (Gibco) supplemented with 10% of FBS. CAD and HeLa cells were
1131 transiently transfected with Gal3-GFP, Arl8b-GFP, fluorescently tagged human histone H2B
1132 (H2B-GFP or H2B-mCherry) plasmids (final concentration: 1 µg for 150,000 cells/35mm Ibidi
1133 µ-dishes, 3 µg for 800.000 cells/T25 flasks) by Lipofectamine 2000 (Invitrogen) according to
1134 the manufacturer's instructions.

1135 To downregulate Arl8b and TFEB, 30 pmol of unique 27mer siRNA duplex against mouse
1136 Arl8b and TFEB (CliniSciences and OriGene respectively) was introduced to CAD cells in
1137 parallel to siRNA scramble (sicontrol) by using Lipofectamine RNAiMAX (Invitrogen)
1138 according to the manufacturer's instructions, and incubated 60h prior to be used in co-culture
1139 experiments and in Western blot analysis.

1140 To induce lysophagy, CAD cells were treated with 1 mM L-Leucyl-L-Leucine methyl ester
1141 (LLOMe) for 3h.

1142

1143 **Generation of stable HeLa mTurquoise-Galectin3 cell line**

1144 In order to generate stable HeLa cell line expressing a mTurquoise-Galectin3 fluorescent
1145 reporter, we used a well-established Sleeping Beauty (SB) transposable system that originates
1146 from an inactive transposon in salmonid fish and belongs to the Tc1/mariner-type transposon
1147 family, as previously described [133,134]. Briefly, the insert sfiI-mTurquoise-Galectin3-sfiI
1148 was amplified from pE mTurquoise-Galectin3 plasmid by polymerase chain reaction (PCR)
1149 where SfiI-mTurquoise-forward (AGG CCT CTG AGG CCG CCA CCA TGG TGA GCA

1150 AGG G) and Gal3-SfiI-reverse (AGG CCT GAC AGG CCT TAT CAT GGT ATA TGA AGC
1151 AC) primers (IDT-DNA Company) were used with Flash Phusion High Fidelity PCR Master
1152 Mix (ThermoFisher Scientific). Next, the insert was cut by sfiI enzyme and inserted into the
1153 constitutive vector pSBbi-PUR, a gift from Eric Kowarz, (Addgene Plasmid #60523) that was
1154 cut by sfiI enzyme and dephosphorylated by Rapid DNA Dephos & Ligation Kit (Roche).
1155 Transformation was performed with on stBL3 competent bacteria following the ligation of sfiI-
1156 pSBbi-PUR-sfiI vector and insert sfiI-mTurquoise-Galectin3-sfiI, and colonies were selected
1157 on LB broth agar plates containing ampicillin. Clones were then sequenced (Eurofins
1158 Genomic) in order to verify the existence of the insert and maxiprep for the pSBbi-PUR-
1159 mTurquoise-Galectin3 plasmid was performed by using the Invitrogen™ PureLink™ HiPure
1160 Plasmid Maxiprep Kit. Next, HeLa cells seeded on 6 well plates (300.000 cells per well) were
1161 co-transfected with 9 µg of pSBbi-PUR-mTurquoise-Galectin3 and 100 ng SB transposase
1162 expression vector pCMV (CAT)T7-SB100, a gift from Eric Kowarz (Addgene plasmid #
1163 34879) by using XtremGene® transfection reagent (Roche). 24 h following the transfection,
1164 cells were subjected to puromycin (1 µg/mL). Selection was carried out for 2 to 10 days. Cells
1165 were then cultivated for four weeks without selection medium and monoclonal selection was
1166 performed on 96 well plates (1 cell/well). Clones exhibited expected mTurquoise fluorescent
1167 were further tested for classical behavior for HeLa cells (low Galectin-3 fluorescent in the
1168 whole cell and a brilliant signal upon vacuole rupture) and used in the experiments described
1169 in the current study.

1170

1171 **Preparation and internalization of α -syn fibrils**

1172 Human wild-type α -syn in pRK172, a construct containing α -syn that lacks cysteine because of
1173 mutagenesis of codon 136 (TAC to TAT) was transformed into *Escherichia coli* BL21 (DE3)
1174 as previously reported. Expression and purification were performed as described previously
1175 [86]. Briefly, the protein concentrations of monomeric α -syn were measured by RP-HPLC as
1176 described previously [86,135]. Purified recombinant α -syn monomers (~5 mg/mL) containing
1177 30 mM Tris-HCl, pH 7.5, 10 mM DTT, and 0.1% sodium azide were incubated at 37°C with
1178 shaking using a horizontal shaker (TAITEC) at 200 rpm. Following the incubation for 7 days,
1179 the samples were ultracentrifuged at 100.000 g for 20 min at room temperature (RT), and the
1180 ppt fraction was recovered as α -syn fibrils. They were re-suspended in saline prior to be
1181 ultracentrifuged again. The pellets were re-suspended in saline and sonicated using a cup horn
1182 sonicator (Sonifier SFX, Branson) at 35% power for 180 s (total 240 s, 30 s on, 10 s off). The

1183 fibrils were labelled with Alexa Fluor 488 or 568 Protein Labelling Kit (Invitrogen) following
1184 the manufacturer's instructions. After the incubation of fibrils with Alexa Fluor dyes, samples
1185 were ultracentrifuged again and the pellets were re-suspended in 30 mM Tris-HCl, pH 7.5 prior
1186 to be ultracentrifuged one more time. Finally, labelled α -syn fibrils were resuspended in saline
1187 containing 0.1% sodium azide and the protein concentration of the fibrils was determined by
1188 RP-HPLC as described before [86,135]. Seeding activity of the fibrils were checked by adding
1189 the labelled fibrils (3 μ g) to 100 μ L of 1 mg/mL α -syn monomer solution in 30 μ M Thioflavin
1190 T and 80 mM Hepes, pH 7.5. Amyloid-like fibril formation was continuously monitored by
1191 measuring the Thioflavin T fluorescence (excitation 442 nm, emission 485 nm) with a
1192 microplate reader (Infinite 200, TECAN).

1193 0.5 μ M Alexa 488 or Alexa 568-tagged α -syn fibrils were diluted in the appropriate medium
1194 and sonicated for 5 min at 80% amplitude with a pulse cycle of 5 s on and 2 s off in an ultrasonic
1195 water bath Vibra-Cell 75,041 (BioBlocks Scientific). Fibrils were then introduced to cells
1196 immediately and incubated for 18 h. Before cells were processed for further procedures (e.g.,
1197 co-culture preparation, fixation, etc.), they were washed 3 times with diluted trypsin (1/3) in
1198 phosphate buffered saline (PBS). In parallel, control cells were subjected to the same treatments
1199 as described above without the addition of α -syn fibrils.

1200

1201 **Immunocytochemistry for lysosomes**

1202 CAD and/or HeLa cells and co-cultures (CAD-CAD and CAD-HeLa) were fixed with 4%
1203 paraformaldehyde (PFA) for 20 min at room temperature (RT). After 3 washes with PBS, cells
1204 were permeabilized with 0.1% Triton X-100 in PBS for 3 min at RT. Cells were then washed
1205 with PBS and nonspecific antibody binding sites were blocked by using 10% of goat serum
1206 (GS) in PBS for 30 min. Cells were then incubated with primary rat monoclonal anti-mouse
1207 LAMP1 (1D4B) or anti-human LAMP1 (H4A3) primary antibodies with the dilution of 1/200
1208 in blocking solution for 1 h. Antibodies were purchased from Developmental Studies
1209 Hybridoma Bank (DSHB), Iowa City, IA, USA. Cells were then washed 3 times with PBS and
1210 incubated for secondary antibodies (anti-rat Alexa-647 or anti-rat Alexa-488 purchased from
1211 Invitrogen, Carlsbad, CA) diluted 1:500 in blocking solution for 2 h at RT. After 3 washes with
1212 PBS, cells were further stained with HCS CellMaskTM Blue (Invitrogen) for 15 min at RT
1213 (diluted 1:5000 in PBS). Cells were then washed 3 times with PBS and further stained for DAPI
1214 (diluted 1:5000 in PBS) for 5 min. Finally, cells were washed and mounted with Aqua-

1215 Poly/Mount (Polysciences, Inc.). Image acquisitions were performed by confocal microscopy
1216 with identical settings.

1217

1218 **Immunocytochemistry for lysophagy**

1219 CAD cells were fixed with 4% paraformaldehyde (PFA) for 20 min at room temperature (RT).
1220 After 3 washes with PBS, cells were permeabilized with 0.1% Triton X-100 in PBS for 3 min
1221 at RT. Cells were then washed with PBS and nonspecific antibody binding sites were blocked
1222 by using 2% of bovine serum albumin (BSA) in PBS for 30 min. Cells were then incubated
1223 with primary rabbit anti-mouse LC3 (1:500, MBL International), mouse anti-Ubiquitin (1:1000,
1224 FK2, Enzo), and rat monoclonal anti-mouse LAMP1 (1D4B) (1:100, DSHB) in blocking
1225 solution for 1 h. Cells were then washed 3 times with PBS and incubated for secondary
1226 antibodies (anti-rabbit Alexa 488, anti-mouse Alexa-647 from Invitrogen, Carlsbad, CA; and
1227 anti-rat CFTM405M from Sigma) diluted 1:500 in blocking solution for 1 h at RT. Finally, cells
1228 were washed and mounted with Aqua-Poly/Mount (Polysciences, Inc.). Image acquisitions
1229 were performed by confocal microscopy with identical settings.

1230

1231 **LysoTracker Deep Red staining, DQ-BSA assay, and Cathepsin B activity assay**

1232 CAD cells were plated on 35 mm Ibidi μ -dishes (100.000 cells/dish). Alexa 568-tagged α -syn
1233 fibrils were introduced or not (control) to the cell culture medium 24 h after plating. Following
1234 18 h of α -syn fibril uptake, 20 nM LysoTracker Deep Red (Invitrogen) was prepared in culture
1235 medium and cells were incubated for 20 min at 37°C. Cells were then fixed with 4% PFA at
1236 RT and stained for HCS CellMaskTM Blue and DAPI as described before. Image acquisitions
1237 were performed by confocal microscopy with identical settings.

1238 To detect Cathepsin B (CathB) activity, CAD cells were plated on 35 mm Ibidi μ -dishes
1239 (100.000 cells/dish). Alexa 488-tagged α -syn fibrils were introduced or not (control) to the cell
1240 culture medium 24 h after plating. Following 18 h of α -syn fibril uptake, cells were treated with
1241 1X Magic Red Cathepsin solution, provided by Magic Red Cathepsin Assay kit
1242 (ImmunoChemistry Technologies LLC) and prepared through the manufacturer's
1243 recommendation, for 15 min at 37°C. Cells were then immediately imaged by confocal
1244 microscopy in live condition. The intracellular activity of CathB was detected as red fluorescent
1245 puncta produced by the hydrolysis of the fluorogenic substrate introduced. All images were
1246 acquired with the identical settings. For both experiments integrated density of LysoTracker
1247 Deep Red and CathB signal were measured by using FiJi software after a region of interest

1248 (ROI) is manually created by the freehand selection tool and the measurements were expressed
1249 in arbitrary unit (AU).

1250 For DQ-BSA assay, CAD cells were plated on 35 mm Ibidi μ -dishes (130.000 cells/dish). Alexa
1251 568-tagged α -syn fibrils were introduced or not (control) to the cell culture medium 24 h after.
1252 Following 18 h of α -syn fibrils uptake, 10 μ g/mL DQ Green BSA (Thermo Fisher Scientific)
1253 was prepared in culture medium and cells were incubated for 90 min at 37°C. Cells were then
1254 fixed with 4% PFA at RT. Image acquisitions were performed by confocal microscopy with
1255 identical settings. Integrated density of DQ-BSA signal were measured by using FiJi software
1256 after a region of interest (ROI) is manually created by the freehand selection tool and the
1257 measurements were expressed in arbitrary unit (AU).

1258

1259 **TNT labelling**

1260 To preserve the structure of TNTs, cells were fixed by a two-step fixation protocol as described
1261 previously [20,129]. Briefly, cells were first fixed with fixative solution-1 (2% PFA, 0.05%
1262 glutaraldehyde (GA) and 0.2 M HEPES in PBS) for 20 min at 37°C, then with fixative solution-
1263 2 (4% PFA and 0.2 M HEPES in PBS) for an additional 20 min at 37°C. After several washes,
1264 cells were labelled with 3.3 μ g/ μ L Wheat Germ Agglutinin (WGA)-Alexa Fluor-488 nm
1265 conjugate solution (Life Technologies) for 20 min at RT for membrane detection. As there is
1266 no specific marker for TNTs, WGA labelling was used to detect TNTs as described in detail in
1267 the quantification section.

1268

1269 **Lysosomal exocytosis analysis**

1270 *Evaluation of released Cathepsin B by ELISA*

1271 CAD cells were plated in B12-wells (80.000 cells/well). Cells were then treated with Alexa
1272 568-tagged α -syn fibrils or not for 18 h. Soluble lysosomal Cathepsin B (CathB) released in
1273 culture medium was evaluated by using Human Cathepsin B ELISA Kit (Abcam) following the
1274 manufacturer's instructions. Briefly, aliquots of culture medium derived from control cells and
1275 cells challenged with α -syn fibrils were incubated in 96-well plates precoated with a CathB
1276 specific mouse monoclonal antibody for 90 min at 37°C. Biotinylated CathB-specific goat
1277 polyclonal antibody was then added on the cells for 60 min at 37°C. Cells were then washed
1278 with tris-buffered saline (TBS) prior to the addition of Avidin-Biotin-Peroxidase Complex for
1279 30 min at 37°C. Unbound conjugates were washed away with TBS buffer five times. 3,3',5,5'-

1280 Tetramethylbenzidine was then used to visualize the horse radish peroxidase (HRP) enzymatic
1281 reaction (O.D. absorbance: 450 nm). Released CathB content is expressed as nanograms of
1282 CathB/mL of culture medium.

1283

1284 *Evaluation of LAMP1 at the plasma membrane*

1285 CAD cells were plated in 35 mm Ibidi μ -dishes (120.000 cells/dish). Cells were then treated
1286 with Alexa 568-tagged α -syn fibrils or not for 18 h. Live cells were then incubated with the
1287 primary rat monoclonal anti-mouse Lamp1 (1D4B) antibody recognizing an epitope at the
1288 luminal region of the protein, diluted in complete medium, for 30 min at 4°C. After washing
1289 with PBS, cells were fixed in 2% PFA in PBS for 10 min at RT. Next, cells were incubated
1290 with the Alexa Fluor 488-conjugated goat anti-rat secondary antibody diluted in PBS for 30
1291 min at RT. Cells were then imaged by confocal microscopy.

1292

1293 **Detection of LMP and seeding**

1294 CAD cells were plated on 35 mm Ibidi μ -dishes (100.000 cells/dish) and transiently transfected
1295 with 1 μ g of Gal3-GFP (for LMP) or 1 μ g of α -syn-GFP plasmids (for seeding). 24 h later cells
1296 were either treated with Alexa 568-tagged α -syn fibrils for 18 h or left untreated. In co-culture
1297 experiments, cells transiently transfected with Gal3-GFP or α -syn-GFP plasmids were co-
1298 cultured for 24 h with donor cells previously treated for 18 h with Alexa 568-tagged α -syn
1299 fibrils or not. Cells were then fixed with 4% PFA for 20 min at RT and stained for DAPI.
1300 Following image acquisition with confocal microscopy, cells were quantified for the presence
1301 of Gal3-GFP or α -syn-GFP puncta by using “Spot detector” tool of the ICY software. Note that
1302 a threshold of five puncta is applied to all images analysed and cells bearing puncta above this
1303 threshold were considered as having LMP.

1304

1305 **Co-culture experiments**

1306 Donor cells were plated on 35 mm well plates (400.000/well) and transfected with suitable
1307 plasmids according to the experiment (LAMP1-GFP, Arl8b-GFP, Gal3-GFP, H2B-mCherry)
1308 or pre-treated with siRNA Arl8b or siRNA-scrambled for 60 h. Myrlysin-KO and KIF1B-5B
1309 dKO HeLa cells were directly used as donors. Donor cells (in parallel to untreated control cells)
1310 were then challenged with Alexa 568-tagged α -syn fibrils for 18 h (or not according to the

1311 experiment). They were then washed once with PBS and 3 times with 1:3 diluted trypsin before
1312 co-culture preparation.

1313 Acceptor cells were plated on T25 flasks (800.000/flask) and transfected with suitable plasmids
1314 according to the experiment (Gal3-GFP, H2B-mCherry, H2B-GFP, α -syn-GFP). HeLa Gal3-
1315 Turquoise cell line was used directly as acceptor cell population. Both donor and acceptor cells
1316 were then detached (mechanically and by trypsinization for CAD and HeLa cells respectively)
1317 and counted. Co-culture was prepared in a 1:1 ratio (100.000 donor and 100.000 acceptors on
1318 35 mm Ibidi μ -dishes) for 24 h. Cells were then fixed with 4% PFA for 20 min at RT and stained
1319 for HCS CellMask™ Blue and DAPI as described before and mounted. Schematic presentation
1320 of different co-culture preparations was presented in S3 Fig.

1321 Of note, co-cultures were named with the predominant treatment of the donor cells: i) co-
1322 cultures having donor cells treated with α -syn fibrils or not were referred to as “ α -syn co-
1323 culture” and “control co-culture” respectively; ii) in the cases where all donor populations were
1324 treated with α -syn fibrils, in order to emphasize the different treatments between donor cells,
1325 co-cultures were named by these treatments (e.g., Arl8b-GFP over-expressing or siArl8b
1326 pretreated donors were referred to as “Arl8b-GFP co-culture” and “siArl8b co-culture”
1327 respectively).

1328

1329 *Secretion test*

1330 In all co-culture conditions, donor cells and acceptor cells were also plated separately during
1331 the co-culture preparation (100.000 cells/35 mm Ibidi μ -dishes) for the total duration of co-
1332 culture incubation (24 h). Then the conditioned medium collected from donor cells were
1333 transferred onto acceptor cells. Acceptor cells were then quantified for the presence of specific
1334 cargos (e.g., lysosomes, α -syn fibrils) to assess the cargo transfer through secretion in each co-
1335 culture condition. Secretion tests for particular experiments were referred to as predominant
1336 treatment of the donor cells as described above (e.g., “control secretion”, “ α -syn secretion”,
1337 “Arl8b-GFP secretion”).

1338

1339 **Confocal microscopy**

1340 After fixation and immunostaining, images were acquired with an inverted laser scanning
1341 confocal microscope LSM700 (Zeiss), with a 63X objective (zoom 1.0). Images were acquired
1342 using the ZEN acquisition software (Zeiss). In all experiments, we acquired Z-stacks covering

1343 the whole volume of cells. For the experiments where integrated density was measured in
1344 control and α -syn treated cells (LysoTracker Deep Red, Magic Red CathB, DQ-BSA assays,
1345 and evaluation of LAMP1 at the plasma membrane in non-permeabilized condition), all settings
1346 (including the laser power and exposure line time) were kept identical. In some experiments
1347 line averaging were also used in order to improve the signal to noise ratio.

1348

1349 **Super-Resolution (SR) Microscopy**

1350 *Sample preparation*

1351 24-well plates containing sterile cover slips (Deckglaser 12 mm) were coated with fibronectin
1352 (25 μ g/mL) diluted in PBS and kept at 37°C for 1 h. Cover slips were then washed 3 times with
1353 PBS. CAD cells were then plated on cover slips (20.000 cells/coverslip). Gal3-GFP or α -syn-
1354 GFP transfected and α -syn treated cells or mixture of donor and acceptor cells (co-cultures
1355 prepared for LMP and seeding experiments) were then plated on coverslips. Cells were then
1356 fixed with 4% PFA for 20 min at RT and immunolabelled with primary rat monoclonal anti-
1357 mouse LAMP1 (1D4B) and secondary anti-rat Alexa 647 antibodies as described before. Cells
1358 were then stained with DAPI and HCS CellMask™ Blue and mounted with Fluoromount-G
1359 (Southern Biotech) mounting medium.

1360

1361 *Structured Illumination Microscopy (SIM)*

1362 SIM was performed on a Zeiss LSM780 Elyra PS1 microscope (Carl Zeiss, Germany) using
1363 100X/1.4 oil Plan Apo objective with a 1.518 refractive index oil (GE Healthcare Life Science)
1364 and an EMCCD Andor Ixon 887 1 K camera for the detection. SIM images were processed
1365 with ZEN software and then aligned with ZEN using 100-nm TetraSpeck microspheres
1366 (ThermoFisher Scientific) embedded in the same conditions as the sample.

1367

1368 *Spinning Disk- Live Super-Resolution (SR) Confocal Microscopy*

1369 Images were acquired with an inverted Eclipse Ti Nikon microscope equipped with a CSU- X1
1370 spinning disk confocal scanning unit (Yokogawa), with an EMCCD Camera (Evolve 512 Delta,
1371 Photometrics), and with Live SR super-resolution module (Gataca systems), using a x100 or
1372 x60 1.4 NA PL-APO VC oil objective lenses controlled by MetaMorph software. SR images
1373 were denoised by using Safir software [136].

1374

1375 **Live imaging microscopy**

1376 Time-lapse microscopy imaging was performed on an inverted Spinning Disk microscope
1377 (Eclipse Ti microscope system, Nikon Instruments, Melville, NY, U.S.A.) using 60X 1.4 NA
1378 CSU oil immersion objective lens and Laser illumination 488 only or together with 561. For
1379 live cell imaging, the 37°C temperature was controlled with an Air Stream Stage Incubator,
1380 which also controlled humidity. Cells were plated in Ibidi μ -Dish 35 mm and incubated with
1381 5% CO₂ during image acquisition. Image processing and movies were realized using
1382 MetaMorph and ImageJ/Fiji software.

1383

1384 **Electron Microscopy**

1385 *Correlative Resin Electron Microscopy*

1386 For correlation of FM and resin-embedded EM of CAD cells, FM imaging was performed prior
1387 to sample preparation in EM. Cells were transiently transfected with LAMP1-GFP using
1388 Lipofectamine 2000 transfection reagent for 24 h and seeded on carbon-coated, gridded
1389 coverslips prepared as described before [76]. 24 h later, they were treated with α -syn- Alexa568
1390 fibrils for 18 h. Cells were then washed in 0.1 M phosphate buffer (PB) and fixed in 4%
1391 formaldehyde in 0.1 M PB buffer after which fluorescent Z-stacks of cells of interest were
1392 obtained for the GFP and Alexa 568 signal. The position of cells relative to the pattern etched
1393 in the coverslip was registered using polarized light. After FM imaging, the same specimens
1394 were prepared for EM by fixing with 2.5% glutaraldehyde + 2% formaldehyde in 0.1 M PB
1395 buffer for 2 h, and post fixation with osmium tetroxide and uranyl acetate, Fixed cells were
1396 dehydrated using a graded ethanol series, and embedded in Epon resin which was polymerized
1397 for 48 h at 65°C. After polymerization, the glass coverslip was removed from the Epon block
1398 by dissolving it in hydrogen fluoride. The exposed Epon surface was thoroughly cleaned with
1399 distilled water and left to harden overnight at 63°C. Areas of the resin block containing the cells
1400 previously imaged by FM were cut out using a clean razor blade, and glued to empty Epon
1401 sample stubs, with the basal side of the cells facing outwards [75,76]. From these blocks, 70
1402 nm sections were cut and collected on formvar and carbon coated copper 50 mesh support grids.
1403 Thin EPON sections were imaged in a Tecnai 12 TEM (Thermo Fischer Scientific, Eindhoven,
1404 The Netherlands) equipped with a Veleta 2k \times 2k CCD camera (EMSIS, Munster, Germany),
1405 operating at 80 kV. For correlation of FM and EM data, the TEM image of a ROI was overlaid
1406 with FM data using Photoshop. Multiple corresponding spots (e.g. nuclei) on images were

1407 manually selected, after which the correct scaling and transformation steps were performed and
1408 high-precision overlays of FM and EM data were generated. We used only linear transformation
1409 options to achieve the overlays shown in the Figures.

1410

1411 *On-section Correlative Microscopy of thawed cryosections*

1412 Similarly, CAD cells were grown on carbon-coated, gridded coverslips, incubated with α -syn
1413 Alexa 568-tagged fibrils for 18 h and fixed in 0.1 M PB (pH 7.4) containing 4% PFA that was
1414 added to an equal volume of medium. Fixed cells were flat embedded in 12% gelatin by keeping
1415 their orientation, cryoprotected in 2.3 M sucrose, and plunge frozen according to previous
1416 protocols [137,138]. 70 nm cryosections were picked up on formvar coated copper grids, after
1417 which they were immunolabelled for LAMP1 with a secondary Alexa 488-tagged rabbit
1418 antibody and 10 nm gold-conjugated Protein A (Cell Microscopy Core, UMC Utrecht, The
1419 Netherlands). Finally, sections were labelled using Hoechst 33342 to outline nuclei for
1420 correlation. The grids were washed with dH₂O and sandwiched between a microscope slide
1421 and a no. 1 coverslip in 2% methylcellulose in dH₂O. Sections were imaged in a Deltavision
1422 RT wide field fluorescence microscope (GE Healthcare, U.S.A.) equipped with a Cascade II
1423 EM-CCD camera (Photometrics, U.S.A.). Grids were first imaged at 40 \times magnification to form
1424 a map of the section, after which regions of interest (ROIs) were selected using 100 \times
1425 magnification. After imaging the grids were removed from the microscope slide, thoroughly
1426 rinsed with H₂O and contrasted for EM and embedded in methylcellulose containing uranyl
1427 acetate. After drying, ROIs were imaged using a Tecnai 12 TEM (Thermo Fischer Scientific)
1428 operating at 80 kV, equipped with a Veleta 2k \times 2k CCD camera (EMSIS, Munster, Germany)
1429 camera, and running serialEM software. Registration of thin section FM and EM data was
1430 performed using Adobe Photoshop, similar to above.

1431

1432 **Western immunoblots**

1433 For the Western blot analysis, cells were rinsed with PBS and then scraped in RIPA buffer (50
1434 mM Tris-HCl, pH 7.5, 150 mM NaCl, 1% Triton X-100, 0.5% sodium deoxycholate, 0.1%
1435 SDS). The resulting soluble fractions were centrifuged at 18,000 g for 5 min at 4 $^{\circ}$ C, and then,
1436 the supernatants were taken as the whole cell lysate, mixed with Laemmli sample buffer (1 M
1437 Tris-HCl, pH 6.8, 20% glycerol, 4% SDS, 5% β -mercaptoethanol, and 0.02% bromophenol
1438 blue), and boiled for 5 min. For Western blots, equal amounts of proteins (30 μ g/lane) were
1439 separated on SDS-PAGE gels and transferred to nitrocellulose membranes (GE Healthcare Life

1440 sciences), following standard procedures. Membranes were then blocked in Tris-buffered saline
1441 containing 0.1% Tween-20 and 5% non-fat dried milk for 1 h and probed overnight at 4°C with
1442 primary antibodies. The membranes were then washed and exposed for 1h at RT to the anti-
1443 rabbit/anti-mouse peroxidase-conjugated antibodies (1:1000) The specific protein bands were
1444 visualized using the ECL-immunoblotting chemiluminescence system (GE Healthcare Life
1445 sciences) and the ImageQuant LAS 500TM camera (GE Healthcare Life sciences). Primary
1446 antibodies used in this study: rat anti-Lamp1 (1:100, DSHB), anti-Arl8b (1:100), rabbit anti-
1447 TFEB (1:1000, Bethyl Laboratories), mouse anti-tubulin (1:1000), rabbit anti-GAPDH (1:5000,
1448 Boster). To determine the apparent molecular weights of the protein bands, a PageRuler plus
1449 prestained protein ladder (Thermo Fisher Scientific) was used.

1450

1451 **Quantification analysis**

1452 *Quantification for lysosomal positioning*

1453 We performed 2D analysis with the Z-projection where we used a two-step detection protocol
1454 in ICY software in order to assess the lysosomal positioning. In the first step, we used a script
1455 to detect two ROIs: i) the limiting membrane of whole cell that was detected with HCS
1456 CellMask™ Blue staining; ii) the nuclear region that was detected by DAPI staining. Important
1457 to note that in the cases where perinuclear region of the cells including microtubule organizing
1458 center (MTOC) was not detected in Z-projection, this ROI was manually corrected. In the
1459 second step of the protocol another script was used where “Spot detector” and “Colocalization”
1460 modules were combined. Thus, we were able to detect the number of lysosomes, the number of
1461 α -syn fibrils puncta, and the number of lysosomes colocalizing with the α -syn fibrils. Number
1462 of peripheral lysosomes were calculated by simply subtracting the number of centrally located
1463 lysosomes from the whole number of lysosomes and the percentages central and peripheral
1464 lysosomes were calculated accordingly. Same protocols were used to quantify the LysoTracker
1465 Deep Red and MagicRed Cathepsin B positive lysosomes where HCS CellMask™ Blue and
1466 Cell Tracker Blue (Invitrogen) staining were used in addition to DAPI staining respectively.

1467

1468 *TNT counting*

1469 A semi-automatized “TNT counting” tool in ICY software was used for TNT counting
1470 experiments as previously described [20,129]. Briefly, total number of cells were counted in
1471 each image and the connection between each cell pair was evaluated by scanning through the
1472 Z-stacks. Cell pairs that are connected by a protrusion that fits to certain criteria that are used

1473 to discriminate TNTs from other cellular protrusions (such as having thin, straight, and
1474 uninterrupted connections that are not touching to the substratum) were counted as “TNTs” and
1475 connected by a line using a free-hand line tool. Total number of cells and number of TNT-
1476 connected cells were automatically counted by the tool. Thus, data were presented as percentage
1477 of TNT connected cells.

1478

1479 *Lysosome size (on-section CLEM)*

1480 FM and EM images from the same section were overlaid and correlated to each other. LAMP1
1481 immunogold labelled organelles (lysosomes) were selected blindly and their size was measured
1482 using the “lasso” tool in Fiji. Afterwards the lysosomes were clustered based on presence of α -
1483 syn fibrils, and their size distribution was plotted.

1484

1485 *Lysosome size (SR microscopy)*

1486 Diameter of lysosomes were measured by using free-hand straight line tool of FiJi software.
1487 For each condition (control lysosomes and lysosomes containing α -syn or not), SR images were
1488 zoomed, and diameter of randomly selected lysosomes was measured.

1489

1490 *Lysosome number*

1491 The average number of lysosomes in control cells and in cells treated with α -syn fibrils were
1492 counted by using the “Spot detector” tool in ICY software.

1493

1494 *Object-based 3D colocalization analysis (Imaris software)*

1495 ROI for each was created by using “Surface” tool in the Surpass mode in Imaris. For each cell
1496 puncta of interest (Gal3-GFP, α -syn-GFP, α -syn fibrils and LAMP1+ puncta) in different colors
1497 were detected by “Spots” tool. Then colocalization was performed first for each pair of interest,
1498 and then for triple presence of the puncta by using “Colocalization” tool.

1499

1500 **Statistical analysis**

1501 Data collected at least from 3 independent experiments was presented as Mean \pm SEM. Exact
1502 number of experiments and number of cells analysed per condition for each experiment is
1503 presented in the Figure legends. All data were first subjected to a D’Agostino-Pearson omnibus
1504 normality test. Values having Gaussian distribution were further analysed by two-tailed *t*-test

1505 and one-way ANOVA followed by Tukey's multiple comparison tests for paired and multiple
1506 comparisons respectively. Values having non-Gaussian distribution were analysed by Whitney-
1507 Mann *U*-test and Kruskal-Wallis nonparametric ANOVA test followed by Dunn's multiple
1508 comparison tests for paired and multiple comparisons respectively. Paired set of data were
1509 analysed by paired-*t* test.

1510 **Acknowledgements**

1511 The authors thank all the lab members for useful discussion. We are grateful to Institut Pasteur
1512 Image Analysis Hub (IAH) for their help in quantitative image analysis, Audrey Salles from
1513 Unit of Technology and Service Photonic BioImaging platform (UTechS PBI, Institut Pasteur)
1514 and Cécile Leduc from Cell Polarity, Migration and Cancer unit, Institut Pasteur, for their help
1515 in SIM acquisitions. UTechS PBI, part of the France–BioImaging infrastructure network (FBI)
1516 acknowledges Agence Nationale de la Recherche (ANR-10-INSB-04), ANR/FBI and the
1517 Région Ile-de-France Domaine d’Intérêt Majeur-Malinf program for the use of SIM. We thank
1518 Alexandre Dufour for writing the script for the lysosomal positioning analysis, Eric Kowarz for
1519 the pSBbi-PUR and pCMV (CAT) T7-SB100 plasmids, Andrea Ballabio (TIGEM) for TFEB-
1520 WT-GFP and TFEB-mut-GFP plasmids, and Jost Enninga (Institut Pasteur) and Kristine
1521 Schauer (Institut Curie) for discussion. We also acknowledge Cilia de Heus (UMCU) for her
1522 assistance in CLEM experiments.

1523 **References**

- 1524 1. Soto C, Pritzkow S. Protein misfolding, aggregation, and conformational strains in
1525 neurodegenerative diseases. *Nat Neurosci.* 2018;21: 1332–1340. doi:10.1038/s41593-
1526 018-0235-9
- 1527 2. Gan L, Cookson MR, Petrucelli L, La Spada AR. Converging pathways in
1528 neurodegeneration, from genetics to mechanisms. *Nat Neurosci.* 2018;21: 1300–1309.
1529 doi:10.1038/s41593-018-0237-7
- 1530 3. Poewe W. Nature Reviews Disease Primers. *Nat Rev Dis Primer.* : 52.
- 1531 4. Volpicelli-Daley LA, Gamble KL, Schultheiss CE, Riddle DM, West AB, Lee VM-Y.
1532 Formation of α -synuclein Lewy neurite-like aggregates in axons impedes the transport
1533 of distinct endosomes. Martin TFJ, editor. *Mol Biol Cell.* 2014;25: 4010–4023.
1534 doi:10.1091/mbc.e14-02-0741
- 1535 5. Braak H, Tredici KD, Rüb U, de Vos RAI, Jansen Steur ENH, Braak E. Staging of brain
1536 pathology related to sporadic Parkinson’s disease. *Neurobiol Aging.* 2003;24: 197–
1537 211. doi:10.1016/S0197-4580(02)00065-9
- 1538 6. Takamatsu Y, Fujita M, Ho GJ, Wada R, Sugama S, Takenouchi T, et al. Motor and
1539 Nonmotor Symptoms of Parkinson’s Disease: Antagonistic Pleiotropy Phenomena
1540 Derived from α -Synuclein Evolvability? *Park Dis.* 2018;2018: 5789424.
1541 doi:10.1155/2018/5789424
- 1542 7. McCann H, Stevens CH, Cartwright H, Halliday GM. α -Synucleinopathy phenotypes.
1543 *Parkinsonism Relat Disord.* 2014;20: 62–67. doi:10.1016/S1353-8020(13)70017-8
- 1544 8. Taguchi K, Watanabe Y, Tsujimura A, Tanaka M. Brain region-dependent differential
1545 expression of alpha-synuclein: α -Synuclein Differential Expression. *J Comp Neurol.*
1546 2016;524: 1236–1258. doi:10.1002/cne.23901
- 1547 9. Chandra S, Chen X, Rizo J, Jahn R, Südhof TC. A Broken α -Helix in Folded α -Synuclein. *J*
1548 *Biol Chem.* 2003;278: 15313–15318. doi:10.1074/jbc.M213128200
- 1549 10. Varkey J, Isas JM, Mizuno N, Jensen MB, Bhatia VK, Jao CC, et al. Membrane Curvature
1550 Induction and Tubulation Are Common Features of Synucleins and Apolipoproteins. *J*
1551 *Biol Chem.* 2010;285: 32486–32493. doi:10.1074/jbc.M110.139576
- 1552 11. Meade RM, Fairlie DP, Mason JM. Alpha-synuclein structure and Parkinson’s disease –
1553 lessons and emerging principles. *Mol Neurodegener.* 2019;14:29: 10.1186/s13024-
1554 019-0329–1. doi:10.1186/s13024-019-0329-1
- 1555 12. Huang M, Wang B, Li X, Fu C, Wang C, Kang X. α -Synuclein: A Multifunctional Player in
1556 Exocytosis, Endocytosis, and Vesicle Recycling. *Front Neurosci.* 2019;13: 28.
1557 doi:10.3389/fnins.2019.00028

- 1558 13. Burré J, Sharma M, Tsetsenis T, Buchman V, Südhof TC. α -Synuclein Promotes SNARE-
1559 Complex Assembly in vivo and in vitro. *Science*. 2011; 1663–1667.
- 1560 14. Sun J, Wang L, Bao H, Premi S, Das U, Chapman ER, et al. Functional cooperation of α -
1561 synuclein and VAMP2 in synaptic vesicle recycling. *Proc Natl Acad Sci*. 2019;116:
1562 11113–11115. doi:10.1073/pnas.1903049116
- 1563 15. Man WK, Tahirbegi B, Vrettas MD, Preet S, Ying L, Vendruscolo M, et al. The docking of
1564 synaptic vesicles on the presynaptic membrane induced by α -synuclein is modulated
1565 by lipid composition. *Nat Commun*. 2021;12: 927. doi:10.1038/s41467-021-21027-4
- 1566 16. Braak H, Rub U, Gai WP, Del Tredici K. Idiopathic Parkinson’s disease: possible routes by
1567 which vulnerable neuronal types may be subject to neuroinvasion by an unknown
1568 pathogen. *J Neural Transm*. 2003;110: 517–536. doi:10.1007/s00702-002-0808-2
- 1569 17. Bae E-J, Yang N-Y, Song M, Lee CS, Lee JS, Jung BC, et al. Glucocerebrosidase depletion
1570 enhances cell-to-cell transmission of α -synuclein. *Nat Commun*. 2014;5:
1571 doi:10.1038/ncomms5755. doi:10.1038/ncomms5755
- 1572 18. Domert J, Sackmann C, Severinsson E, Agholme L, Bergström J, Ingelsson M, et al.
1573 Aggregated Alpha-Synuclein Transfer Efficiently between Cultured Human Neuron-
1574 Like Cells and Localize to Lysosomes. Witt SN, editor. *PLOS ONE*. 2016;11: e0168700.
1575 doi:10.1371/journal.pone.0168700
- 1576 19. Abounit S, Bousset L, Loria F, Zhu S, Chaumont F, Pieri L, et al. Tunneling nanotubes
1577 spread fibrillar α -synuclein by intercellular trafficking of lysosomes. *EMBO J*. 2016;35:
1578 2120–2138. doi:10.15252/embj.201593411
- 1579 20. Dilsizoglu Senol A, Pepe A, Grudina C, Sassoon N, Reiko U, Bousset L, et al. Effect of
1580 tolytoxin on tunneling nanotube formation and function. *Sci Rep*. 2019;9: 5741.
1581 doi:10.1038/s41598-019-42161-6
- 1582 21. Loria F, Vargas JY, Bousset L, Syan S, Salles A, Melki R, et al. α -Synuclein transfer
1583 between neurons and astrocytes indicates that astrocytes play a role in degradation
1584 rather than in spreading. *Acta Neuropathol (Berl)*. 2017;134: 789–808.
1585 doi:10.1007/s00401-017-1746-2
- 1586 22. Vargas JY, Loria F, Wu Y, Córdova G, Nonaka T, Bellow S, et al. The Wnt/Ca²⁺ pathway is
1587 involved in interneuronal communication mediated by tunneling nanotubes. *EMBO J*.
1588 2019;38: e101230. doi:10.15252/embj.2018101230
- 1589 23. Desplats P, Lee H-J, Bae E-J, Patrick C, Rockenstein E, Crews L, et al. Inclusion formation
1590 and neuronal cell death through neuron-to-neuron transmission of α -synuclein. *Proc*
1591 *Natl Acad Sci*. 2009;106: 13010–13015. doi:10.1073/pnas.0903691106
- 1592 24. Luk KC, Kehm V, Carroll J, Zhang B, O’Brien P, Trojanowski JQ, et al. Pathological -
1593 Synuclein Transmission Initiates Parkinson-like Neurodegeneration in Nontransgenic
1594 Mice. *Science*. 2012;338: 949–953. doi:10.1126/science.1227157

- 1595 25. Recasens A, Dehay B, Bové J, Carballo-Carbajal I, Dovero S, Pérez-Villalba A, et al. Lewy
1596 body extracts from Parkinson disease brains trigger α -synuclein pathology and
1597 neurodegeneration in mice and monkeys: LB-Induced Pathology. *Ann Neurol*. 2014;75:
1598 351–362. doi:10.1002/ana.24066
- 1599 26. Kordower JH, Chu Y, Hauser RA, Freeman TB, Olanow CW. Lewy body–like pathology in
1600 long-term embryonic nigral transplants in Parkinson’s disease. *Nat Med*. 2008;14:
1601 504–506. doi:10.1038/nm1747
- 1602 27. Masuda-Suzukake M, Nonaka T, Hosokawa M, Kubo M, Shimozawa A, Akiyama H, et al.
1603 Pathological alpha-synuclein propagates through neural networks. 2014;2:
1604 <http://www.actaneurocomms.org/content/2/1/88>.
- 1605 28. Ayers JI, Brooks MM, Rutherford NJ, Howard JK, Sorrentino ZA, Riffe CJ, et al. Robust
1606 Central Nervous System Pathology in Transgenic Mice following Peripheral Injection of
1607 α -Synuclein Fibrils. *J Virol*. 2017;91: e02095-16.
- 1608 29. Brundin P, Melki R, Kopito R. Prion-like transmission of protein aggregates in
1609 neurodegenerative diseases. *Nat Rev Mol Cell Biol*. 2010;11: 301–307.
1610 doi:10.1038/nrm2873
- 1611 30. Masuda-Suzukake M, Nonaka T, Hosokawa M, Oikawa T, Arai T, Akiyama H, et al. Prion-
1612 like spreading of pathological α -synuclein in brain. *Brain*. 2013;136: 1128–1138.
1613 doi:10.1093/brain/awt037
- 1614 31. Rey NL, Wesson DW, Brundin P. The olfactory bulb as the entry site for prion-like
1615 propagation in neurodegenerative diseases. *Neurobiol Dis*. 2018;109: 226–248.
1616 doi:10.1016/j.nbd.2016.12.013
- 1617 32. Victoria GS, Zurzolo C. The spread of prion-like proteins by lysosomes and tunneling
1618 nanotubes: Implications for neurodegenerative diseases. *J Cell Biol*. 2017;216: 2633–
1619 2644. doi:10.1083/jcb.201701047
- 1620 33. Angot E, Steiner JA, Lema Tomé CM, Ekström P, Mattsson B, Björklund A, et al. Alpha-
1621 Synuclein Cell-to-Cell Transfer and Seeding in Grafted Dopaminergic Neurons In Vivo.
1622 Mosley RL, editor. *PLoS ONE*. 2012;7: e39465. doi:10.1371/journal.pone.0039465
- 1623 34. Hansen C, Angot E, Bergström A-L, Steiner JA, Pieri L, Paul G, et al. α -Synuclein
1624 propagates from mouse brain to grafted dopaminergic neurons and seeds aggregation
1625 in cultured human cells. *J Clin Invest*. 2011;121: 715–725. doi:10.1172/JCI43366
- 1626 35. Vargas JY, Grudina C, Zurzolo C. The prion-like spreading of α -synuclein: From in vitro to
1627 in vivo models of Parkinson’s disease. *Ageing Res Rev*. 2019;50: 89–101.
1628 doi:10.1016/j.arr.2019.01.012
- 1629 36. Dieriks BV, Park TI-H, Fourie C, Faull RLM, Dragunow M, Curtis MA. α -synuclein transfer
1630 through tunneling nanotubes occurs in SH-SY5Y cells and primary brain pericytes from
1631 Parkinson’s disease patients. *Sci Rep*. 2017;7: 42984. doi:10.1038/srep42984

- 1632 37. Rustom A. Nanotubular Highways for Intercellular Organelle Transport. *Science*.
1633 2004;303: 1007–1010. doi:10.1126/science.1093133
- 1634 38. Abounit S, Zurzolo C. Wiring through tunneling nanotubes - from electrical signals to
1635 organelle transfer. *J Cell Sci*. 2012;125: 1089–1098. doi:10.1242/jcs.083279
- 1636 39. Marzo L, Gousset K, Zurzolo C. Multifaceted Roles of Tunneling Nanotubes in
1637 Intercellular Communication. *Front Physiol*. 2012;3: doi: 10.3389/fphys.2012.00072.
1638 doi:10.3389/fphys.2012.00072
- 1639 40. Gerdes H-H, Bukoreshtliev NV, Barroso JFV. Tunneling nanotubes: A new route for the
1640 exchange of components between animal cells. *FEBS Lett*. 2007;581: 2194–2201.
1641 doi:10.1016/j.febslet.2007.03.071
- 1642 41. Cordero Cervantes D, Zurzolo C. Peering into tunneling nanotubes—The path forward.
1643 *EMBO J*. 2021 [cited 29 Mar 2021]. doi:10.15252/embj.2020105789
- 1644 42. Chinnery HR, Pearlman E, McMenemy PG. Cutting Edge: Membrane Nanotubes In
1645 Vivo: A Feature of MHC Class II⁺ Cells in the Mouse Cornea. *J Immunol*. 2008;180:
1646 5779–5783. doi:10.4049/jimmunol.180.9.5779
- 1647 43. Lou E, Fujisawa S, Morozov A, Barlas A, Romin Y, Dogan Y, et al. Tunneling Nanotubes
1648 Provide a Unique Conduit for Intercellular Transfer of Cellular Contents in Human
1649 Malignant Pleural Mesothelioma. Yang P-C, editor. *PLoS ONE*. 2012;7: e33093.
1650 doi:10.1371/journal.pone.0033093
- 1651 44. Pasquier J, Guerrouahen BS, Al Thawadi H, Ghiabi P, Maleki M, Abu-Kaoud N, et al.
1652 Preferential transfer of mitochondria from endothelial to cancer cells through
1653 tunneling nanotubes modulates chemoresistance. *J Transl Med*. 2013;11: 94.
1654 doi:10.1186/1479-5876-11-94
- 1655 45. Osswald M, Jung E, Sahm F, Solecki G, Venkataramani V, Blaes J, et al. Brain tumour
1656 cells interconnect to a functional and resistant network. *Nature*. 2015;528: 93–98.
1657 doi:10.1038/nature16071
- 1658 46. Seyed-Razavi Y, Hickey MJ, Kuffová L, McMenemy PG, Chinnery HR. Membrane
1659 nanotubes in myeloid cells in the adult mouse cornea represent a novel mode of
1660 immune cell interaction. *Immunol Cell Biol*. 2013;91: 89–95. doi:10.1038/icb.2012.52
- 1661 47. Alarcon-Martinez L, Villafranca-Baughman D, Quintero H, Kacerovsky JB, Dotigny F,
1662 Murai KK, et al. Interpericyte tunnelling nanotubes regulate neurovascular coupling.
1663 *Nature*. 2020;585: 91–95. doi:10.1038/s41586-020-2589-x
- 1664 48. Sartori-Rupp A, Cordero Cervantes D, Pepe A, Gousset K, Delage E, Corroyer-Dulmont S,
1665 et al. Correlative cryo-electron microscopy reveals the structure of TNTs in neuronal
1666 cells. *Nat Commun*. 2019;10: <https://doi.org/10.1038/s41467-018-08178-7>.
1667 doi:10.1038/s41467-018-08178-7

- 1668 49. Zurzolo C. Tunneling nanotubes: Reshaping connectivity. *Curr Opin Cell Biol.* 2021;71:
1669 139–147. doi:10.1016/j.ceb.2021.03.003
- 1670 50. Gousset K, Schiff E, Langevin C, Marijanovic Z, Caputo A, Browman DT, et al. Prions
1671 hijack tunnelling nanotubes for intercellular spread. *Nat Cell Biol.* 2009;11: 328–336.
1672 doi:10.1038/ncb1841
- 1673 51. Victoria GS, Arkhipenko A, Zhu S, Syan S, Zurzolo C. Astrocyte-to-neuron intercellular
1674 prion transfer is mediated by cell-cell contact. *Sci Rep.* 2016;6: 20762.
1675 doi:10.1038/srep20762
- 1676 52. Abounit S, Wu JW, Duff K, Victoria GS, Zurzolo C. Tunneling nanotubes: A possible
1677 highway in the spreading of tau and other prion-like proteins in neurodegenerative
1678 diseases. *Prion.* 2016;10: 344–351. doi:10.1080/19336896.2016.1223003
- 1679 53. Costanzo M, Abounit S, Marzo L, Danckaert A, Chamoun Z, Roux P, et al. Transfer of
1680 polyglutamine aggregates in neuronal cells occurs in tunneling nanotubes. *J Cell Sci.*
1681 2013;126: 3678–3685. doi:10.1242/jcs.126086
- 1682 54. Tardivel M, Bégard S, Bousset L, Dujardin S, Coens A, Melki R, et al. Tunneling nanotube
1683 (TNT)-mediated neuron-to neuron transfer of pathological Tau protein assemblies.
1684 *Acta Neuropathol Commun.* 2016;4: 117. doi:10.1186/s40478-016-0386-4
- 1685 55. Chastagner P, Loria F, Vargas JY, Tois J, I Diamond M, Okafo G, et al. Fate and
1686 propagation of endogenously formed Tau aggregates in neuronal cells. *EMBO Mol*
1687 *Med.* 2020;12. doi:10.15252/emmm.202012025
- 1688 56. Grudina C, Kouroupi G, Nonaka T, Hasegawa M, Matsas R, Zurzolo C. Human NPCs can
1689 degrade α -syn fibrils and transfer them preferentially in a cell contact-dependent
1690 manner possibly through TNT-like structures. *Neurobiol Dis.* 2019;132: 104609.
1691 doi:10.1016/j.nbd.2019.104609
- 1692 57. Luzio JP, Parkinson MDJ, Gray SR, Bright NA. The delivery of endocytosed cargo to
1693 lysosomes. *Biochem Soc Trans.* 2009;37: 1019–1021. doi:10.1042/BST0371019
- 1694 58. Luzio JP, Pryor PR, Bright NA. Lysosomes: fusion and function. *Nat Rev Mol Cell Biol.*
1695 2007;8: 622–632. doi:10.1038/nrm2217
- 1696 59. Singh R, Cuervo AM. Autophagy in the Cellular Energetic Balance. *Cell Metab.* 2011;13:
1697 495–504. doi:10.1016/j.cmet.2011.04.004
- 1698 60. Rabinowitz JD, White E. Autophagy and Metabolism. *Science.* 2010;330: 1344–1348.
1699 doi:10.1126/science.1193497
- 1700 61. Settembre C, Fraldi A, Medina DL, Ballabio A. Signals from the lysosome: a control
1701 centre for cellular clearance and energy metabolism. *Nat Rev Mol Cell Biol.* 2013;14:
1702 283–296. doi:10.1038/nrm3565

- 1703 62. Settembre C, Ballabio A. Lysosomal Adaptation: How the Lysosome Responds to
1704 External Cues. *Cold Spring Harb Perspect Biol.* 2014;6: a016907–a016907.
1705 doi:10.1101/cshperspect.a016907
- 1706 63. Lim C-Y, Zoncu R. The lysosome as a command-and-control center for cellular
1707 metabolism. *J Cell Biol.* 2016;214: 653–664. doi:10.1083/jcb.201607005
- 1708 64. Perera RM, Zoncu R. The Lysosome as a Regulatory Hub. *Annu Rev Cell Dev Biol.*
1709 2016;32: 223–253. doi:10.1146/annurev-cellbio-111315-125125
- 1710 65. Shin HR, Zoncu R. The Lysosome at the Intersection of Cellular Growth and Destruction.
1711 *Dev Cell.* 2020;54: 226–238. doi:10.1016/j.devcel.2020.06.010
- 1712 66. Fraldi A, Klein AD, Medina DL, Settembre C. Brain Disorders Due to Lysosomal
1713 Dysfunction. *Annu Rev Neurosci.* 2016;39: 277–295. doi:10.1146/annurev-neuro-
1714 070815-014031
- 1715 67. Chu Y, Dodiya H, Aebischer P, Olanow CW, Kordower JH. Alterations in lysosomal and
1716 proteasomal markers in Parkinson’s disease: Relationship to alpha-synuclein
1717 inclusions. *Neurobiol Dis.* 2009;35: 385–398. doi:10.1016/j.nbd.2009.05.023
- 1718 68. Dehay B, Bove J, Rodriguez-Muela N, Perier C, Recasens A, Boya P, et al. Pathogenic
1719 Lysosomal Depletion in Parkinson’s Disease. *J Neurosci.* 2010;30: 12535–12544.
1720 doi:10.1523/JNEUROSCI.1920-10.2010
- 1721 69. Mazzulli JR, Zunke F, Isacson O, Studer L, Krainc D. α -Synuclein–induced lysosomal
1722 dysfunction occurs through disruptions in protein trafficking in human midbrain
1723 synucleinopathy models. *Proc Natl Acad Sci.* 2016;113: 1931–1936.
1724 doi:10.1073/pnas.1520335113
- 1725 70. Hoffmann A-C, Minakaki G, Menges S, Salvi R, Savitskiy S, Kazman A, et al. Extracellular
1726 aggregated alpha synuclein primarily triggers lysosomal dysfunction in neural cells
1727 prevented by trehalose. *Sci Rep.* 2019;9: 544. doi:10.1038/s41598-018-35811-8
- 1728 71. Mazzulli JR, Xu Y-H, Sun Y, Knight AL, McLean PJ, Caldwell GA, et al. Gaucher Disease
1729 Glucocerebrosidase and α -Synuclein Form a Bidirectional Pathogenic Loop in
1730 Synucleinopathies. *Cell.* 2011;146: 37–52. doi:10.1016/j.cell.2011.06.001
- 1731 72. Boya P. Lysosomal Function and Dysfunction: Mechanism and Disease. *Antioxid Redox*
1732 *Signal.* 2012;17: 766–774. doi:10.1089/ars.2011.4405
- 1733 73. Freeman D, Cedillos R, Choyke S, Lukic Z, McGuire K, Marvin S, et al. Alpha-Synuclein
1734 Induces Lysosomal Rupture and Cathepsin Dependent Reactive Oxygen Species
1735 Following Endocytosis. Kahle PJ, editor. *PLoS ONE.* 2013;8: e62143.
1736 doi:10.1371/journal.pone.0062143
- 1737 74. Flavin WP, Bousset L, Green ZC, Chu Y, Skarpathiotis S, Chaney MJ, et al. Endocytic
1738 vesicle rupture is a conserved mechanism of cellular invasion by amyloid proteins.
1739 *Acta Neuropathol (Berl).* 2017;134: 629–653. doi:10.1007/s00401-017-1722-x

- 1740 75. Jongsma ML, Bakker J, Cabukusta B, Liv N, Elsland D, Fermie J, et al. SKIP - HOPS recruits
1741 TBC 1D15 for a Rab7-to-Arl8b identity switch to control late endosome transport.
1742 EMBO J. 2020;39. doi:10.15252/embj.2019102301
- 1743 76. Fermie J, Liv N, ten Brink C, van Donselaar EG, Müller WH, Schieber NL, et al. Single
1744 organelle dynamics linked to 3D structure by correlative live-cell imaging and 3D
1745 electron microscopy. *Traffic*. 2018;19: 354–369. doi:10.1111/tra.12557
- 1746 77. Meel E, Klumperman J. Imaging and imagination: understanding the endo-lysosomal
1747 system. *Histochem Cell Biol*. 2008;129: 253–266. doi:10.1007/s00418-008-0384-0
- 1748 78. Klumperman J, Raposo G. The Complex Ultrastructure of the Endolysosomal System.
1749 *Cold Spring Harb Perspect Biol*. 2014;6: a016857–a016857.
1750 doi:10.1101/cshperspect.a016857
- 1751 79. Mohammadian S, Fokkema J, Agronskaia AV, Liv N, de Heus C, van Donselaar E, et al.
1752 High accuracy, fiducial marker-based image registration of correlative microscopy
1753 images. *Sci Rep*. 2019;9: 3211. doi:10.1038/s41598-019-40098-4
- 1754 80. Cortese K, Vicidomini G, Gagliani MC, Boccacci P, Diaspro A, Tacchetti C. High Data
1755 Output Method for 3-D Correlative Light-Electron Microscopy Using Ultrathin
1756 Cryosections. In: Sousa AA, Kruhlak MJ, editors. *Nanoimaging*. Totowa, NJ: Humana
1757 Press; 2013. pp. 417–437. doi:10.1007/978-1-62703-137-0_23
- 1758 81. Calafate S, Flavin W, Verstreken P, Moechars D. Loss of Bin1 Promotes the Propagation
1759 of Tau Pathology. *Cell Rep*. 2016;17: 931–940. doi:10.1016/j.celrep.2016.09.063
- 1760 82. Papadopoulos C, Kirchner P, Bug M, Grum D, Koerver L, Schulze N, et al. VCP /p97
1761 cooperates with YOD 1, UBXD 1 and PLAA to drive clearance of ruptured lysosomes by
1762 autophagy. *EMBO J*. 2017;36: 135–150. doi:10.15252/embj.201695148
- 1763 83. Oku Y, Murakami K, Irie K, Hoseki J, Sakai Y. Synthesized A β 42 Caused Intracellular
1764 Oxidative Damage, Leading to Cell Death, via Lysosome Rupture. *Cell Struct Funct*.
1765 2017;42: 71–79. doi:10.1247/csf.17006
- 1766 84. Maejima I, Takahashi A, Omori H, Kimura T, Takabatake Y, Saitoh T, et al. Autophagy
1767 sequesters damaged lysosomes to control lysosomal biogenesis and kidney injury.
1768 *EMBO J*. 2013;32: 2336–2347. doi:10.1038/emboj.2013.171
- 1769 85. Jiang P, Gan M, Yen S-H, McLean PJ, Dickson DW. Impaired endo-lysosomal membrane
1770 integrity accelerates the seeding progression of α -synuclein aggregates. *Sci Rep*.
1771 2017;7: 7690. doi:10.1038/s41598-017-08149-w
- 1772 86. Nonaka T, Watanabe ST, Iwatsubo T, Hasegawa M. Seeded Aggregation and Toxicity of
1773 α -Synuclein and Tau: CELLULAR MODELS OF NEURODEGENERATIVE DISEASES. *J Biol*
1774 *Chem*. 2010;285: 34885–34898. doi:10.1074/jbc.M110.148460

- 1775 87. Shrivastava AN, Bousset L, Renner M, Redeker V, Savistchenko J, Triller A, et al.
1776 Differential Membrane Binding and Seeding of Distinct α -Synuclein Fibrillar
1777 Polymorphs. *Biophys J*. 2020;118: 1301–1320. doi:10.1016/j.bpj.2020.01.022
- 1778 88. Yang X, Williams JK, Yan R, Mouradian MM, Baum J. Increased Dynamics of α -Synuclein
1779 Fibrils by β -Synuclein Leads to Reduced Seeding and Cytotoxicity. *Sci Rep*. 2019;9:
1780 17579. doi:10.1038/s41598-019-54063-8
- 1781 89. Sangwan S, Sahay S, Murray KA, Morgan S, Guenther EL, Jiang L, et al. Inhibition of
1782 synucleinopathic seeding by rationally designed inhibitors. *eLife*. 2020;9: e46775.
1783 doi:10.7554/eLife.46775
- 1784 90. Guardia CM, Farías GG, Jia R, Pu J, Bonifacino JS. BORC Functions Upstream of Kinesins
1785 1 and 3 to Coordinate Regional Movement of Lysosomes along Different Microtubule
1786 Tracks. *Cell Rep*. 2016;17: 1950–1961. doi:10.1016/j.celrep.2016.10.062
- 1787 91. Pu J, Guardia CM, Keren-Kaplan T, Bonifacino JS. Mechanisms and functions of
1788 lysosome positioning. *J Cell Sci*. 2016;129: 4329–4339. doi:10.1242/jcs.196287
- 1789 92. Cabukusta B, Neefjes J. Mechanisms of lysosomal positioning and movement. *Traffic*.
1790 2018;19: 761–769. doi:10.1111/tra.12587
- 1791 93. Jongsma MLM, Berlin I, Wijdeven RHM, Janssen L, Janssen GMC, Garstka MA, et al. An
1792 ER-Associated Pathway Defines Endosomal Architecture for Controlled Cargo
1793 Transport. *Cell*. 2016;166: 152–166. doi:10.1016/j.cell.2016.05.078
- 1794 94. Bajaj L, Lotfi P, Pal R, Ronza A di, Sharma J, Sardiello M. Lysosome biogenesis in health
1795 and disease. *J Neurochem*. 2019;148: 573–589. doi:10.1111/jnc.14564
- 1796 95. Medina DL, Fraldi A, Bouche V, Annunziata F, Mansueto G, Spampanato C, et al.
1797 Transcriptional Activation of Lysosomal Exocytosis Promotes Cellular Clearance. *Dev*
1798 *Cell*. 2011;21: 421–430. doi:10.1016/j.devcel.2011.07.016
- 1799 96. Willett R, Martina JA, Zewe JP, Wills R, Hammond GRV, Puertollano R. TFEB regulates
1800 lysosomal positioning by modulating TMEM55B expression and JIP4 recruitment to
1801 lysosomes. *Nat Commun*. 2017;8: 1580. doi:10.1038/s41467-017-01871-z
- 1802 97. Zhang J, Johnson JL, He J, Napolitano G, Ramadass M, Rocca C, et al. Cystinosin, the
1803 small GTPase Rab11, and the Rab7 effector RILP regulate intracellular trafficking of the
1804 chaperone-mediated autophagy receptor LAMP2A. *J Biol Chem*. 2017;292: 10328–
1805 10346. doi:10.1074/jbc.M116.764076
- 1806 98. Hofmann I, Munro S. An N-terminally acetylated Arf-like GTPase is localised to
1807 lysosomes and affects their motility. *J Cell Sci*. 2006;119: 1494–1503.
1808 doi:10.1242/jcs.02958
- 1809 99. Bagshaw RD, Callahan JW, Mahuran DJ. The Arf-family protein, Arl8b, is involved in the
1810 spatial distribution of lysosomes. *Biochem Biophys Res Commun*. 2006;344: 1186–
1811 1191. doi:10.1016/j.bbrc.2006.03.221

- 1812 100. Pu J, Schindler C, Jia R, Jarnik M, Backlund P, Bonifacino JS. BORG, a Multisubunit
1813 Complex that Regulates Lysosome Positioning. *Dev Cell*. 2015;33: 176–188.
1814 doi:10.1016/j.devcel.2015.02.011
- 1815 101. Nakata T, Hirokawa N. Point mutation of adenosine triphosphate-binding motif
1816 generated rigor kinesin that selectively blocks anterograde lysosome membrane
1817 transport. *J Cell Biol*. 1995;131: 1039–1053. doi:10.1083/jcb.131.4.1039
- 1818 102. Rosa-Ferreira C, Munro S. Arl8 and SKIP Act Together to Link Lysosomes to Kinesin-1.
1819 *Dev Cell*. 2011;21: 1171–1178. doi:10.1016/j.devcel.2011.10.007
- 1820 103. Korolchuk VI, Saiki S, Lichtenberg M, Siddiqi FH, Roberts EA, Imarisio S, et al. Lysosomal
1821 positioning coordinates cellular nutrient responses. *Nat Cell Biol*. 2011;13: 453–460.
1822 doi:10.1038/ncb2204
- 1823 104. Matsushita M, Tanaka S, Nakamura N, Inoue H, Kanazawa H. A Novel Kinesin-Like
1824 Protein, KIF1B β 3 Is Involved in the Movement of Lysosomes to the Cell Periphery in
1825 Non-Neuronal Cells: Novel Kinesin Motor for Lysosomal Movement. *Traffic*. 2004;5:
1826 140–151. doi:10.1111/j.1600-0854.2003.00165.x
- 1827 105. Bentley M, Decker H, Luisi J, Banker G. A novel assay reveals preferential binding
1828 between Rabs, kinesins, and specific endosomal subpopulations. *J Cell Biol*. 2015;208:
1829 273–281. doi:10.1083/jcb.201408056
- 1830 106. Naphade S, Sharma J, Gaide Chevonnay HP, Shook MA, Yeagy BA, Rocca CJ, et al. Brief
1831 Reports: Lysosomal Cross-Correction by Hematopoietic Stem Cell-Derived
1832 Macrophages Via Tunneling Nanotubes: Lysosomal Cross-Correction by Stem Cells Via
1833 TNTs. *STEM CELLS*. 2015;33: 301–309. doi:10.1002/stem.1835
- 1834 107. Del Tredici K, Braak H. Review: Sporadic Parkinson’s disease: development and
1835 distribution of α -synuclein pathology. *Neuropathol Appl Neurobiol*. 2016;42: 33–50.
1836 doi:10.1111/nan.12298
- 1837 108. Usenovic M, Tresse E, Mazzulli JR, Taylor JP, Krainc D. Deficiency of ATP13A2 Leads to
1838 Lysosomal Dysfunction, α -Synuclein Accumulation, and Neurotoxicity. *J Neurosci*.
1839 2012;32: 4240–4246. doi:10.1523/JNEUROSCI.5575-11.2012
- 1840 109. Chen PM, Gombart ZJ, Chen JW. Chloroquine treatment of ARPE-19 cells leads to
1841 lysosome dilation and intracellular lipid accumulation: possible implications of
1842 lysosomal dysfunction in macular degeneration. *Cell Biosci*. 2011;1: 10.
1843 doi:10.1186/2045-3701-1-10
- 1844 110. Boya P, Kroemer G. Lysosomal membrane permeabilization in cell death. *Oncogene*.
1845 2008;27: 6434–6451. doi:10.1038/onc.2008.310
- 1846 111. Radulovic M, Schink KO, Wenzel EM, Nähse V, Bongiovanni A, Lafont F, et al. ESCRT -
1847 mediated lysosome repair precedes lysophagy and promotes cell survival. *EMBO J*.
1848 2018;37. doi:10.15252/embj.201899753

- 1849 112. Skowrya ML, Schlesinger PH, Naismith TV, Hanson PI. Triggered recruitment of ESCRT
1850 machinery promotes endolysosomal repair. *Science*. 2018;360: eaar5078.
1851 doi:10.1126/science.aar5078
- 1852 113. Lynch-Day MA, Mao K, Wang K, Zhao M, Klionsky DJ. The Role of Autophagy in
1853 Parkinson's Disease. *Cold Spring Harb Perspect Med*. 2012;2: a009357–a009357.
1854 doi:10.1101/cshperspect.a009357
- 1855 114. Cui L, Zhao L-P, Ye J-Y, Yang L, Huang Y, Jiang X-P, et al. The Lysosomal Membrane
1856 Protein Lamp2 Alleviates Lysosomal Cell Death by Promoting Autophagic Flux in
1857 Ischemic Cardiomyocytes. *Front Cell Dev Biol*. 2020;8: 31.
1858 doi:10.3389/fcell.2020.00031
- 1859 115. Lashuel HA, Petre BM, Wall J, Simon M, Nowak RJ, Walz T, et al. α -Synuclein, Especially
1860 the Parkinson's Disease-associated Mutants, Forms Pore-like Annular and Tubular
1861 Protofibrils. *J Mol Biol*. 2002;322: 1089–1102. doi:10.1016/S0022-2836(02)00735-0
- 1862 116. Tosatto L, Andrighetti AO, Plotegher N, Antonini V, Tessari I, Ricci L, et al. Alpha-
1863 synuclein pore forming activity upon membrane association. *Biochim Biophys Acta*
1864 *BBA - Biomembr*. 2012;1818: 2876–2883. doi:10.1016/j.bbamem.2012.07.007
- 1865 117. Volles MJ, Lansbury PT. Vesicle Permeabilization by Protofibrillar α -Synuclein Is
1866 Sensitive to Parkinson's Disease-Linked Mutations and Occurs by a Pore-like
1867 Mechanism [†]. *Biochemistry*. 2002;41: 4595–4602. doi:10.1021/bi0121353
- 1868 118. Butler D, Bahr BA. Oxidative Stress and Lysosomes: CNS-Related Consequences and
1869 Implications for Lysosomal Enhancement Strategies and Induction of Autophagy.
1870 *Antioxid Redox Signal*. 2006;8: 185–196. doi:10.1089/ars.2006.8.185
- 1871 119. Perier C, Tieu K, Guegan C, Caspersen C, Jackson-Lewis V, Carelli V, et al. Complex I
1872 deficiency primes Bax-dependent neuronal apoptosis through mitochondrial oxidative
1873 damage. *Proc Natl Acad Sci*. 2005;102: 19126–19131. doi:10.1073/pnas.0508215102
- 1874 120. Bourdenx M, Dehay B. What lysosomes actually tell us about Parkinson's disease?
1875 *Ageing Res Rev*. 2016;32: 140–149. doi:10.1016/j.arr.2016.02.008
- 1876 121. Trinkaus VA, Riera-Tur I, Martínez-Sánchez A, Guo Q, Arzberger T, Baumeister W, et al.
1877 In situ architecture of neuronal α -Synuclein inclusions. : 46.
- 1878 122. Matteoni R, Kreis TE. Translocation and Clustering of Endosomes and Lysosomes
1879 Depends on Microbules. *J Cell Biol*. 1987;105: 1253–1265.
- 1880 123. Nakamura S, Shigeyama S, Minami S, Shima T, Akayama S, Matsuda T, et al. LC3
1881 lipidation is essential for TFEB activation during the lysosomal damage response to
1882 kidney injury. *Nat Cell Biol*. 2020;22: 1252–1263. doi:10.1038/s41556-020-00583-9
- 1883 124. Decressac M, Mattsson B, Weikop P, Lundblad M, Jakobsson J, Bjorklund A. TFEB-
1884 mediated autophagy rescues midbrain dopamine neurons from α -synuclein toxicity.
1885 *Proc Natl Acad Sci*. 2013;110: E1817–E1826. doi:10.1073/pnas.1305623110

- 1886 125. Gousset K, Marzo L, Commere P-H, Zurzolo C. Myo10 is a key regulator of TNT
1887 formation in neuronal cells. *J Cell Sci.* 2013;126: 4424–4435. doi:10.1242/jcs.129239
- 1888 126. Wang Y, Cui J, Sun X, Zhang Y. Tunneling-nanotube development in astrocytes depends
1889 on p53 activation. *Cell Death Differ.* 2011;18: 732–742. doi:10.1038/cdd.2010.147
- 1890 127. Shi Z, Sachs J, Rhoades E, Baumgart T. Biophysics of α -synuclein induced membrane
1891 remodelling. 2015; 19.
- 1892 128. Qi Y, Wang JKT, McMillian M, Chikaraishi DM. Characterization of a CNS Cell Line, CAD,
1893 in which Morphological Differentiation Is Initiated by Serum Deprivation. *J Neurosci.*
1894 1997;17: 1217–1225. doi:10.1523/JNEUROSCI.17-04-01217.1997
- 1895 129. Abounit S, Delage E, Zurzolo C. Identification and Characterization of Tunneling
1896 Nanotubes for Intercellular Trafficking. *Curr Protoc Cell Biol.* 2015;67: doi:
1897 10.1002/0471143030.cb1210s67. doi:10.1002/0471143030.cb1210s67
- 1898 130. Zhu S, Abounit S, Korth C, Zurzolo C. Transfer of disrupted-in-schizophrenia 1
1899 aggregates between neuronal-like cells occurs in tunnelling nanotubes and is
1900 promoted by dopamine. *Open Biol.* 2017;7: 160328. doi:10.1098/rsob.160328
- 1901 131. Delage E, Cervantes DC, Pénard E, Schmitt C, Syan S, Disanza A, et al. Differential
1902 identity of Filopodia and Tunneling Nanotubes revealed by the opposite functions of
1903 actin regulatory complexes. *Sci Rep.* 2016;6: 39632. doi:10.1038/srep39632
- 1904 132. Jia R, Guardia CM, Pu J, Chen Y, Bonifacino JS. BORC coordinates encounter and fusion
1905 of lysosomes with autophagosomes. *Autophagy.* 2017;13: 1648–1663.
1906 doi:10.1080/15548627.2017.1343768
- 1907 133. Kowarz E, Löscher D, Marschalek R. Optimized Sleeping Beauty transposons rapidly
1908 generate stable transgenic cell lines. *Biotechnol J.* 2015;10: 647–653.
1909 doi:10.1002/biot.201400821
- 1910 134. Mátés L, Chuah MKL, Belay E, Jerchow B, Manoj N, Acosta-Sanchez A, et al. Molecular
1911 evolution of a novel hyperactive Sleeping Beauty transposase enables robust stable
1912 gene transfer in vertebrates. *Nat Genet.* 2009;41: 753–761. doi:10.1038/ng.343
- 1913 135. Nonaka T, Iwatsubo T, Hasegawa M. Ubiquitination of α -Synuclein[†]. *Biochemistry.*
1914 2005;44: 361–368. doi:10.1021/bi0485528
- 1915 136. Boulanger J, Kervrann C, Bouthemy P, Elbau P, Sibarita J-B, Salamero J. Patch-Based
1916 Nonlocal Functional for Denoising Fluorescence Microscopy Image Sequences. *IEEE*
1917 *Trans Med Imaging.* 2010;29: 442–454. doi:10.1109/TMI.2009.2033991
- 1918 137. Oorschot V, de Wit H, Annaert WG, Klumperman J. A Novel Flat-embedding Method to
1919 Prepare Ultrathin Cryosections from Cultured Cells in Their In Situ Orientation. *J*
1920 *Histochem Cytochem.* 2002;50: 1067–1080. doi:10.1177/002215540205000809
- 1921 138. Slot JW, Geuze HJ. Cryosectioning and immunolabeling. *Nat Protoc.* 2007;2: 2480–2491.
1922 doi:10.1038/nprot.2007.365

1923 **Supporting information**

1924 **S1 Fig. EM images of control CAD cells.** (A) Resin embedded EM images of control CAD
1925 cells. Three examples of control lysosomes (indicated by blue squares) selected from different
1926 regions (indicated by red squares) of three different cells are presented. Scale bar for the cells:
1927 5 μm , for the selected regions: 1 μm , and for lysosomes: 0.2 μm . (B) On-section EM images of
1928 control CAD cells immunogold labelled with LAMP1¹⁰. Two examples of lysosomes were
1929 presented in insets selected from regions indicated by red and blue squares. Scale bar: 1 μm
1930 (for the insets: 0.2 μm).

1931

1932 **S2 Fig. α -Syn fibrils are transferred from donor to acceptor cells inside of lysosomes**
1933 **through TNTs.** Representative image of a TNT having a lysosome containing α -syn fibrils
1934 which is formed between α -syn loaded donor cell for 18 h (D) and H2B-GFP transfected
1935 acceptor cell (A) in 24 h of CAD-CAD co-culture. Z projection of donor and acceptor cells and
1936 lysosomes labelled with LAMP1 is presented (upper panels). Z projection of merged image
1937 with an additional staining of HCS CellMaskTM Blue, a bottom section (section no:3) where
1938 TNT is not visible and an upper section (section no:8) where TNT is visible are presented
1939 (middle panels). Arrows in the orthogonal view of the upper section and in insets are indicating
1940 the lysosome containing α -syn fibrils inside of the TNT (lower panels). Scale bar: 10 μm (for
1941 insets: 5 μm).

1942

1943 **S3 Fig. Schematic presentation of experimental designs.** (A) CAD cells were transiently
1944 transfected with Gal3-GFP (1), α -syn-GFP (2), or TFEB-WT-GFP (3) and treated with Alexa
1945 568- tagged α -syn fibrils for 18 h; cells were then analysed for the presence of Gal3-GFP
1946 puncta, α -syn-GFP puncta, or nuclear TFEB respectively. (B) Donor CAD cells were
1947 transiently transfected with LAMP1-GFP and either treated with Alexa 568-tagged α -syn fibrils
1948 for 18 h (co-culture prepared from these donors was referred to as “ α -syn co-culture”) or left
1949 untreated (co-culture prepared from these donors was referred to as “control co-culture”).
1950 Donor cells were then co-cultured with acceptor CAD cells transiently transfected with H2B-
1951 mCherry for 24 h. Efficiency of the LAMP1-GFP+ lysosome transfer was measured in each
1952 condition. (C) Donor CAD cells were transiently transfected with Arl8b-GFP (co-culture
1953 prepared from these donors was referred to as “Arl8b co-culture”) or not (co-culture prepared
1954 from these donors was referred to as “control co-culture”) prior to be loaded with Alexa 568-

1955 tagged α -syn fibrils for 18 h. Arl8b-GFP expressing donors (having more peripheral lysosomes)
1956 and control donors were then co-cultured with acceptor CAD cells that were transiently
1957 transfected with H2B-GFP for 24 h. Efficiency of the α -syn fibrils' transfer was measured in
1958 each condition. **(D)** Donor HeLa cells were transiently transfected with Arl8b-GFP (co-culture
1959 prepared from these donors was referred to as "Arl8b co-culture") or not transfected (co-culture
1960 prepared from these donors was referred to as "control co-culture") prior to be loaded with
1961 Alexa 568-tagged α -syn fibrils for 18 h. Arl8b-GFP expressing donors (having more peripheral
1962 lysosomes) and control donors were then co-cultured with acceptor HeLa cells that were
1963 transiently transfected with H2B-GFP for 24 h. Efficiency of the α -syn fibrils' transfer was
1964 measured in each condition. **(E)** Three donor CAD cell populations were prepared: untreated
1965 control cells, cells pretreated with sicontrol (scramble) or with siArl8b. Co-cultures were
1966 referred to as "control", "sicontrol", and "siArl8b" co-cultures to distinguish the treatments
1967 applied to the donor cells. Donors having perinuclear lysosomes (siArl8b pretreated) and
1968 control donors (sicontrol pretreated or untreated) were loaded with Alexa 568-tagged α -syn
1969 fibrils for 18 h prior to be co-cultured with acceptor CAD cells transfected with H2B-GFP for
1970 24 h. Efficiency of the α -syn fibrils' transfer was measured in each condition. **(F)** Donor control
1971 cells (WT HeLa) or myrlysin-KO HeLa cells or KIF1B-5B dKO HeLa cells were treated with
1972 Alexa 568-tagged α -syn fibrils for 18 h. Control donors (WT HeLa) and donors having
1973 perinuclear lysosomes (myrlysin-KO and KIF1B-5B dKO HeLa cells) were then co-cultured
1974 with the acceptor WT HeLa cells transiently transfected with H2B-GFP for 24 h. Co-cultures
1975 were referred to as "control", "myrlysin-KO", and "KIF1B-5B dKO" co-cultures to distinguish
1976 the treatments applied to the donor cells. Efficiency of the α -syn fibrils' transfer was measured
1977 in each condition. **(G)** Donor CAD cells were either transfected with H2B-mCherry (co-culture
1978 prepared from these donors was referred to as "control co-culture") or treated with Alexa 568-
1979 tagged α -syn fibrils for 18 h (co-culture prepared from these donors was referred to as " α -syn
1980 co-culture") were co-cultured with acceptor CAD cells were either transiently transfected with
1981 Gal3-GFP (1) or α -syn-GFP (2). Donor and acceptor cells were then co-cultured for 24 h.
1982 Acceptors cells were analysed for the presence of Gal3-GFP or α -syn-GFP puncta, respectively.
1983 **(H)** Donor CAD cells transiently transfected with Gal3-GFP and treated with Alexa 568-tagged
1984 α -syn fibrils for 18 h were co-cultured with acceptor HeLa cells stably expressing Gal3-
1985 Turquoise for 24 h. Co-cultures were either immunolabelled with LAMP1 (mouse) antibody or
1986 LAMP1 (human) antibody to detect lysosomes derived from donor and acceptor cells,
1987 respectively. **(I)** Secretion test: in parallel to co-culture preparations where donor and acceptor
1988 cells were mixed in 1:1 ratio, donors and acceptor cells were also plated separately and medium

1989 of acceptor cells were replaced by the conditioned medium collected from donor cells. Acceptor
1990 cells were then analysed for the presence of different cargos (e.g., α -syn fibrils, lysosomes) in
1991 order to evaluate cargo transfer from donor to acceptor cells through secretion.

1992

1993 **S4 Fig. α -Syn fibrils do not induce lysophagy.** Representative confocal images of CAD cells
1994 control, treated with 1 mM LLOMe for 3 h, or treated with Alexa 568-tagged α -syn fibrils for
1995 18 h and immunolabelled with LC3-Alexa 488, Ubiquitin FK2-Alexa 647, and Lamp1-
1996 CFTM405M (pseudo colored in grey) antibodies. Light blue arrows indicate lysosomes under
1997 lysophagy. $n=3$ (60 cells analysed per condition). Scale bar: 10 μ m.

1998

1999 **S5 Fig. Timeframes of the S1 and S2 Movies of CAD cells overexpressing soluble α -syn-**
2000 **GFP treated or not with Alexa 568-tagged α -syn fibrils up to 4 h. (A)** Timeframes at
2001 0/1/2/3/4 hours of the S1 Movie of CAD cells overexpressing soluble α -syn-GFP monitored
2002 after the administration of α -syn fibrils. **(B)** Timeframes at 0/1/2/3/4 hours of the S2 Movie of
2003 CAD cells overexpressing soluble α -syn-GFP.

2004

2005 **S6 Fig. Lysosome positioning affects the efficiency of α -syn fibrils' transfer in HeLa cells.**

2006 **(A)** Representative confocal images of donor and acceptor HeLa cells after 24 h of co-culture.
2007 Donor cells were either treated with Alexa 568-tagged α -syn fibrils for 18 h (referred as “control
2008 co-culture”) or they were transfected with Arl8b-GFP prior to be treated with α -syn fibrils
2009 (referred as “Arl8b-GFP co-culture”). Acceptor cells were transfected with H2B-GFP. 24 h
2010 later, co-cultures were labelled with HCS CellMaskTM Blue and DAPI. Arrows indicate the α -
2011 syn fibrils received by acceptor cells and asterisks indicate the cells having α -syn fibrils in each
2012 co-culture condition. Scale bar: 10 μ m. **(B)** % of acceptor cells received α -syn fibrils in control
2013 co-culture ($28 \pm 3\%$), Arl8b-GFP co-culture ($60 \pm 5\%$), control secretion ($1 \pm 1\%$), and Arl8b-
2014 GFP secretion ($8 \pm 3\%$) is presented (left graph); average number of α -syn puncta in control
2015 co-culture (3 ± 1), Arl8b-GFP co-culture (5 ± 1), control secretion (1 ± 0.0), and in Arl8b-GFP
2016 secretion (2 ± 0.2) is presented (right graph). Mean \pm S.E.M, $n=3$ (70 acceptor cells per
2017 condition). ns=not significant, *** $P=0.0001$ by Kruskal-Wallis nonparametric ANOVA test
2018 followed by Dunn's multiple comparison tests. **(C)** Representative confocal images of donor
2019 and acceptor HeLa cells after 24 h of co-culture. WT, myrlysin-KO, and KIF1B-5B dKO HeLa
2020 cells were loaded with Alexa 568-tagged α -syn fibrils (referred as control, myrlysin-KO, and
2021 KIF1B-5B dKO co-cultures, respectively) and co-cultured with acceptor cells transfected with

2022 H2B-GFP. Co-cultures were labelled with HCS CellMask™ Blue and DAPI. Arrows indicate
2023 the α -syn fibrils received by acceptor cells and asterisks indicate the cells having α -syn fibrils
2024 in each co-culture condition. Scale bar: 10 μ m. **(D)** % of acceptor cells received α -syn fibrils in
2025 control co-culture ($29 \pm 2\%$), myrlysin-KO co-culture ($16 \pm 2\%$), KIF1B-5B dKO co-culture
2026 ($12 \pm 2\%$), control secretion ($5 \pm 2\%$), myrlysin-KO secretion ($6 \pm 1\%$), and KIF1B-5B dKO
2027 secretion ($6 \pm 1\%$) is presented (left graph); average number of α -syn in control co-culture ($2 \pm$
2028 0.3), myrlysin-KO co-culture (2 ± 0.3), KIF1B-5B dKO co-culture (2 ± 0.4), control secretion
2029 (1 ± 0.4), myrlysin-KO secretion (1 ± 0.2), and KIF1B-5B dKO secretion (1 ± 0.2) is presented
2030 (right graph). Mean \pm S.E.M, $n=3$ (90 acceptor cells per condition). ns=not significant,
2031 ** $P=0.016$, **** $P<0.0001$ by Kruskal-Wallis nonparametric ANOVA test followed by Dunn's
2032 multiple comparison tests. The data underlying this Figure may be found in S1 Data.

2033

2034 **S7 Fig. Validation of CAD-HeLa co-culture system with additional information. (A)**

2035 Representative confocal image of donor CAD cells loaded with Alexa 568-tagged α -syn fibrils
2036 (18 h) co-cultured with HeLa Gal3-Turquoise acceptor cells for 24 h. In acceptor HeLa cells,
2037 arrows indicate α -syn fibrils. Scale bar: 10 μ m. **(B)** % of acceptor HeLa cells received α -syn
2038 fibrils in co-culture ($65 \pm 3\%$) and in secretion test ($7 \pm 2\%$) is presented (left graph). Mean \pm
2039 S.E.M. **** $P<0.0001$ by two-tailed t -test. Average number of α -syn fibrils puncta per acceptor
2040 cell in co-culture (4 ± 0.2) and in secretion test (2 ± 0.2) is presented (right graph). ns=not
2041 significant by Mann-Whitney U -test. **(C)** Representative confocal image of donor CAD cells
2042 loaded with Alexa 568-tagged α -syn fibrils (18 h) co-cultured with acceptor WT HeLa cells
2043 transfected with α -syn-GFP for 24 h. Red arrows indicate α -syn fibrils, green arrows indicate
2044 α -syn-GFP puncta formation (seeding) in acceptor HeLa cells. Scale bar: 10 μ m. **(D)**
2045 Representative confocal image of Gal3-GFP transfected and Alexa 568-tagged α -syn fibril
2046 loaded donor CAD cells (18 h) co-cultured with HeLa Gal3-Turquoise cells for 24 h. In donor
2047 CAD cell, green arrows indicate Gal3-GFP puncta formation. Scale bar: 10 μ m. **(E)** % of donor
2048 CAD cells under LMP in control ($2 \pm 2\%$) and in α -syn ($11 \pm 4\%$) co-cultures is presented (left
2049 graph); average number of Gal3-GFP puncta in donor cells under LMP in control (10 ± 2) and
2050 in α -syn (14 ± 4) co-cultures is presented (right graph). Mean \pm S.E.M. ns=not significant, by
2051 * $P=0.04$ Mann-Whitney U -test. **(F)** HeLa Gal3-Turquoise acceptor cell under LMP labelled for
2052 LAMP1 human Alexa 647 antibody (pseudo colored in grey). Colocalization between Gal3-
2053 Turquoise puncta and LAMP1 (indicated by arrows) is presented in a selected region indicated
2054 by the square. Scale bar: 10 μ m (for the inset: 1 μ m). **(G)** HeLa Gal3-Turquoise acceptor cell

2055 under LMP labelled with LAMP1 mouse Alexa 647 antibody (pseudo colored in grey).
2056 Colocalization between Gal3-Turquoise puncta and donor's lysosome (white arrows), and
2057 colocalization between α -syn fibrils puncta and donor's lysosome (red arrows) are presented in
2058 a selected region indicated by a square. Scale bar: 10 μ m (for the inset: 1 μ m). **(H)**
2059 Representative confocal image of Alexa 568-tagged α -syn fibril-treated donor CAD cells for
2060 18 h co-cultured with HeLa Gal3-Turquoise cells (pseudo colored in yellow) for 24 h. Higher
2061 magnification of a selected region (white square) in donor CAD cell is presented. Arrows
2062 indicate a Gal3-Turquoise puncta detected in a donor CAD cell. "Merge" image is saturated for
2063 the better visualization of the Gal3-Turquoise puncta. Scale bar: 10 μ m (for the inset: 2 μ m).
2064 **(I)** % of donor CAD cells received Gal3-Turquoise puncta in control ($0.3 \pm 0.3\%$) and in α -syn
2065 ($4 \pm 1\%$) co-cultures. Mean \pm S.E.M. ****** $P=0.003$ by Mann-Whitney *U*- test. In CAD-HeLa co-
2066 culture model, data was collected from seven independent experiments in which four and three
2067 of them were labelled with anti-LAMP1 mouse and human antibodies, respectively. According
2068 to the experiment, in average 100 acceptor or donor cells were analysed for each condition per
2069 experiment. The data underlying this Figure may be found in S1 Data.

2070

2071 **S1 Movie. Seeding of α -syn-GFP aggregates in CAD cells overexpressing soluble α -syn-**
2072 **GFP treated with α -syn fibrils up to 4 h.** Timeframes of the max projection of 36 slides (step
2073 size: 0.20 μ m) with a total physical thickness of 7.2 μ m, with 5 minutes of interval time. Video
2074 was acquired using laser 488 in a Spinning Disk microscope.

2075

2076 **S2 Movie. Monitoring of CAD cells overexpressing soluble α -syn-GFP up to 4 h.**
2077 Timeframes of the max projection of 21 slides (step size: 0.48 μ m) with a total physical
2078 thickness of 9.55 μ m, with 15 minutes of interval time. Video was acquired using laser 488 in
2079 a Spinning Disk microscope.

Figure-1

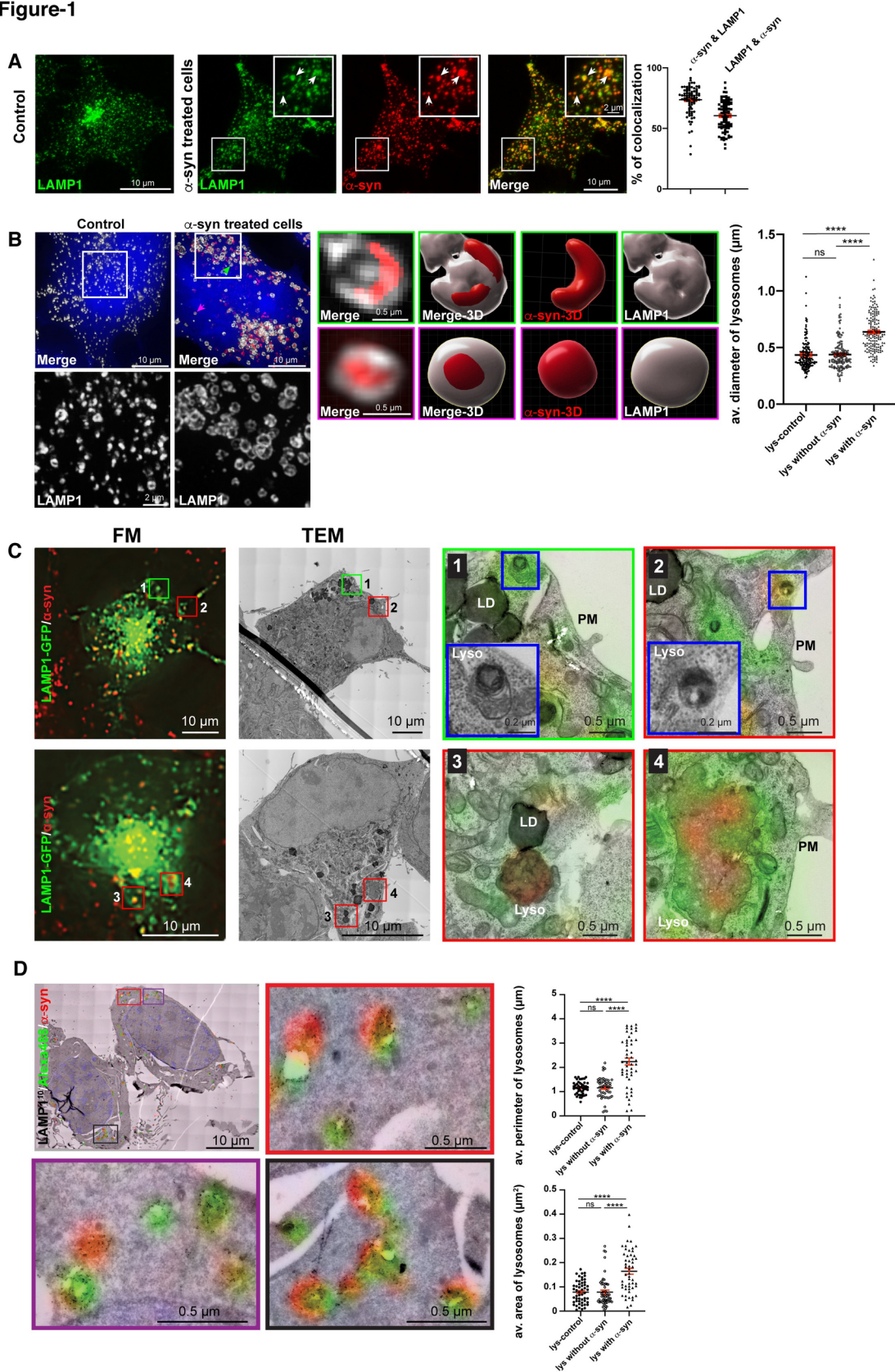


Figure-2

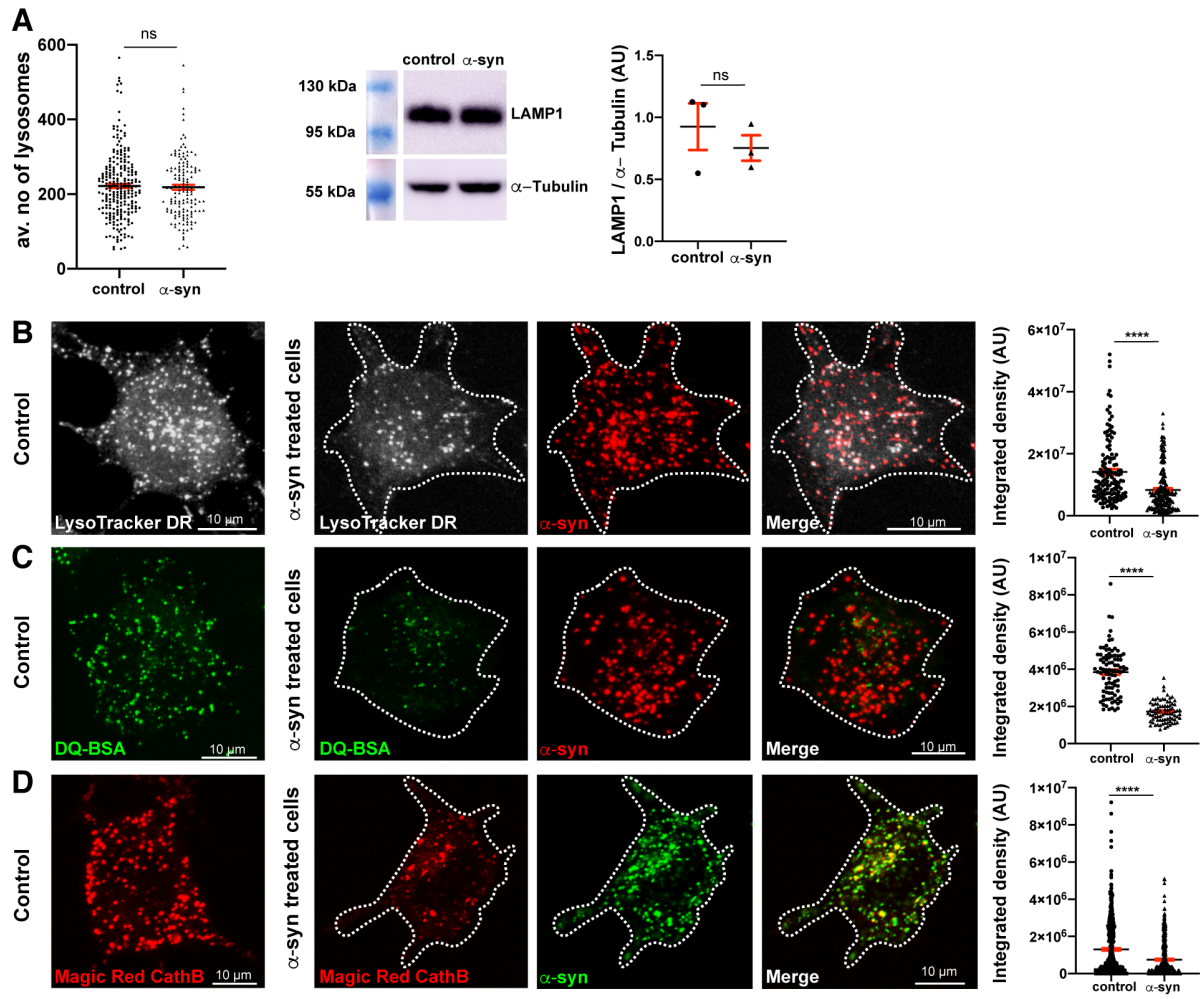


Figure-3

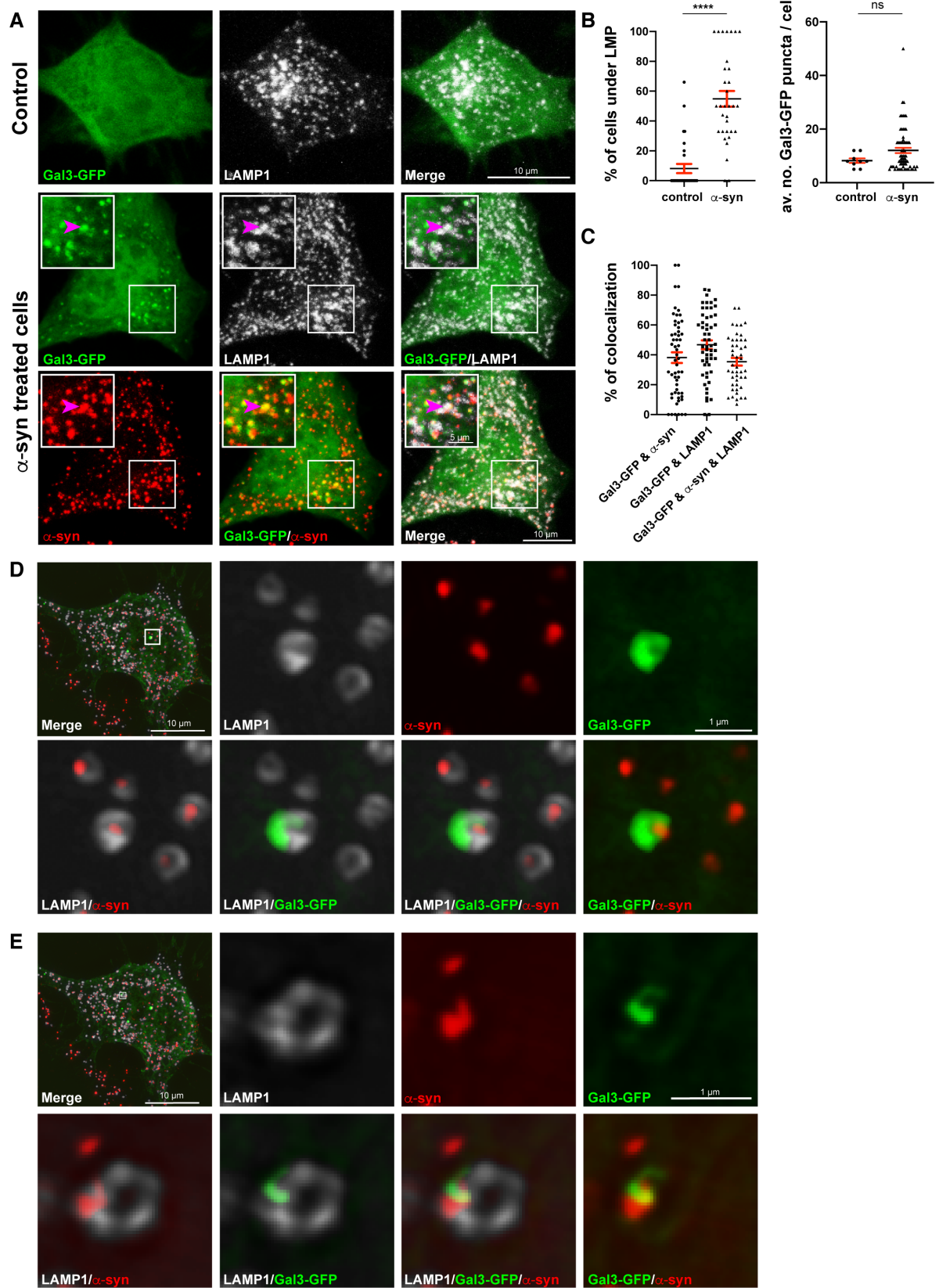


Figure-4

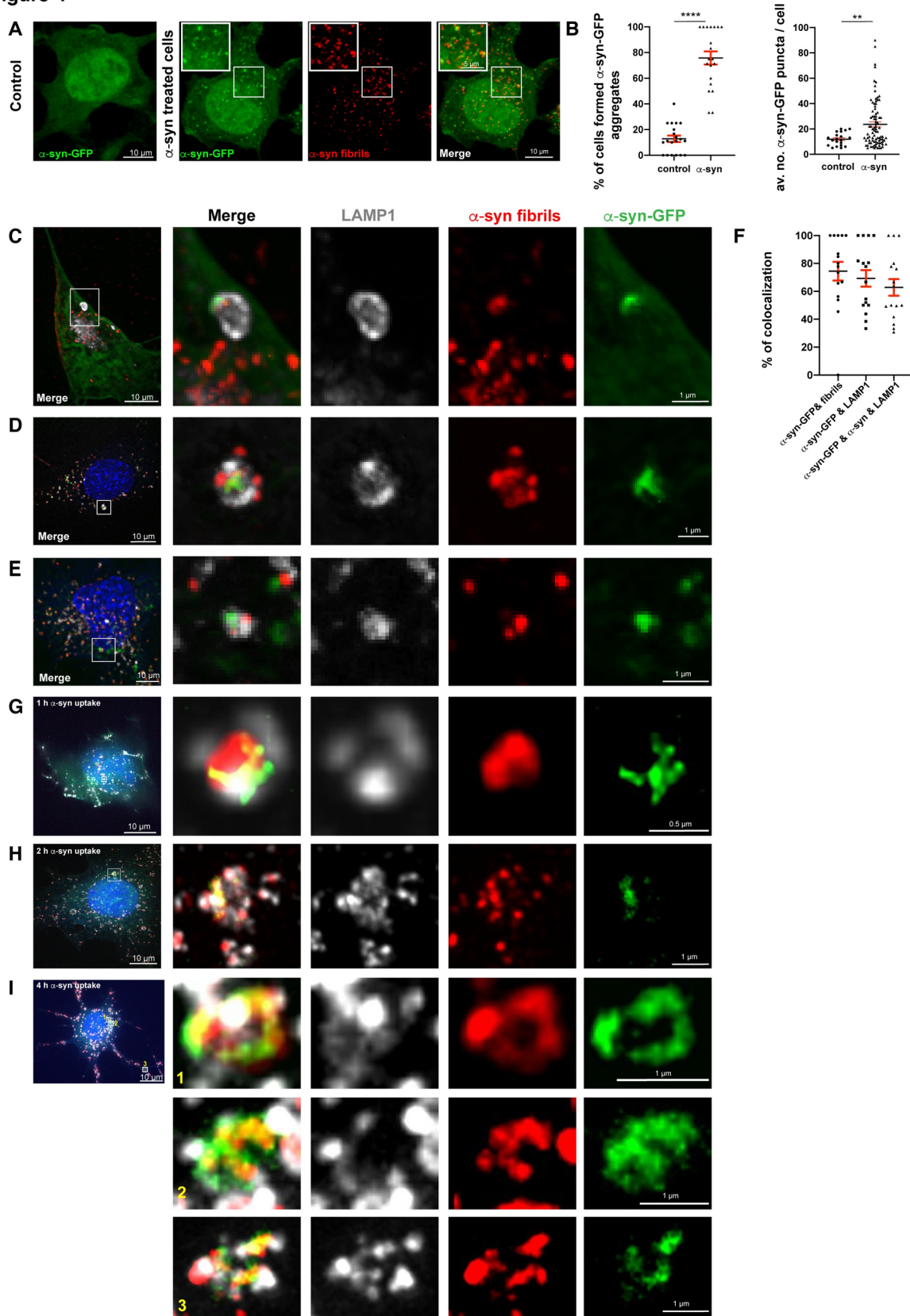


Figure-5

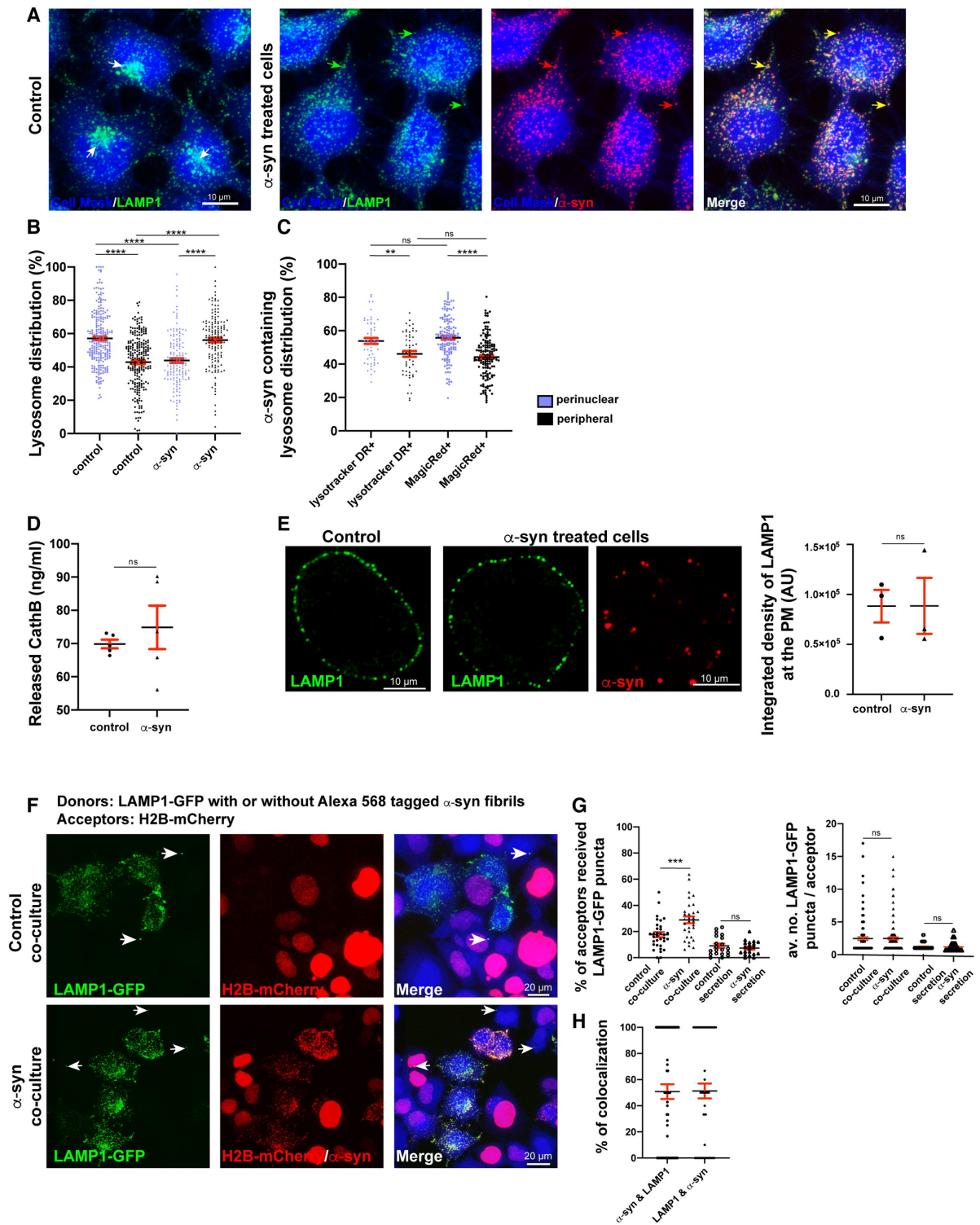


Figure-6

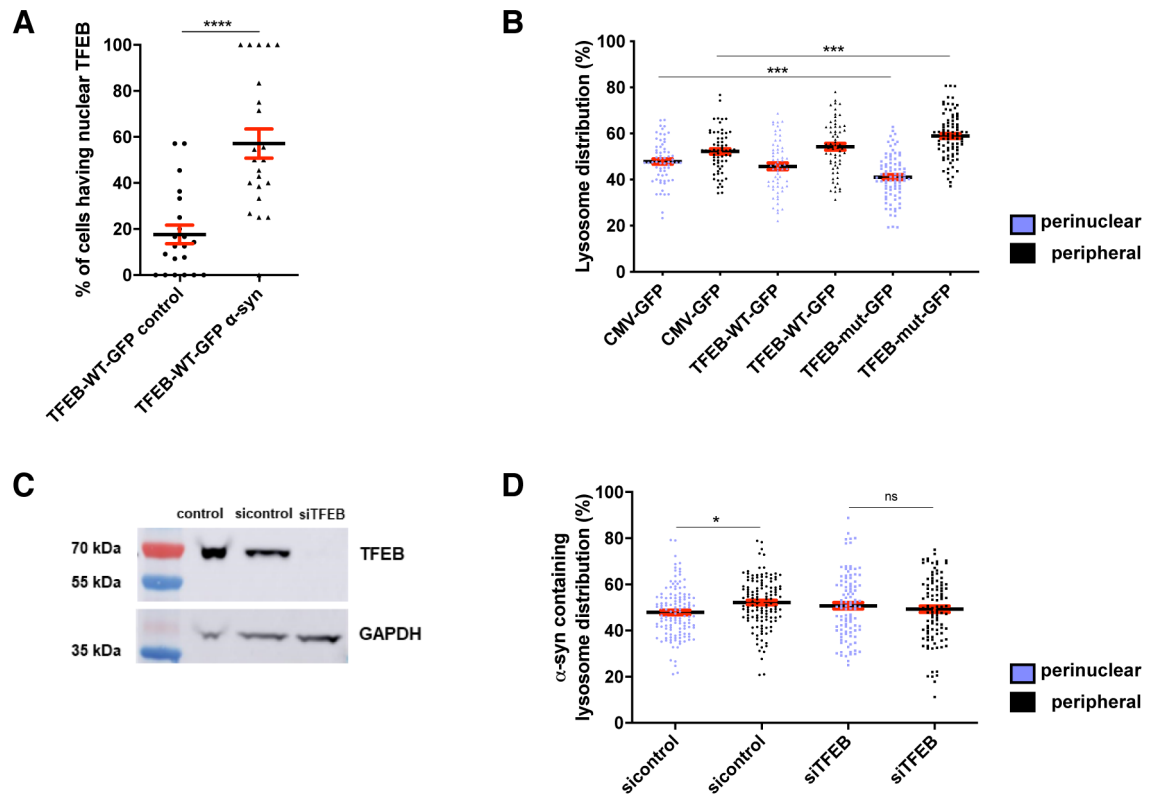


Figure-7

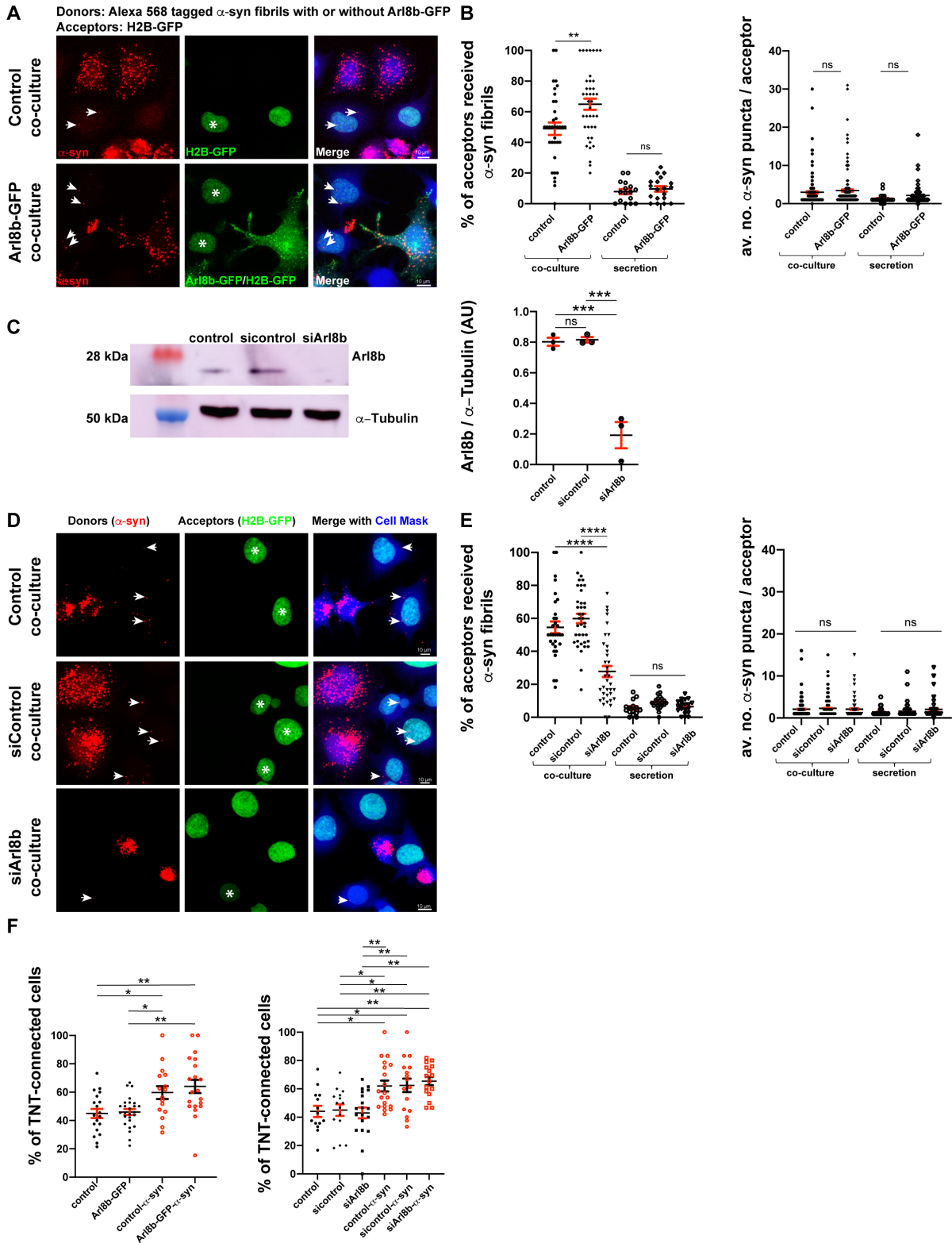


Figure-8

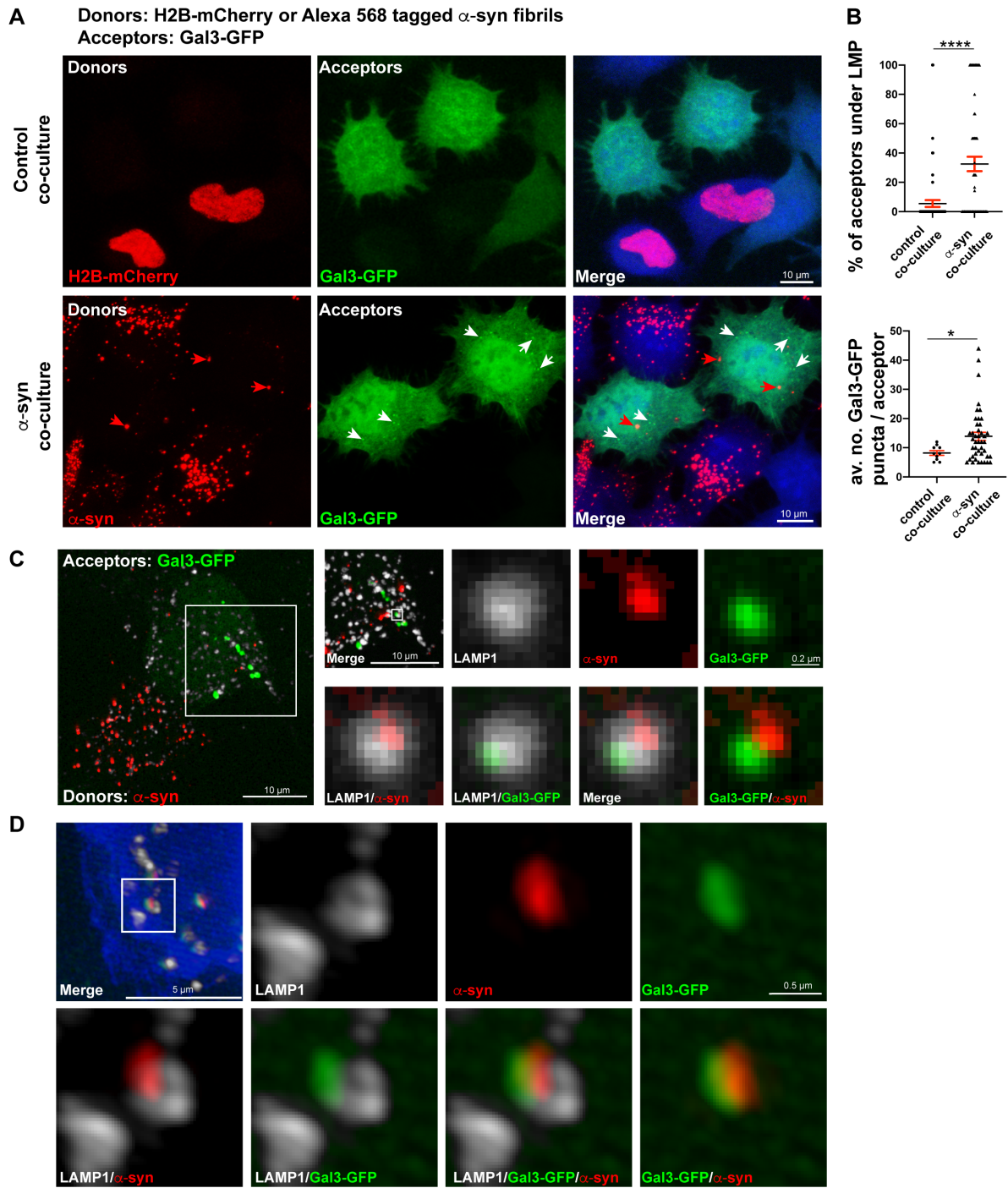


Figure-9

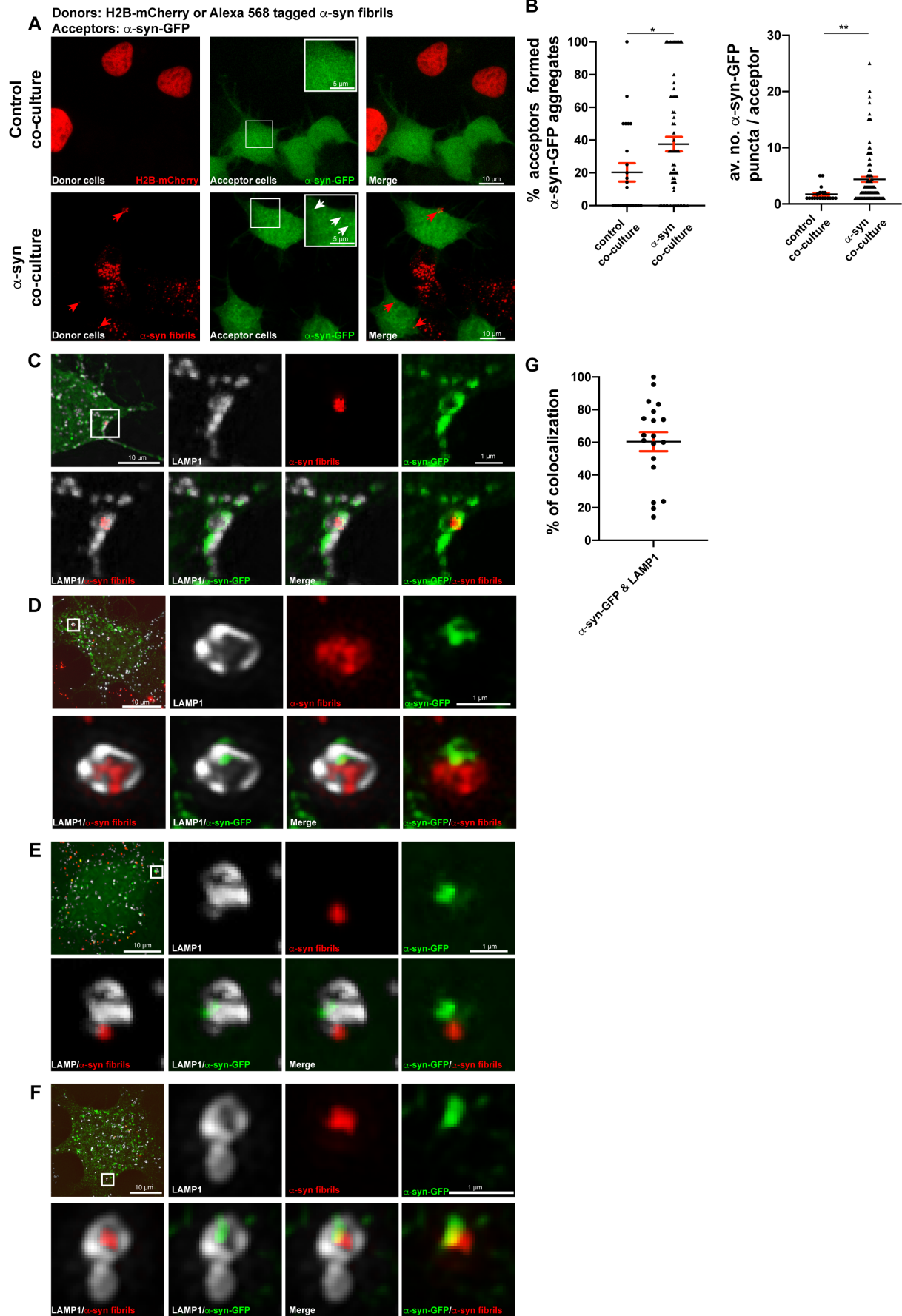


Figure-10

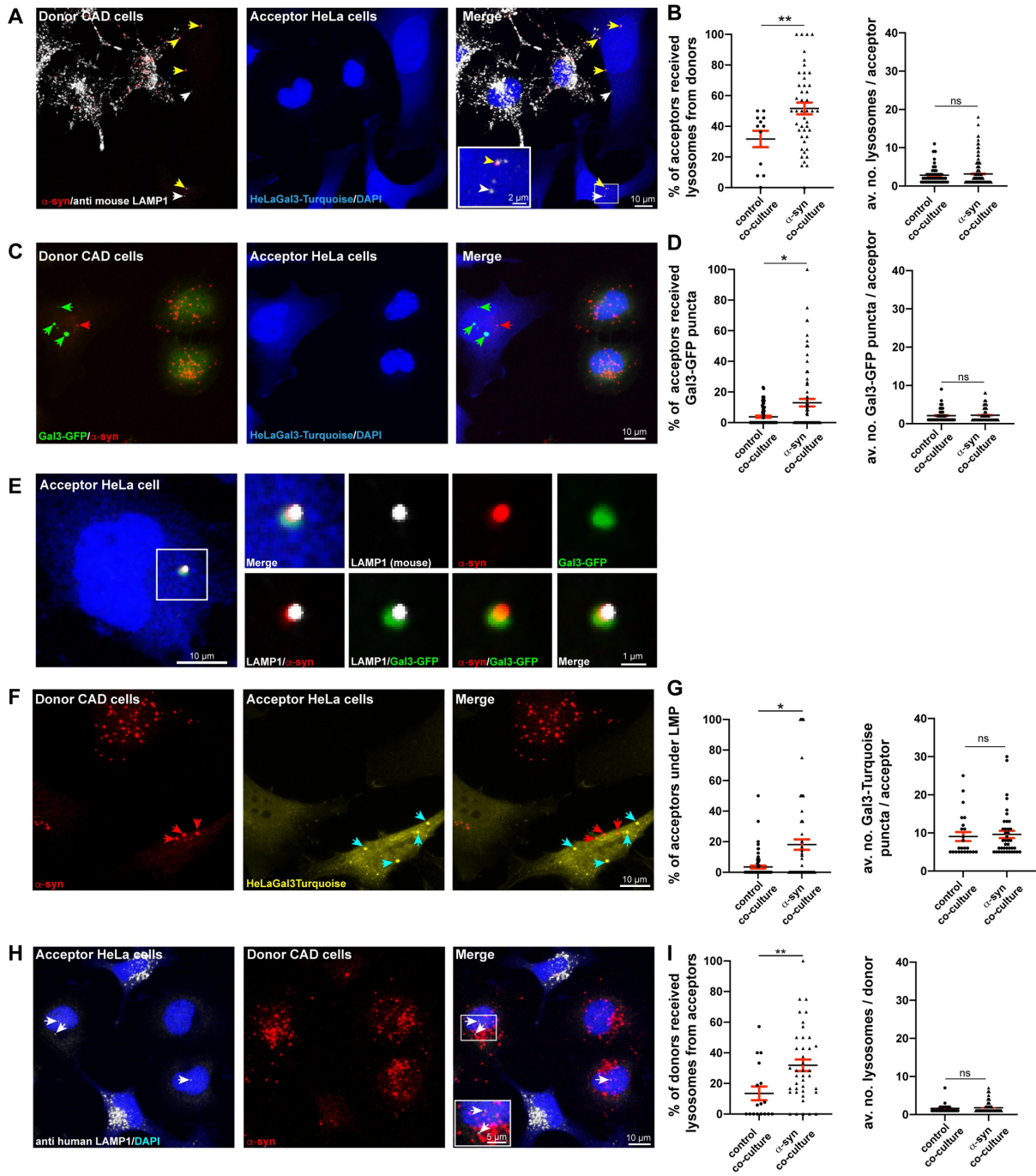


Figure-11

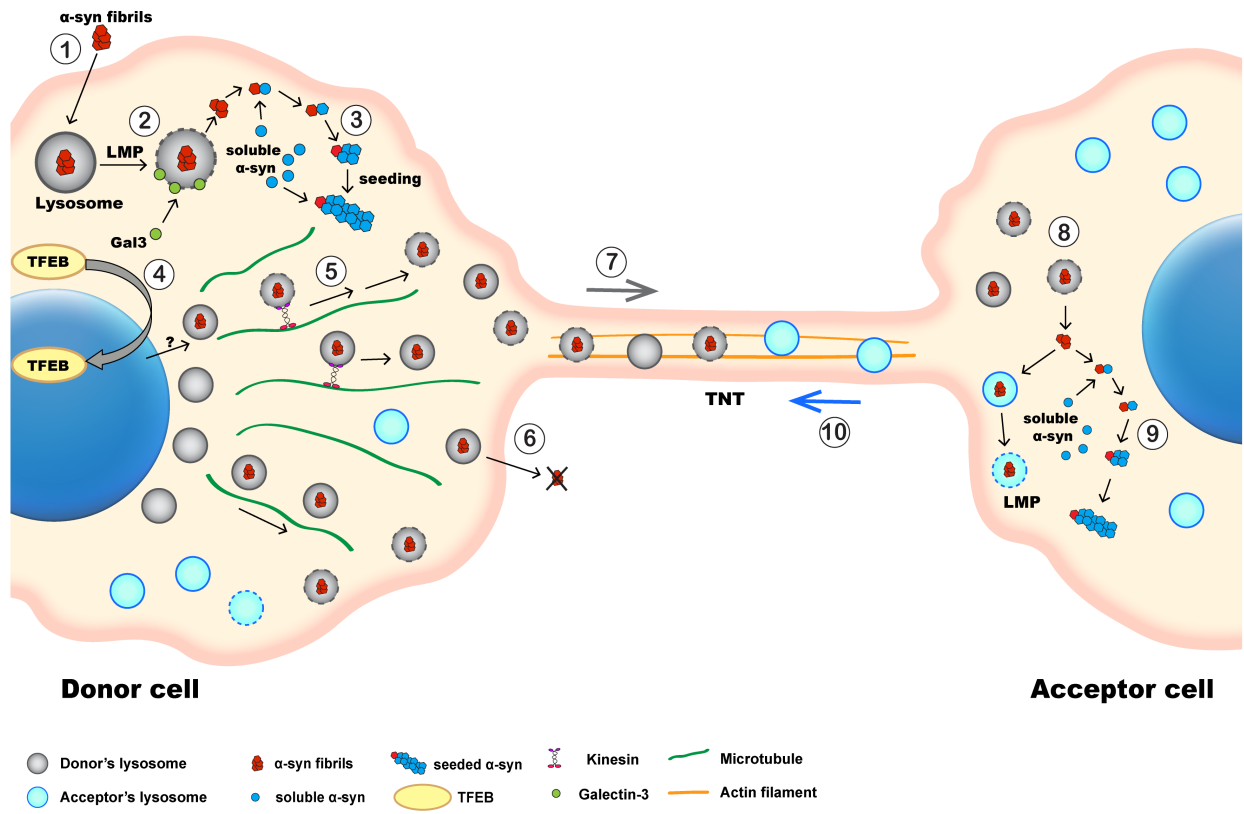


Figure S1

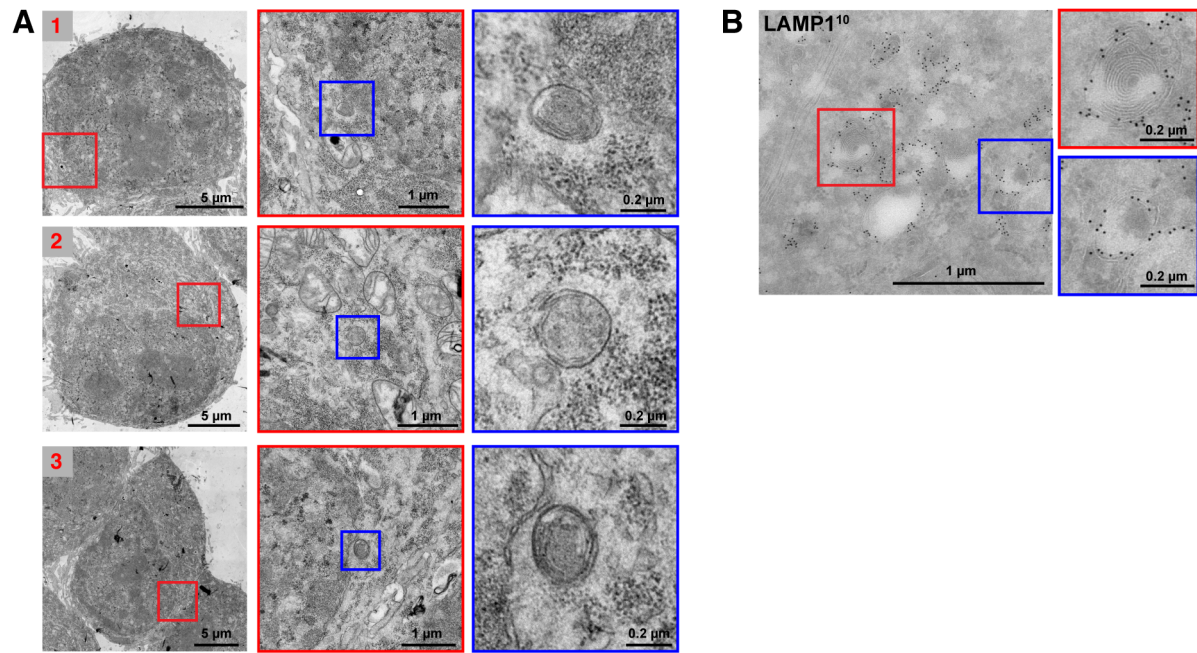


Figure S2

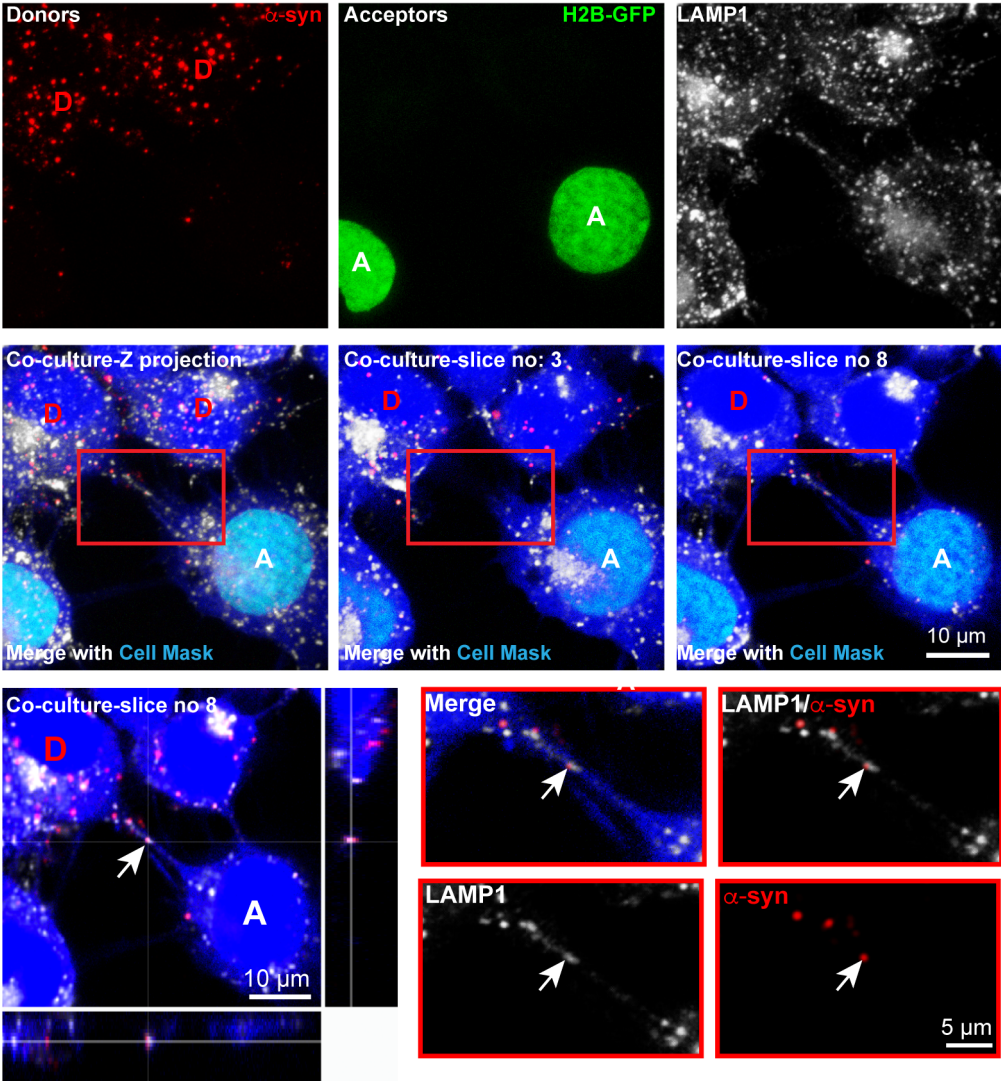
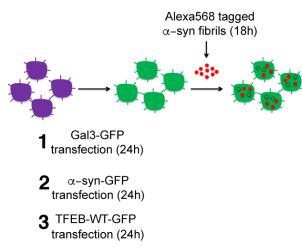
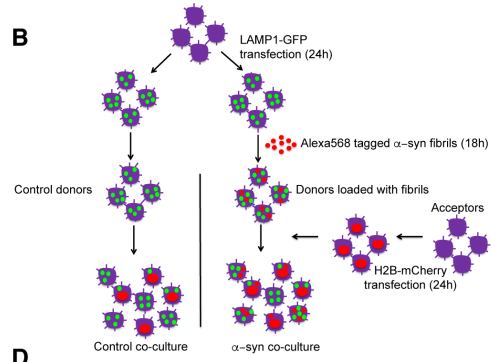


Figure S3

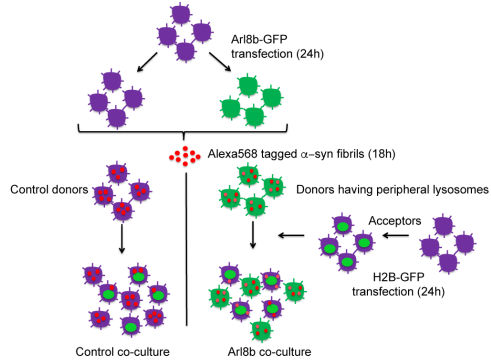
A



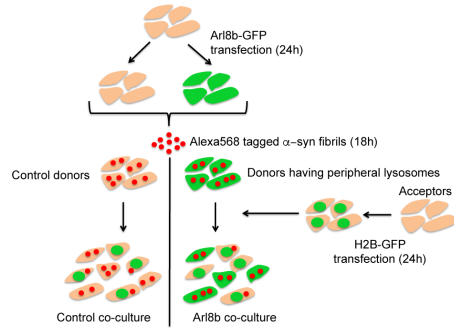
B



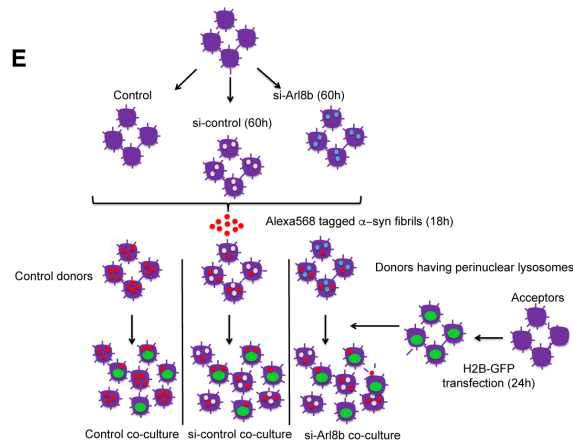
C



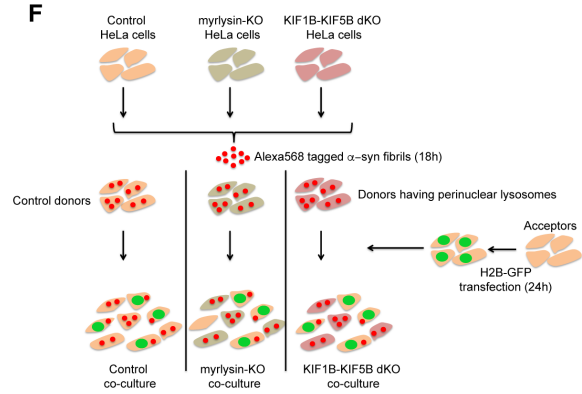
D



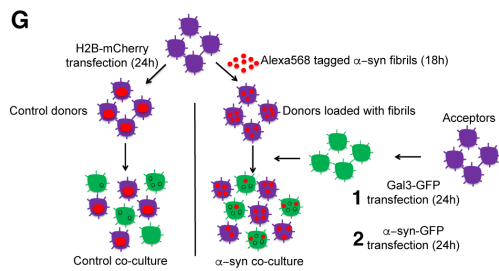
E



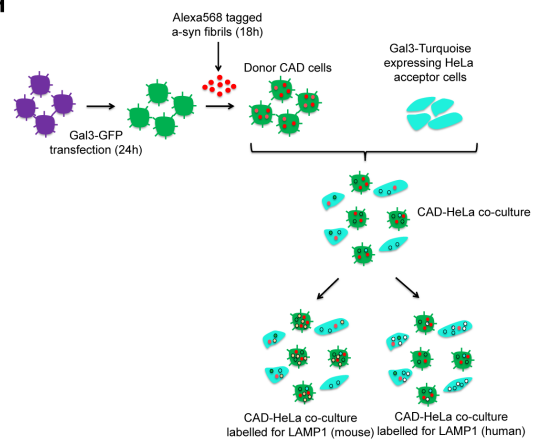
F



G



H



I

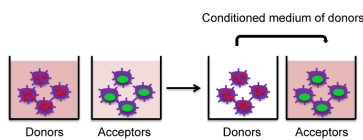


Figure S4

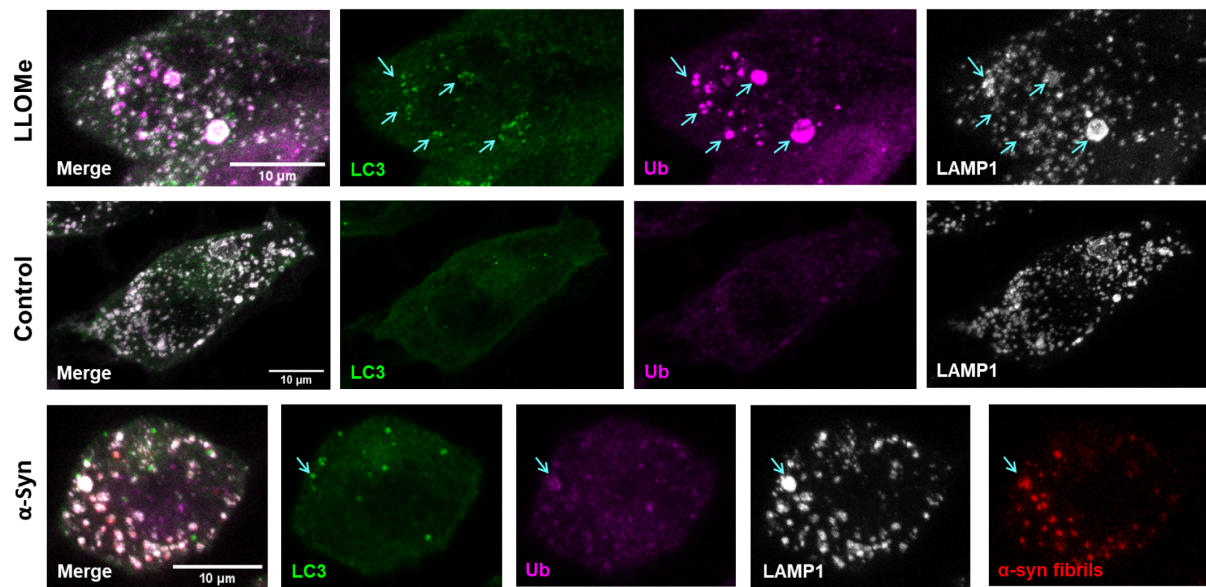


Figure S5

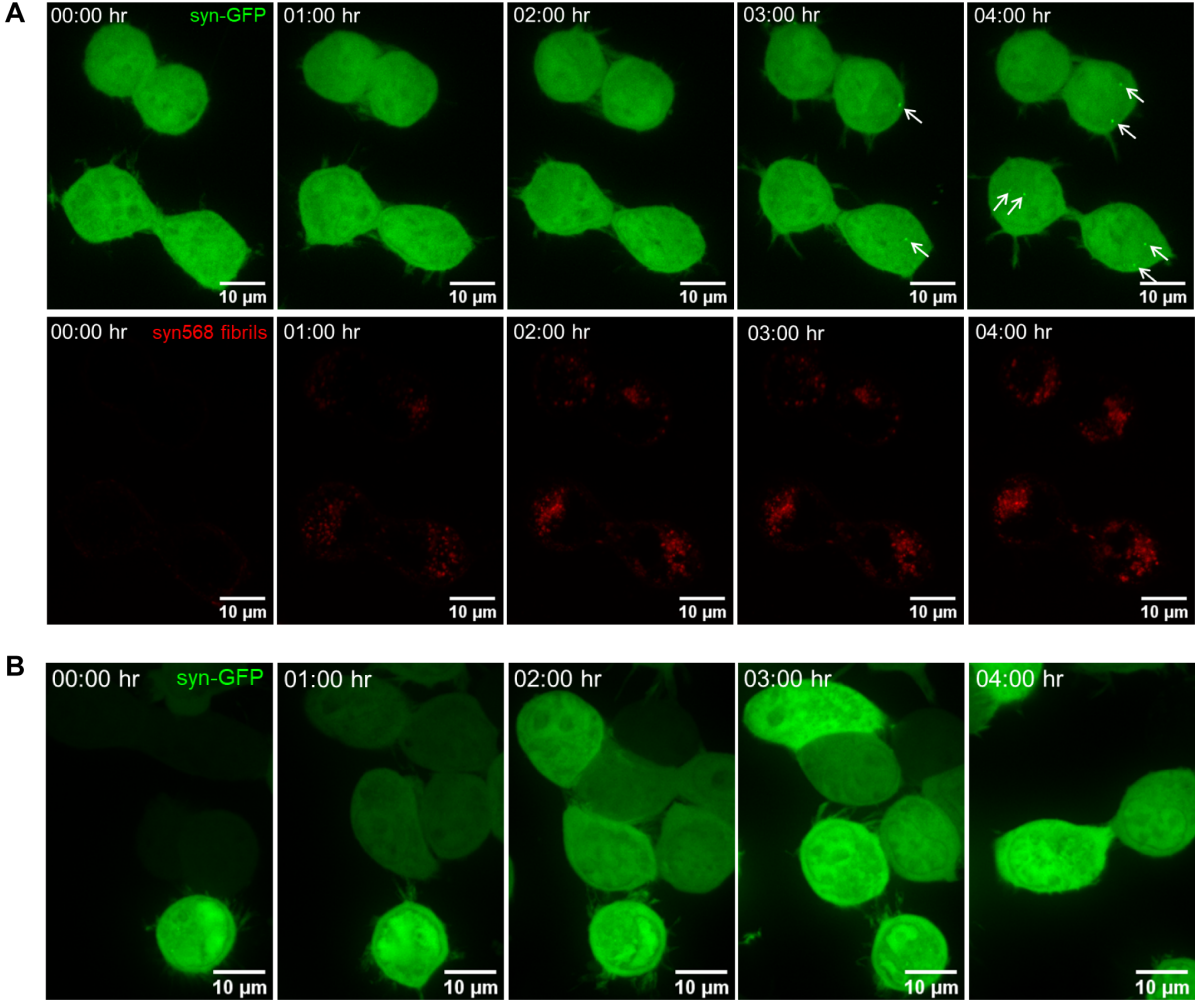


Figure S6

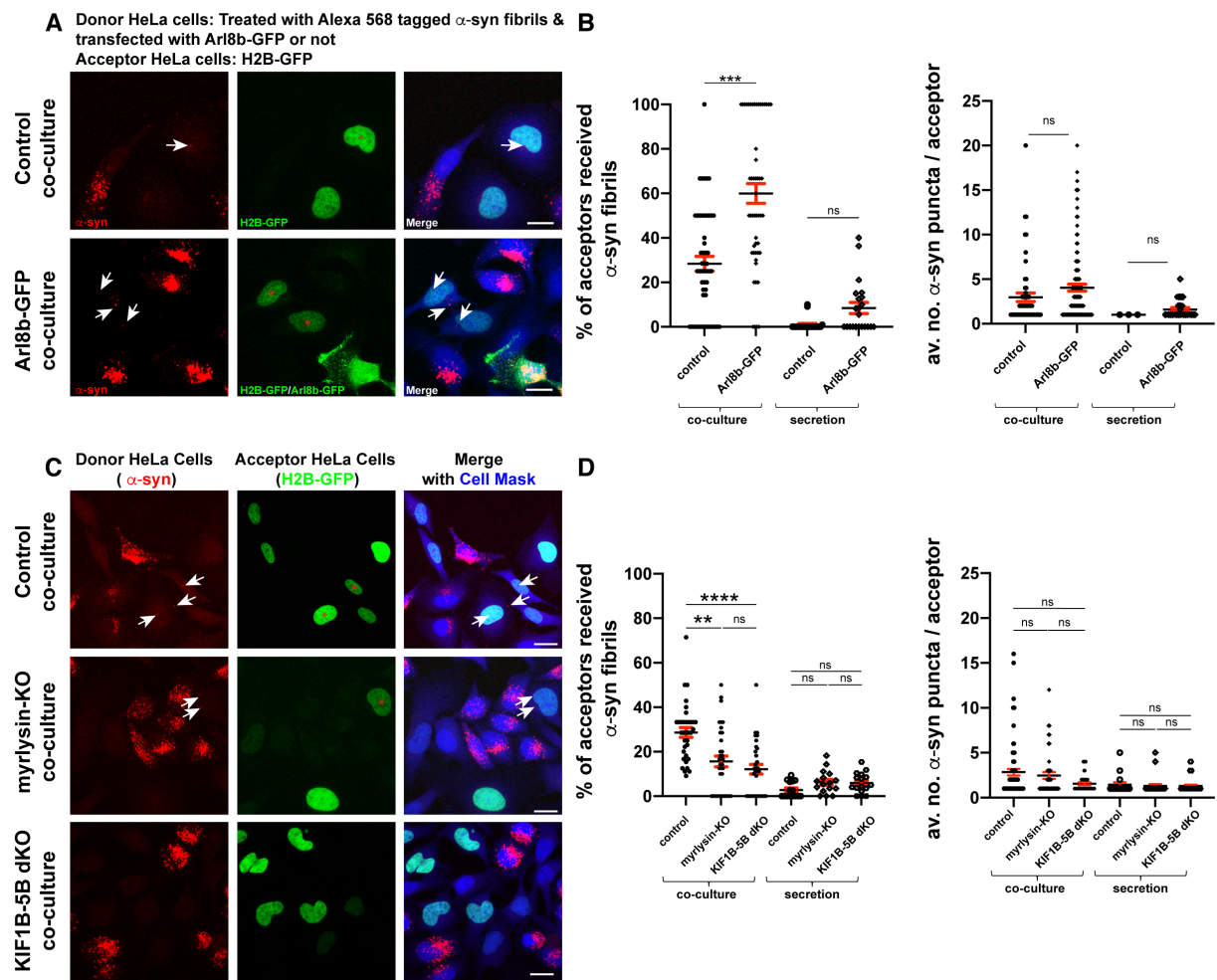
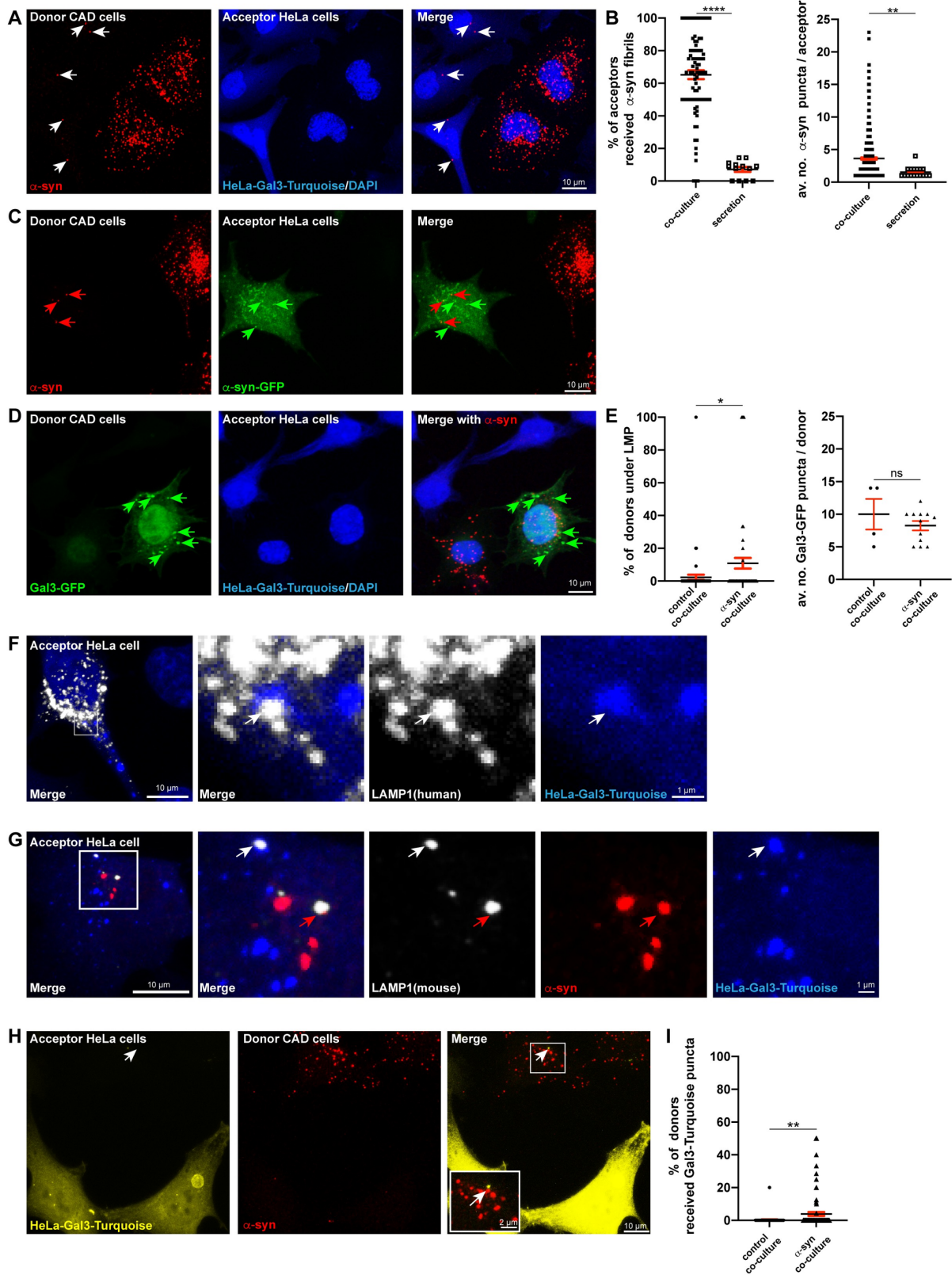


Figure S7



Funding

Association pour la Recherche sur la Sclérose Latérale Amyotrophique et Autres Maladies du Motoneurone (ARSLA 2016), INNOV 39-2019 Flash Start (Institut Pasteur) supported ADS, Access to Correlative Light and Electron Microscopy Flagship Node was supported by Euro-BioImaging grant (EuBI_AYDI109) for ADS,

MS was supported by France Alzheimer (S-FB17026) and the Marie Skłodowska-Curie Action H2020-MSCA-IF-2019 EU project 897378

Agence Nationale de la Recherche (ANR-16-CE16-0019-01), Fondation pour la Recherche Médicale (FRM-2016-DEQ20160334896) and LECMA-Vaincre Alzheimer (2016 / FR-16020) and France Alzheimer (AAP SM 2017#1674) foundations financially supported CZ,

Intramural Program of NICHD (project ZIA HD001607) supported JSB, Grant-in-Aids for Scientific Research (JP26117005), CREST, JST (JP18071300) and AMED Brain/MINDS (JP18dm0207019) supported MH, Brain Science Foundation supported TN, NL was supported by the Netherlands Organization for Scientific Research (NWO) through a ZonMW-TOP grant (91216006) to JK.

Agence Nationale de la Recherche (ANR-10-INSB-04), ANR/FBI and the Région Ile-de-France Domaine d'Intérêt Majeur-Malinf program supported the use of structured illumination microscopy (SIM) at the BioImagerie Photonic platform at Institut Pasteur